INVESTIGATION OF CONTROL STRATEGIES AND DEVELOPMENT OF A HYDRAULIC ACTUATOR MECHANISM FOR ACCURATE POSITIONING OF SUBSEA ROBOTS

KAREN JULIE MUGGERIDGE

INVESTIGATION OF CONTROL STRATEGIES AND DEVELOPMENT OF A HYDRAULIC ACTUATOR MECHANISM FOR ACCURATE POSITIONING OF SUBSEA ROBOTS

BY

© KAREN JULIE MUGGERIDGE, B.ENG.

A thesis submitted to the School of Graduate Studies in partial fulfillment of the requirements for the degree of Master of Engineering

Faculty of Engineering and Applied Science

Memorial University of Newfoundland

September 1994

St. John's Newfoundland Canada

To Steve and my family

Definition of research:

Research is what I'm doing when I don't know what I'm doing.

Wernher von Braun

Apollo Rocket Engineer

ABSTRACT

Subsea robot control must be robust in the face of dynamic uncertainties encountered in the unstructured ocean environment. In this thesis, the main control strategies are examined and evaluated in terms of their potential for underwater robot control. It is concluded that robust control would be achieved with a mix of supervisory and classical control strategies. In particular, neural networks and fuzzy logic combined with error-driven compensation are recommended for high performance underwater control.

A new propulsion device for short duration fine-positioning control of small subsea robots is proposed. This device uses a hydraulic actuator mechanism operated from an energy source of compressed gas to mimic the jet propulsion of squids. Experimental work conducted demonstrated the potential of the proposed propulsion device.

ACKNOWLEDGMENTS

The author gratefully acknowledges financial support from: the Department of Education, Government of Newfoundland and Labrador (Career Development Award); the Centre for Cold Ocean Resources Engineering (C-CORE Fellowship); and the author's supervisor, Dr. M. J. Hinchey.

The author is greatly indebted to Dr. Hinchey, Department Head of Mechanical Engineering, for his excellent guidance, support and understanding. Dr. Hinchey has helped the author gain a great deal of knowledge in the area of underwater robot control and a practical insight into research.

Special thanks are also due to the technical staff in the engineering fluids and structures labs, especially Mr. A. Bursey, who made their services readily available throughout the project.

CONTENTS

LIST OF FIGURES

LIST OF TABLES

LIST OF SYMBOLS

γ	negative constant
Δt	sampling interval
ε	boundary layer width
λ	bandwidth
ϕ	boundary layer thickness
C	term which accounts for wake drag
C°	best estimate for term which accounts for wake drag
d	safe operating depth
D	disturbance force from the surroundings
D°	best estimate of disturbance force from the surroundings
e	exponential
E	difference between desired and actual robot position
E_d	relay dead zone
E_h	relay hysteresis level
E_N	difference between the neural network output and the target output
f	squashing function
F	force generated by the propulsion system
F°	best estimate of force generated by the propulsion system
I	command or desired robot position
I_N	network input

K_D derivative gain

K_I integral gain

K_P proportional gain

K_R relay gain

M inherent and added water mass of the robot

M^o best estimate of inherent and added water mass of the robot

M_N squashed output from middle layer neuron

O actual robot position

O_N network output

O_T target output

Q forcing due to uncertainty

R wave steepness

S measure of the algebraic distance to the sliding surface, S(t)

S(t) sliding surface

t time

T wave period

V Liapunov function

W_I input weight

W_{IB} input weight for input bias neuron

W_{IM} input weight for middle layer neuron

W_O output weight

W_{OB} output weight for middle layer bias neuron

W_{OM} output weight for middle layer neuron

LIST OF ABBREVIATIONS

AUV autonomous underwater vehicle

DOF degree of freedom

LVDT linear variable differential transformer

PID proportional, integral and derivative

ROV remotely operated vehicle

1 INTRODUCTION

With the recent flybys of the outer planets and their moons, we now know more about the outer solar system than we know about the oceans (Blidberg and Yoerger, 1990). Humans have not been able to explore the full but finite depths of the oceans, which cover 70 percent of the earth's surface and are a vital part of the existence of mankind.

In the field of marine science, there is a vast wealth of knowledge to be discovered through ocean exploration. Areas for potential technological advancement in marine science include: marine biology; marine chemistry; marine geology and geophysics; and marine physics. These areas encompass the effects of biological and geological processes and mankind on global systems such as global resources and changes in climate. Effective management of these global systems is necessary to maintain their delicate balance.

Commercially, the ocean environment has become of ever-increasing interest in the world, since reserves of nonrenewable resources on the earth's land areas are diminishing. The need for exploration and development of these resources from the seabed has emphasized the role of robot technology for performing various underwater tasks. Examples of the use of robotics for

underwater operations include: support for offshore oil and gas development; oceanic mining; subsea survey and ocean mapping; inspection and maintenance; and salvage and burial tasks.

The increasing depth requirements for underwater tasks has promoted the use of remotely operated vehicles (ROVs) for such operations. The depth range for divers is approximately 450 metres, while the depth range for ROVs is between 1800 and 6000 metres depending on the degree of sophistication of the vehicle. A ROV is connected to the surface by an umbilical cord through which all communications, power and control are transmitted. The length of the umbilical cord is the limiting factor in determining the maximum depth for a ROV, since longer tethers can become entangled, require large cranes and winches and produce large drag forces. This dilemma has prompted the development of autonomous underwater vehicles (AUVs), which do not have umbilical cords connecting them to the surface. AUVs would be preprogrammed and contain their own power supply.

Unfortunately, ROVs and AUVs lack high performance characteristics due to problems in adapting control strategies for the underwater environment and inefficiencies in current propulsion mechanisms and sensors.

There are two main project objectives presented in this thesis. The first

objective was to provide a comprehensive investigation of the main control strategies in terms of their potential for effective underwater control. Although there have been many studies on different theories for subsea control, there is a remarkable lack of literature which describe the various control strategies in an understandable form.

The second thesis objective was to develop a propulsion device to provide fine-positioning control for a subsea robot as an application of subsea control theory. This positioning device was a new idea which had never been tested. The author started with the concept of the device and built a test apparatus to determine if the device was feasible.

This thesis begins with an overview of underwater control (chapter two) which includes a discussion of control considerations for subsea operations and an objective review of previous work conducted in the area of underwater control. Chapter three gives detailed descriptions of how each of the main control strategies would operate and their suitability for subsea control. An overview of current propulsion mechanisms is presented in chapter four, while chapter five gives a description of the new positioning device and preliminary experiments conducted with this device. Concluding remarks and recommendations regarding future work are contained in chapter six and seven, respectively.

2 OVERVIEW OF UNDERWATER ROBOT CONTROL

The designer of an underwater robot control system must consider many nonlinearities and modelling uncertainties. These considerations are associated with the high density, nonuniform, and unstructured ocean environment. Technologies developed for on-land systems cannot be directly adapted for subsea robotics since different dynamic characteristics are present. Underwater control considerations and previous work on adapting control strategies for subsea applications are discussed and evaluated in the following sections. Detailed descriptions of the main control strategies are given in chapter three.

2.1 Underwater Control Considerations

Robot control in the ocean environment is complicated by factors including: characteristics of the ocean environment itself; real fluid considerations; and the forces due to real fluids.

The ocean environment, in terms of a vertical profile, consists of three regimes: the atmosphere above the water surface, the water column, and the sea floor. All these regimes influence submersible design, although the water column is of primary importance. A summary of factors affecting submersible design for various regions of the ocean profile is given in Figure 2.1.

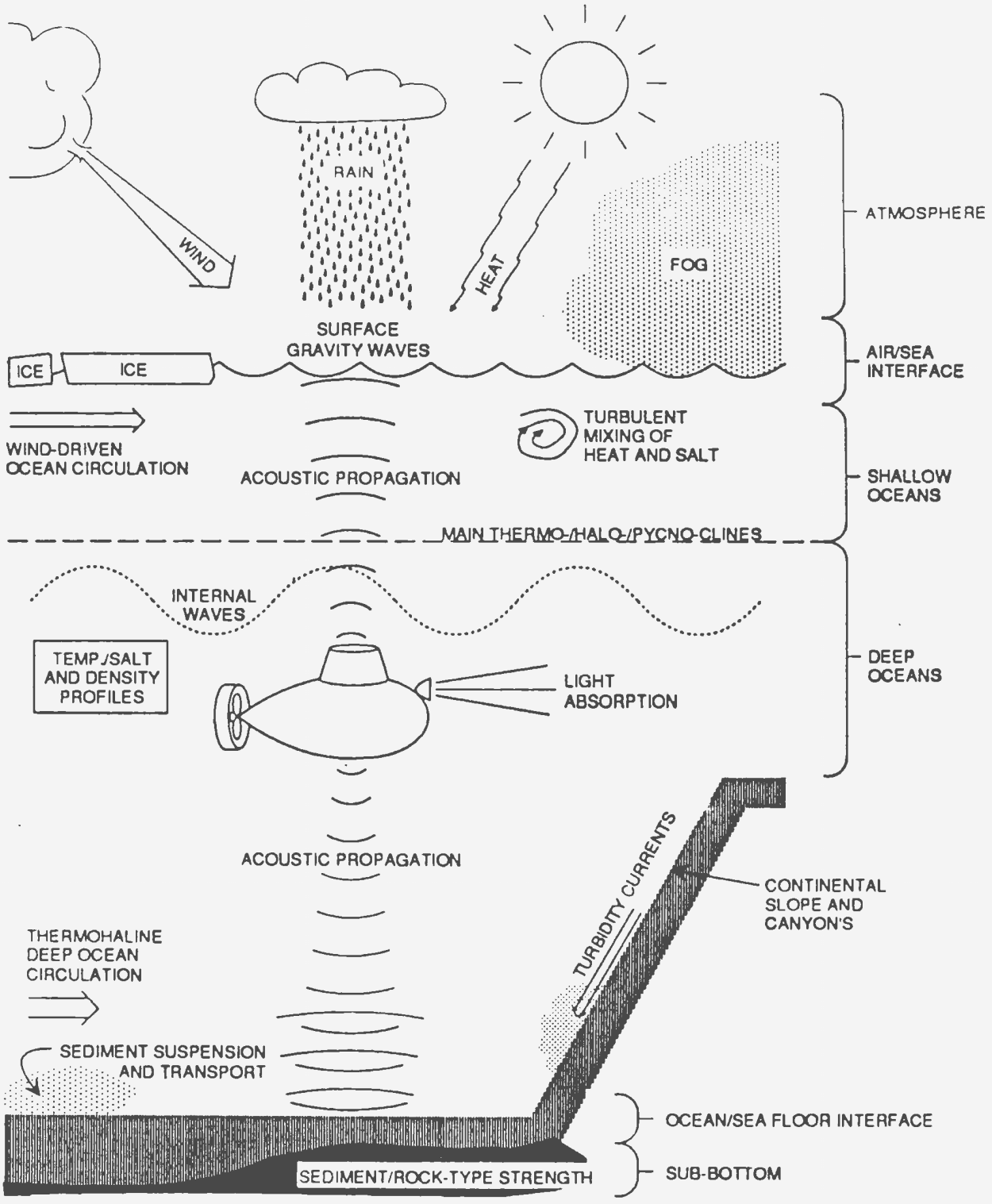

Figure 2.1 Factors Affecting Submersible Design (Irish and Brown, 1990)

In the water column, environmental factors influencing submersible design include: surface gravity waves; internal gravity waves; wave generation drag; and temperature, salinity, pressure and density of seawater. All these factors should be considered for vehicles operating near the ocean surface and in areas of maximum density gradients, where internal gravity waves are significant. Generally, ROVs operate well below the surface where most of these factors are not predominant. For example, wave drag associated with the energy of wind generated waves is negligible at a depth of 300 metres for waves with a period of 20 seconds (Irish and Brown, 1990).

Deep water currents, however, often do affect ROV operation. A number of ROVs that are regularly deployed are incapable of operating in a moderate cross current (Baker and Sayer, 1990). ROVs also have difficulties operating in the wake of a nearby structure or operating a manipulator arm in the wake of the vehicle body. Many ROVs have open frame bodies that generate eddies which add turbulence. In the ocean, the levels of turbulence are relatively high from an operational point of view and can vary for the reasons just mentioned. High levels of turbulence create drag forces and moments on a ROV which impede vehicle performance and make it difficult to control.

Drag forces are dependent on the shape and size of the body, characteristics of the fluid flow and the drag coefficient. Drag coefficients are determined

empirically for different Reynolds numbers. The Reynolds number is dependent on the size of the body and the characteristics of the fluid flow. The pattern of vortex shedding is also a function of the Reynolds number. Asymmetric vortices can lead to oscillating transverse forces and transverse body motions which can cause vehicle instability.

The main problem in dealing with ROV design and control is that it is impossible to treat the hydrodynamics of a ROV undergoing arbitrary unsteady motions analytically. Even the treatment of steady motions is difficult, since it relies heavily on experimental data and hydrodynamic coefficients for ROVs are known only for specific configurations. Most studies of ROV motion assume quasi-steady flow, which means that flows are set up quickly and resemble steady flows. This is a reasonable assumption for slow moving bodies.

The main concerns for underwater control are basically the same as any other environment, but because of the number of uncertainties associated with the ocean environment robustness is of key importance. The primary concerns for underwater control are:

- stability
- computational efficiency
- accuracy
- robustness

The system must be stable to be of any practical value. System stability implies that, given some input, the system will not oscillate violently or drive itself to some limiting value, but instead attain some useful response. The computational efficiency refers to the time required to perform the necessary calculations within the control loop. A low computational efficiency would slow the control loop significantly and thus degrade the performance. Accuracy is the ability to reduce the difference between the actual and the desired position or state of the system to a tolerable value and is necessary for positioning in underwater tasks. The robustness of the system refers to the ability to perform a task in the presence of disturbances. It is of particular importance for underwater tasks since various disturbances may be encountered. The control strategies adapted for underwater applications must be evaluated in light of these main control concerns (Muggeridge and Hinchey, 1991).

2.2 Previous Work

The growth of the offshore oil and gas industry has prompted the use and development of ROVs to perform various underwater tasks. ROVs are application driven and have been widely used for tasks such as: high resolution pipeline survey; deep water drilling and production support; and structural integrity support. As the future need for offshore oil and gas increases, so will the trend towards increased capabilities and participation of ROVs.

Over the past 20 years, the trend in undersea vehicles has progressed from manned submersibles to remotely operated vehicles to autonomous underwater vehicles. The progression has been toward minimizing the need of man's physical presence and intervention underwater. The objective of this trend is to develop a self-contained, preprogrammed, decision making AUV independent of external control (Busby and Vadus, 1990). Research in the area of autonomous underwater vehicles is being conducted by the military, universities and industry in different countries around the world.

Development to increase the autonomy of underwater vehicles is not easy, since current technologies are limited and current conventional technologies cannot be directly adapted to the unstructured, high density seawater environment (Yuh, 1990). The dynamic nonlinearities of the undersea environment require robustness in control for underwater robot tasks. Work is on-going to gain robustness through the incorporation of adaptive control strategies such as: sliding mode, neural networks, and fuzzy logic. The term adaptive control may be applied to a strategy that is capable of learning on-line and modifying its own behaviour with the goal of improving system performance (Farbrother and Stacey, 1993).

The main developments in the area of underwater robot control are discussed in this section and elaboration is given for the most significant work. Detailed

descriptions of the main control strategies considered for underwater robot control are given in chapter three.

The sliding mode control strategy, in simple terms, is a combination of computed load control with a switching type of error-driven compensation which is used to direct the system towards the command state. Sliding mode control has received considerable attention in the Soviet Union, where the method was applied to the control of linear systems with discontinuous control action. This control method has been extended for use in nonlinear systems with continuous control action. Cristi, Papoulias and Healey (1990) and Yoerger, Cooke and Slotine (1990) have studied sliding mode control for underwater vehicles.

Cristi, Papoulias and Healey (1990) showed the effectiveness of combining the adaptivity of a direct adaptive control algorithm and the robustness of sliding mode for control of autonomous underwater vehicles in the dive plane. The equations of motion were determined using a simplified model of a symmetrical body while considering only the dive plane. These equations were found to be coupled, nonlinear and not in the same form as the standard approach to sliding mode control used by Slotine and Sastry (1983) and Yoerger and Slotine (1985). In order to circumvent this problem, while maintaining the robust features of a sliding controller, an approximate model, linearized around nominal

operating conditions was used. The dynamic model was separated into its linear component and nonlinear state dependent disturbance. Normally, sliding mode would consist of a control input determined on the basis of a nominal model (a full nonlinear model) and a term which compensates for deviations from ideal performances due to uncertainty. Cristi, Papoulias and Healey's nominal model was based on the linearized dynamics around the operating conditions of the vehicle and changes in the nominal speed. An adaptive controller was used to compensate for the uncertainties of the linear part of the vehicle dynamics, while not affecting the nonlinear part.

Numerical simulation results from a three dimensional real-time simulation of an AUV were given, where vehicle motion was dynamically simulated from the complete set of equations of motion. Responses of the linear and nonlinear model under sliding mode control were compared and the sliding mode controller's ability to handle unmodelled nonlinearities was demonstrated. Robustness tests were performed on the controller and the vehicle's response remained stable even with wide parametric variation. Similar robustness tests were performed by applying the nominal control law (with the linearized term) to the nonlinear vehicle model under a wide variation in certain essential hydrodynamic and hydrostatic parameters. The results showed stable vehicle response and consistent performance for different parametric values. Simulations for the adaptive algorithm were also given and results showed

tracking of the depth signal for different operating conditions.

Another paper by Yoerger, Cooke and Slotine (1990) showed that sliding mode techniques could be used to compensate for the influence of thruster dynamics on the behaviour of an underwater vehicle. Thruster dynamics were investigated because they were believed to dominate vehicle dynamics. A nonlinear parametric model of a torque controlled thruster was developed and experimentally tested. A quasi-linear analysis using describing functions showed that the dynamics of the thrusters produced a strong bandwidth constraint and a limit cycle, both of which have been commonly seen in practice. In order to compensate for the thruster dynamics, three compensation schemes were tested. The first method of compensation tested was a linear lead model. This model was easy to implement and was found to be better than the uncompensated system, but it did not perform uniformly over the entire operating range of the thruster. The second compensation scheme tried to cancel the nonlinear filtering effect of the thruster. It was found to be effective over the entire operating range of the thruster, as long as an accurate thruster model was used. The third method of compensation, an adaptive sliding controller, was found to out-perform the uncompensated system as well as the other two compensation techniques. The adaptive sliding controller was found to be effective over the entire thruster operating range and was able to compensate for uncertainties or thruster degradation.

The sliding controller for the thruster model was developed according to the scheme presented by Slotine (1984) and Slotine and Coetsee (1986). A boundary layer was used to avoid the chattering effect produced around the sliding line by the discontinuous (nonlinear) control law. The sliding controller design was made adaptive to parameter uncertainty by coupling it to an on-line parameter estimator. Active adaptation only occurred when the system was outside the boundary layer and was proportional to the algebraic distance to the boundary layer. Thus, adaptation only occurred when the actual dynamic uncertainty exceeded the current estimate and adaptation stopped once inside the boundary layer. Triggers of the adaptation mechanism included: thruster fouling; motor or propeller degradation; or complex flow effects.

The sliding mode controller and the other methods of compensation were tested through a hybrid simulation, which combined an instrumented thruster with a real-time mathematical model. The nonlinear adaptive controller was shown to preserve system performance in the presence of uncertainty, through the ability of the controller to adapt on-line to changes in model parameters.

Preliminary testing and simulation of sliding mode control strategy showed some interesting results, however, verification of this strategy's ability to perform in actual vehicle operating conditions is required. The sliding mode strategy, even with the adaptive controller, requires good estimates of the parameters which

are not easy to obtain for subsea vehicle operation.

Neural networks are a powerful technology which is making its way from the laboratory to practical applications. Neural networks, as a control strategy, may be described in simple terms as similar to a polynomial input/output fit, where weights in the network are analogous to coefficients in a polynomial fit (Hinchey, 1994). Research in neural networks began with early research into intelligent machines in the 1950's and has been inspired by on-going studies of the brain and nervous system. Neural networks are capable of processing information in a dynamic, self-organizing manner which is similar to the way that humans process information. A neural network is made up of simple, highly interconnected processing elements which respond in parallel to inputs presented to it. Knowledge within the neural network is not stored in a certain location, but in the way the processing elements are connected and in the importance (weighting value) of each input to the processing elements (Caudill, 1987). The networks have the capability to 'learn' given a large number of examples. Derivation or programming of inverse transformation equations is not necessary and natural and unforseen changes will automatically be incorporated into the network (Josin, 1988). Neural networks have been found to be particularly useful in situations which conventional methods have found unmanageable such as: continuous speech recognition and synthesis, pattern recognition, vision, and autonomous vehicles (Caudill, 1987).

A hierarchical neural network model for robotic applications has been proposed by Kawato, Uno, Isobe and Suzuki (1988) for control of voluntary movements with application to robotics. Physiological information of the human central nervous system was used as the basis of the neural network model. This method was successfully applied by Miyamoto, Kawato, Setoyama and Suzuki (1988) to control an industrial robotic manipulator.

Yuh (1990) showed that it was feasible to use neural networks to control an underwater robot vehicle in the presence of unpredictable changes in the dynamics of the vehicle and its environment. It is one of the few published cases where neural networks have been applied to underwater vehicles. Yuh developed a new approach to neural networks by using an on-line direct-learning scheme. He reasoned that since the dynamic behaviour of underwater vehicles is nonlinear and time varying, the indirect off-line approach used by most researchers was not appropriate.

Yuh's proposed method used a multilayered neural network and an error back-propagation scheme for training the neural network. Normally, the error back-propagation scheme requires the value of the control signal which provides the desired performance of the controlled system. Since this value is not known in advance, direct training of the network using this scheme is not possible. However, Yuh determined that if an estimate of the error signal was obtained,

error back-propagation could be used for direct controller training. The estimate of the error signal was found to be solely dependent on the upper bound of the inertia matrix (Yuh, Lakshmi, Lee and Oh, 1990).

Computer simulation was performed for the plane motion of a vehicle modelled after the Dolphin 3K vehicle, presented by Nomoto and Hattori (1986), to investigate the feasibility of on-line neural network control for the vehicle. A three-layer network was used and the simulation showed, for the examples given, that the on-line learning trajectory overlapped the desired trajectory. If training was stopped, the simulation showed that the vehicle no longer tracked the desired trajectory and its behaviour was unpredictable. Limit cycle-type oscillations were found to occur when the magnitude of the ocean current velocity was suddenly changed to the same velocity as the maximum desired vehicle velocity. The results of the simulation showed that the control system adjusted its weights to provide a proper control signal in order to maintain the desired velocity.

Yuh also claimed that this technique required fewer learning cycles than off-line learning, since his approach required the desired control signal to be learned (the objective of the control system). This method differed from previous approaches which required the model of the system dynamics to be learned. Yuh's strategy only required the upper bound of the inertia model rather than

the explicit vehicle dynamic model. Vehicle dynamics cannot be completely defined, even with expensive hydrodynamic testing of the vehicle, because of unsteady fluid motion effects and variation of model parameters with vehicle configuration and environment. Yuh's idea of trying to bypass the problem of determining a complete dynamic model is reasonable, since, as stated, a good dynamic model presently does not exist and may never exist. The test of this approach will be to see if this method, when implemented on a real vehicle, will be able to produce appropriate control signals quickly enough (because learning takes time) to maintain vehicle performance in the face of uncertainties and abrupt changes in surroundings.

In Japan, at the Institute of Industrial Science, University of Tokyo, another group of scientists are developing a motion control system for autonomous underwater vehicles using neural networks (Fujii and Ura, 1990 and Ura, 1990). A series of autonomous underwater vehicles have been developed through the 'PTEROA project' which was formed in 1986 to develop cruising-type robots to survey the deep-sea bed. The vehicles include: PTEROA60 (a small model with body length of 0.60 m); PTEROA150 (a pilot model with body length of 1.5 m); and PTEROA250 (a prototype vehicle with body length of 2.5 m). Of the three vehicles, the PTEROA60 was the only vehicle to be tested with the project's Self-Organizing Neural-net Controller System (SONCS).

The general architecture of SONCS consists of a controller network, a forward-model controller network, and an evaluation mechanism. The controller network was connected to both the vehicle and the forward-model network and the controller network operated them simultaneously. State variables of the vehicle were used as inputs for the controller network and its outputs were control inputs. The network and the error back-propagation scheme used were based on a connectionist model presented by Rumelhart, Hinton and Williams (1986). The forward-model network was introduced to allow the dynamics of the vehicle to be considered for adaptive adjustment of the controller. The inputs of the forward model network were state variables of the vehicle at a previous time step and the corresponding control inputs. Its outputs were state variables at each time step. The output of the vehicle was compared to the desired output through the evaluation mechanism and weights were adjusted in the controller network in order to match desired and actual vehicle motion.

The organizing process of the SONCS architecture consisted of two phases, one for initialization and the other for control during vehicle task operation. Fuzzy logic was used to form a simple fuzzy premature controller, which was used to keep the vehicle in a stable state with limited knowledge of vehicle dynamics while an initial set of weights for the controller was obtained. Initially, the premature fuzzy controller controlled the vehicle and, on the basis of motion and control data, the controller network adjusted its weights so it had the same

ability as the premature controller. The forward-model network was also initialized through learning from the motion controlled by the premature fuzzy controller. Once the controller network and the forward-model network were initialized, the vehicle's motion was controlled through the controller network. The resultant vehicle motion was compared to the output of the forward-model network. The difference was used to update the weights in the controller network through back-propagation in an attempt to achieve the same vehicle motion as the target motion of the vehicle.

SONCS was demonstrated with the use of the model vehicle PTEROA60, which was linked to a computer on the surface through an umbilical cord in a flume tank. The model was found to follow the mission of constant depth swimming after four adaptations once the learning to initialize the controllers was complete. The limited data given in the papers showed promising results, however, it would be interesting to see tank test results for additional scenarios.

Fuzzy logic is being widely used in Japan for all sort of products from auto-focusing cameras to industrial assembly controllers. Companies in other parts of the world, however, are only beginning to realize the versatility of this control strategy (Self, 1990). Fuzzy logic, as a control strategy, can be simply described as a set of linguistic IF/THEN fits to rules-of-thumb of a human

operator. A practical example of fuzzy-logic control is Japan's Sendi subway system for which Hitachi granted contracts in 1991. Fuzzy-logic control improved stop position by a factor of three, reduced power setting by a factor of two and total power use was reduced by ten percent (Togai, 1991).

Fuzzy logic (Cox, 1992 and Lee, 1990) has evolved from the concept of a 'fuzzy set' developed by Zadeh (1965) of the University of California at Berkeley. The value of fuzzy logic lies in its ability to simulate human thinking by incorporating imprecision which is inherent in all physical systems. Fuzzy logic uses linguistic terms such as 'large', 'medium' and 'small' to describe the values of the variables. Linguistic concepts are treated mathematically and human 'experts' are used to provide a set of linguistic IF/THEN rules. The IF/THEN structure is similar to expert systems, however, unlike expert systems, fuzzy logic is easier on its human 'experts' because they are not required to determine outputs for every possible set of inputs. Typically, a simple graphical procedure is used to determine outputs in fuzzy-logic control. In many papers this is difficult to ascertain due to overuse of set theory and its jargon (Jain 1980). However, fuzzy logic, like expert systems, generates poor predictions for inputs outside its data range.

As mentioned earlier, Fujii and Ura (1990) used an elementary version of fuzzy logic to control one of a series of small submersibles being developed in Japan.

Fuzzy logic has also been used for error-driven control. In fact, the earliest practical application of fuzzy logic was of this type (Mamdani and Sembi, 1980).

A layered type of control called subsumption has been developed by Brooks (1991) and his colleagues at Massachusetts Institute of Technology for mobile robots. Brooks has a different approach to intelligence than most researchers in the field of artificial intelligence. He believes human intelligence is too complex and too little understood to be correctly broken down into the correct subpieces and to know the appropriate interfaces between them. Instead, Brooks suggests it is better to start with a number of levels (each of relatively simple intelligence) and to incrementally build up the capabilities of intelligent systems (which Brooks refers to as Creatures). Each intelligent system is made up of independent, parallel activity producers (layers) which all interface directly to the world through perception and action.

Using subsumption architecture, Brooks and his colleagues have built a successful series of mobile robots which operate independently in an office environment. The subsumption architecture for these robots is divided into three layers: avoid, wander and explore. Each layer is built on top of existing layers and lower layers never rely on the existence of higher layers. These robots operate autonomously in a complex dynamic environment and are claimed to

operate at a level close to simple insect level intelligence. These ideas merit attention and it will be interesting to follow the development of Brooks' Creatures.

Subsumption is being considered by International Submarine Engineering Ltd. for control of its submersibles (Zheng, Jackson and Kao, 1990). Layered strategies have been used by Yoerger (1990); Zheng, Jackson and Kao (1990); and Hall and Adams (1992) to make small submersibles operate autonomously in the unstructured subsea environment.

Previous work in underwater robot control is limited. Research mainly includes the use of oversimplified models tested mostly with numerical simulations. Few model tank tests have been used to demonstrate robust control strategies. Realistic tank testing and testing on actual vehicles in their normal working environment is required. The advanced control strategies are poorly described in the literature and it seems they are not fully understood by many researchers, even by some of those who have attempted to apply the strategies themselves. Thus, chapter three attempts to deal with this problem by investigating how each strategy really works in order to ascertain its suitability for underwater robot control.

3 CONTROL STRATEGIES

Strategies for robotic control can be divided into two main categories: classical and supervisory control, each of which can further be divided into a number of different control strategies. These strategies are described in the following sections in a fundamental manner using simple terms with limited use of the jargon found in most of the literature.

A simple example of depth control of a small subsea robot is used to aid in strategy descriptions. Each strategy will be summarized in terms of its advantages and disadvantages, especially with respect to robustness and computational efficiency.

3.1 Classical Control Strategies

The four principal classical control strategies are:

- combination of proportional, integral and derivative
- switching
- computed load
- sliding mode

These control strategies are normally referred to as classical since they have been used for robotic applications for many years. The first two strategies are

error-driven, while the remaining strategies are based on the governing equations for the system. Each of these classical strategies is described in the following sections. More information pertaining to the first three strategies may be found in numerous text books on control (for instance, Ogata, 1990). Details of sliding mode may be found in *Robot Analysis and Control* by Asada and Slotine, 1986.

Newer control strategies such as neural networks, expert systems and fuzzy logic may be used for classical control problems, however, since they may also be used for supervisory control they are described in the supervisory control section to avoid redundancy.

3.1.1 Proportional, Integral and Derivative

The proportional, integral and derivative control strategy, often referred to as the PID control strategy, incorporates proportional, integral, and derivative controllers in a conventional feedback loop. This type of control is considered to be pure error-driven or closed-loop control since drive signals are generated based on the state error, the difference between what should be happening versus what is actually happening. A block diagram of a typical feedback control system is shown in Figure 3.1. The desired state or position is referred to as the command signal. The response of the system is multiplied by

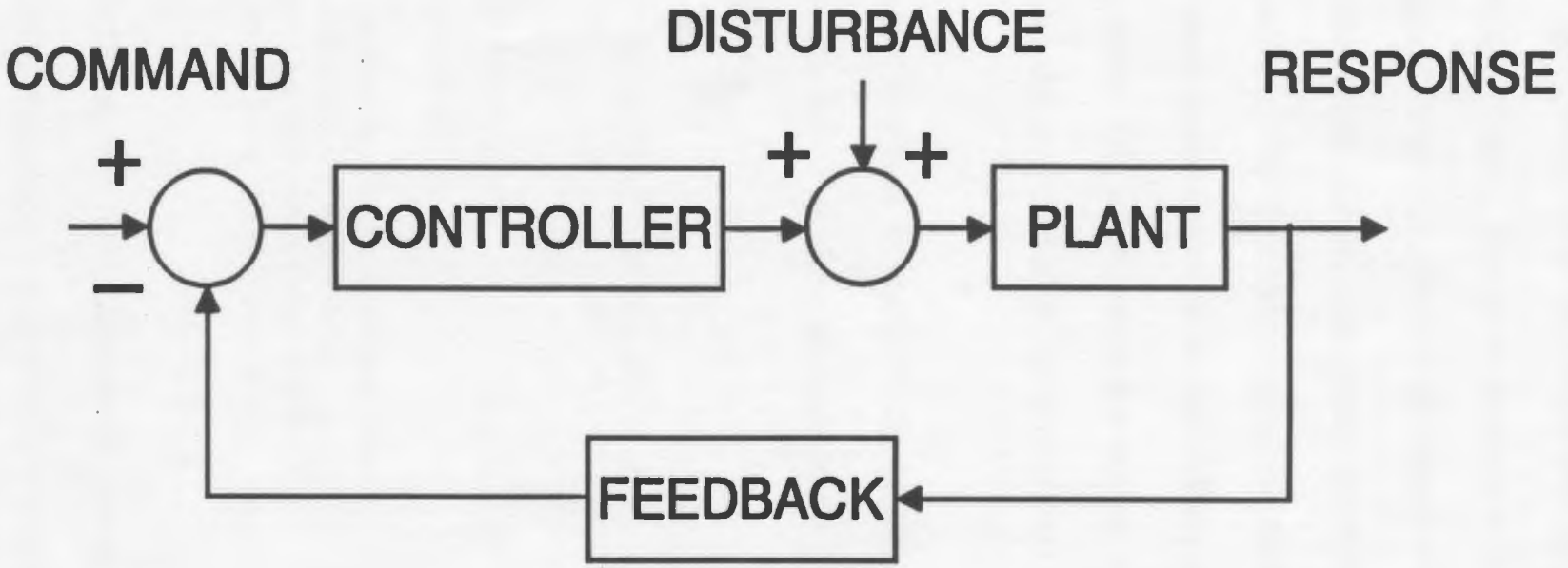

Figure 3.1 Block Diagram of Typical Feedback Control System

feedback elements and returned to the beginning of the loop, where it is compared to a command signal. The difference between the command signal and the returned signal is then passed through the controller. In the case of PID control, the controller would consist of a combination of proportional, integral and derivative controllers. The disturbance is added to the loop and passed on to the plant. The plant is the machine or tool which is to be controlled, for instance a subsea robot. The response is the actual state or position of the system (for instance, the actual position of the robot).

For example, consider the task of dynamically positioning the small subsea robot shown in Figure 3.2. For slow up and down motions, the governing equation is of the form:

$$M \frac{d^2O}{dt^2} + C \frac{dO}{dt} \left|\frac{dO}{dt}\right| = F + D \qquad (3.1)$$

where:

O = actual robot position
t = time
M = inherent and added water mass of the robot
C = term which accounts for wake drag
F = force generated by the propulsion system
D = disturbance force from the surroundings

Generally, M, C and D are not known exactly. Pure error-driven control lets the force generated by the propulsion system, F, be a function of the error, E. The error is equal to the difference between the command position of the robot and

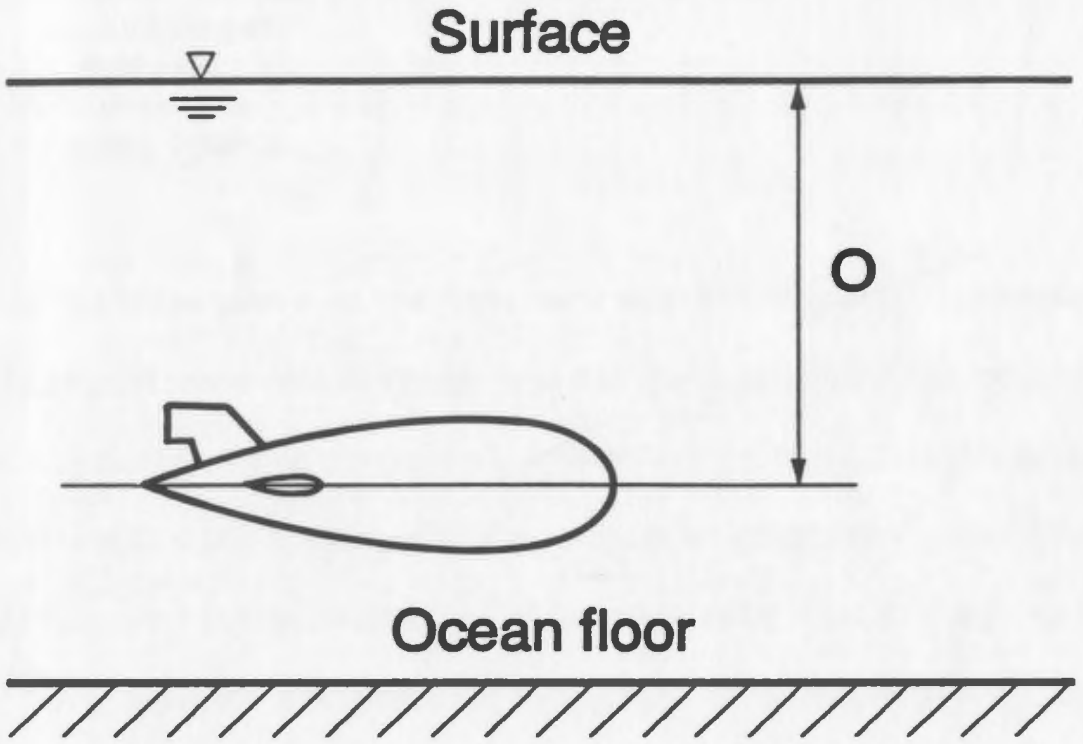

Figure 3.2 Vertical Positioning of Subsea Robot

the actual position. For example, in a digital control loop, the lowest level PID scheme lets F be

$$F = K_P E + K_I \Sigma E \Delta t + K_D \frac{\Delta E}{\Delta t} \qquad (3.2)$$

where:

F = force generated by the propulsion system
E = difference between desired and actual position
K_P = proportional gain
K_I = integral gain
K_D = derivative gain
Δt = sampling interval

Each of the three terms on the right hand side of Equation 3.2 represent the contribution of proportional, integral and derivative control action, respectively. A proportional controller is essentially an amplifier with an adjustable gain, since corrective action is proportional to the error. In an integral controller, the value of the controller output is changed at a rate proportional to the error signal. Thus, the correction is proportional to the time integral of the error, which is approximated by the term $\Sigma E \Delta t$ for a small time interval, Δt. For derivative control action, sometimes called rate control, the magnitude of the controller output is proportional to the rate of change of the error signal. A correction is made which is proportional to the time derivative of the error, which is approximated by the change in the error over a small time interval, Δt.

Proportional, integral and derivative controllers each have their own advantages

and disadvantages. Proportional controllers provide good stability characteristics but deal poorly with system disturbances. Integral controllers provide good disturbance rejection because they tend to eliminate any steady-state system error. A problem with integral control is that it tends to overshoot, producing an oscillatory response which can lead to system instability. Derivative controllers are useful because they respond to the rate of change of the error. They are often said to be able to 'anticipate' the error since they can produce significant corrective actions before the error becomes too large. Unfortunately, derivative controllers will not respond to steady-state error and, therefore, must be used in combination with other control actions.

Combining proportional, integral and derivative control strategies allows the advantages of each type of strategy to be used. A tuned mix of the strategies is generally used in practice and, as a rule-of-thumb, the sampling interval should be at least 10 times smaller than the time constant of the dominant motion of the subsea robot in order for the loop to work properly.

The advantages of the PID control strategy mix for subsea robots are high computational efficiency, stability and the ability to be made adaptive if the control signal is computer generated. High computational efficiency means that time needed to complete the control loop is small, which in turn, does not create problems with analog to digital or digital to analog conversions. These

conversions are necessary to convert analog sensor inputs to digital inputs to allow computer-generated control and then to convert digital outputs to analog for command signals. Control can be made adaptive by making the proportional, integral and derivative control gains (K_P, K_I and K_D) dependent on the state of the system or system surroundings.

The disadvantage of basic PID control for subsea robots is its lack of robustness. The basic PID control strategy has difficulty dealing with the many disturbances and uncertainties of the ocean environment and thus, in most cases, is not well suited for underwater tasks. Adaptive PID, on the other hand, has good potential for such tasks.

3.1.2 Switching

The three main types of switching control strategies are:

- ideal relay
- relay with dead zone or deadband
- relay with hysteresis

These switching techniques may be used together and in combination with other control strategies. The input-output characteristic curves for an ideal relay, a relay with a dead zone and a relay with hysteresis are shown in Figure 3.3. The curve for the ideal relay shows that any positive input results in a

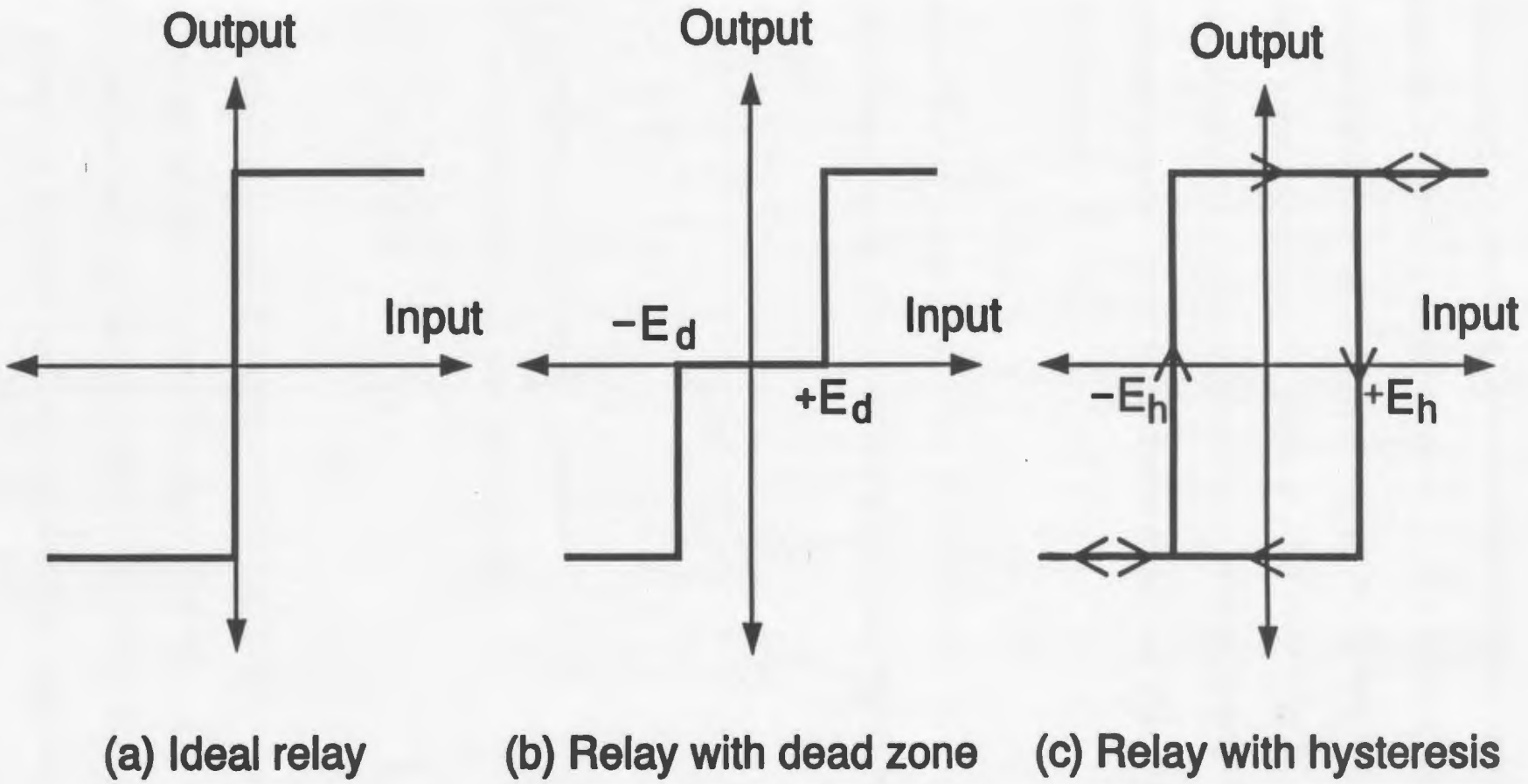

Figure 3.3 Characteristics of a Relay

constant positive output and any negative input results in a constant negative output. A dead zone refers to a range of inputs ($\pm E_d$) which will result in zero output. Hysteresis phenomenon is a lag or a delay in a change in output until a specific input value is reached. For the case of a relay with hysteresis, the input value must return to a value E_h before the contact will break. Computers can generate very complex mixes of deadband and hysteresis, which provide braking and damping.

For the case of simple depth positioning of a subsea robot, an ideal relay switching control strategy lets F be equal to the relay gain multiplied by the sign of the error:

$$F = K_R \, sign(E) \tag{3.3}$$

where:

F = force generated by the propulsion system
K_R = relay gain
E = difference between desired and actual position

sign (E) = + 1 if E > 0
sign (E) = - 1 if E < 0

Generally, this strategy causes mechanical systems to undergo finite amplitude or limit cycle oscillations about the command position. However, modifications such as the addition of deadband and hysteresis allow limit cycles to be eliminated. Switching schemes often have very good performance and are

normally easy to implement in control hardware.

3.1.3 Computed Load

Computed load is a control strategy based on the equations of motion for the system. This type of control is a form of open-loop control which computes drive loads corresponding to desired motions and control signals are sent to the drives in an attempt to generate the appropriate loads.

For the simple case of depth positioning of a subsea robot, computed load gives the force generated by the propulsion system, F, to be

$$F = M \frac{d^2O}{dt^2} + C \frac{dO}{dt}\left|\frac{dO}{dt}\right| - D \qquad (3.4)$$

where:

F = force generated by the propulsion system
O = actual robot position
M = inherent and added water mass of the robot
C = term which accounts for wake drag
D = disturbance force from the surroundings

Unfortunately, the equation of motion parameters, M and C, and disturbance, D, are not known exactly making it difficult to obtain an accurate value for the required propulsion force, F.

Computed load is not expected to be accurate for subsea applications, since the coefficients in the equation of motion are not known exactly due to the lack of hydrodynamic data (even for a specific vehicle configuration) and the uncertainty associated with the unstructured ocean environment. Computed load control strategy is also computationally expensive, because it requires complex computations which slow the control loop down considerably. For remotely operated subsea robots, whose control signals are generated from the surface, the time delays associated with such a computationally expensive strategy would produce poor robot performance.

3.1.4 Sliding Mode

The sliding mode control strategy combines the computed load technique with a switching type of error-driven compensation. Switching helps counteract uncertainties and is said to make control more robust. It ensures that there is always some measure of control when uncertainties have known upper bounds.

Sliding mode control is based on the concept of the 'sliding condition' requiring all trajectories to converge on a time-varying sliding surface, S(t) (see Figure 3.4). The sliding surface is often referred to as the switching surface and is an idealized state trajectory. A state trajectory is a quantitative description of the condition or state of the system through a period of time. High speed switching

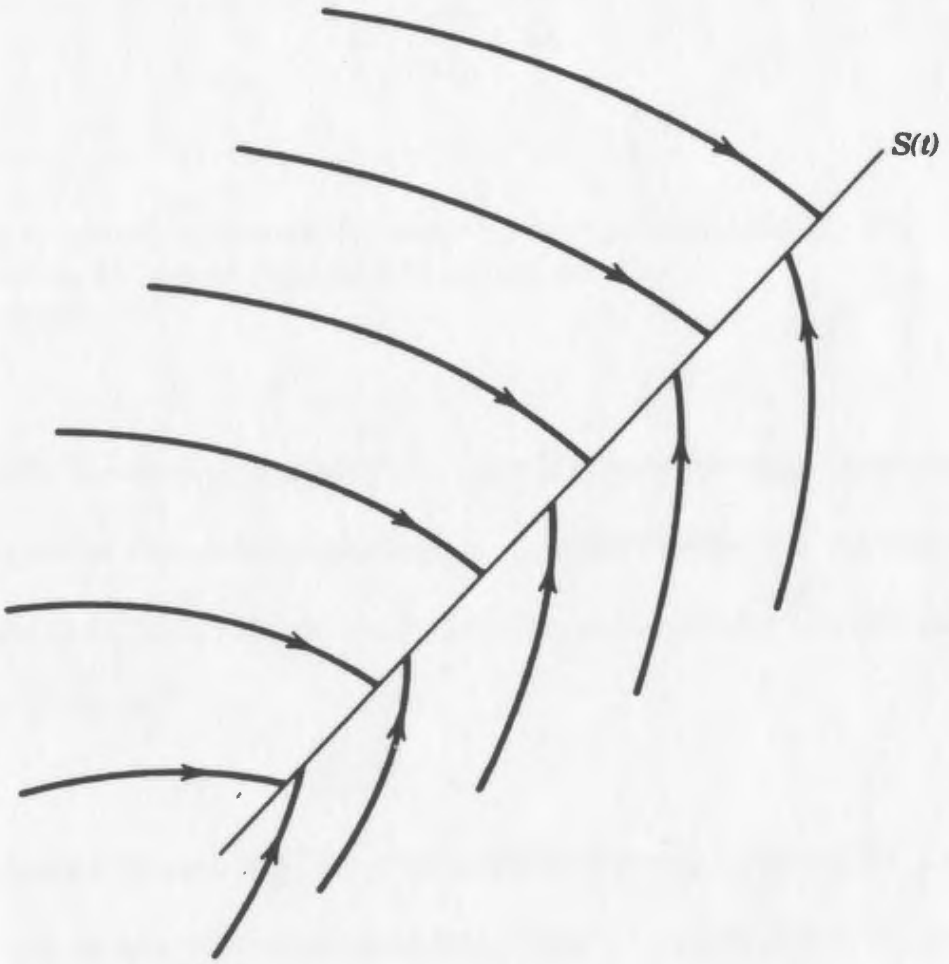

Figure 3.4 The Sliding Condition (Asada and Slotine, 1986)

feedback control is used in attempt to make the state trajectory lie along the switching surface, S = 0.

For the case of depth positioning of a subsea robot, one starts by defining, as shown in Figure 3.4, the sliding line:

$$S = \frac{dE}{dt} + \lambda E \tag{3.5}$$

where:

S = measure of the algebraic distance to the sliding surface, S(t)
E = difference between desired and actual position
λ = bandwidth

As is generally the case, the sliding equation is one order lower than the system order. The goal of this control strategy is to make S zero. If S, which drives E, can be made zero, then E must decay and the actual robot position will match the desired position.

Sliding mode control uses the Liapunov stability method, specifically Liapunov's direct method, to ensure system stability. When the control input(s) satisfy the 'sliding condition' the control algorithm is said to be a true Liapunov function. Liapunov's theory is based on the fact that for the system to remain stable the system energy must decrease with time until it comes to rest at its equilibrium state or position. Liapunov introduced a fictitious energy function, named the

Liapunov function, since there is no simple way of defining an energy term mathematically. A Liapunov function, denoted as V, is a scalar function satisfying Liapunov's stability theorems and is based on the state variables for the system. State variables are a set of variables which completely define the system at any instant in time. The time derivative of the Liapunov function establishes the stability of the system: If the time derivative, dV/dt, is negative the system is stable. This method determines system stability without solving state equations, which is quite advantageous for nonlinear and time-varying systems that have complex state equations.

For the case of simple depth positioning of a subsea robot, the Liapunov function, V, and its time derivative may be defined as

$$V = \frac{M}{2} S^2$$

$$\frac{dV}{dt} = S\ M\ \frac{dS}{dt} \qquad (3.6)$$

The time derivative of the Liapunov function must be negative to ensure system stability. This condition which constrains trajectories to be directed toward the

sliding line is called the sliding condition:

$$\frac{dV}{dt} \leq \gamma \ |S| \tag{3.7}$$

where:

γ = negative constant

In order to determine the value for dV/dt which will ensure system stability, S and dS/dt must be defined in terms of the state variables (F, M, C and D) and substituted into Equation 3.6.

Substituting the tracking error, which is normally defined as the desired position of the robot minus the actual position (E = I - O), into the sliding equation (Equation 3.5) gives

$$S = \frac{dI}{dt} - \frac{dO}{dt} + \lambda I - \lambda O \tag{3.8}$$

Its time derivative is

$$\frac{dS}{dt} = \frac{d^2I}{dt^2} - \frac{d^2O}{dt^2} + \lambda\frac{dI}{dt} - \lambda\frac{dO}{dt} \tag{3.9}$$

where:

I = desired robot position
O = actual robot position

Rearranging the equation of motion (Equation 3.1) gives

$$\frac{d^2O}{dt^2} = \frac{F}{M} + \frac{D}{M} - \frac{C}{M}\frac{dO}{dt}\left|\frac{dO}{dt}\right| \tag{3.10}$$

Substitution of Equation 3.10 into Equation 3.9 gives

$$\frac{dS}{dt} = \frac{C}{M}\frac{dO}{dt}\left|\frac{dO}{dt}\right| - \frac{F}{M} - \frac{D}{M} + \frac{d^2I}{dt^2} + \lambda\frac{dI}{dt} - \lambda\frac{dO}{dt} \tag{3.11}$$

Equation 3.11 gives the value of dS/dt in terms of the state variables, but unfortunately, the parameters M and C and the disturbance, D, are unknown. Let M°, C° and D° be the best estimates of uncertain parameters M and C and disturbance, D. If these values for M, C and D were exact, then the force F° that would keep S fixed is

$$F^o = C^o\frac{dO}{dt}\left|\frac{dO}{dt}\right| - D^o + M^o\frac{d^2I}{dt^2} + M^o\,\lambda\,\frac{dI}{dt} - M^o\,\lambda\,\frac{dO}{dt} \tag{3.12}$$

In order to satisfy the sliding condition despite uncertainty, a discontinuous control term is added to the continuous control law. The lowest level sliding mode control strategy uses ideal relay compensation and lets

$$F = F^o + K_R\,sign(S) \tag{3.13}$$

where:

K_R = relay gain

sign (S) = + 1 if S > 0
sign (S) = - 1 if S < 0

Through substitution of Equation 3.12 into Equation 3.13 and substitution of the resultant equation for F into Equation 3.11, the dS/dt equation becomes

$$\frac{dS}{dt} = \frac{(C - C^o)}{M} \frac{dO}{dt}\left|\frac{dO}{dt}\right| - \frac{(D - D^o)}{M} + \left(1 - \frac{M^o}{M}\right)\frac{d^2I}{dt^2}$$

$$+ \lambda\left(1 - \frac{M^o}{M}\right)\frac{dI}{dt} - \lambda\left(1 - \frac{M^o}{M}\right)\frac{dO}{dt} - \frac{K_R}{M}\,sign(S) \qquad (3.14)$$

Equation 3.14 with exact values for M, C and D reduces to

$$\frac{dS}{dt} = -\frac{K_R}{M}\,sign(S) \qquad (3.15)$$

In this case, S would go to zero and cause E to decay. With inexact M, C and D, a sliding mode control strategy tries to adjust the relay gain, K_R, so that the time derivative of V is always more negative than $\gamma|S|$.

Substitution of Equation 3.14 into Equation 3.6 gives a general form for dV/dt:

$$\frac{dV}{dt} = \left[(C - C^o) \frac{dO}{dt} \left| \frac{dO}{dt} \right| - (D - D^o) + (M - M^o) \frac{d^2I}{dt^2} \right.$$
$$\left. + \lambda (M - M^o) \frac{dI}{dt} - \lambda (M - M^o) \frac{dO}{dt} - K_R \, sign(S) \right] S$$

$$= [(P - P^o) - K_R \, sign(S)] \, S \qquad (3.16)$$

where:

(P - P°) = error in estimating values for M, C and D for the system

This gives for K_R

$$K_R = |P - P^o| - \gamma \qquad (3.17)$$

The value for the relay gain, K_R, must be large enough to ensure stabilization. A good estimate of |P - P°| is necessary for sliding mode control to function properly. Unfortunately, it is very difficult to estimate values for the uncertain parameters M and C and the disturbance, D, and thus obtaining a good estimate of |P - P°| is close to impossible.

Another problem with sliding mode control is the 'chattering' effect which results from the use of ideal relay compensation. Since infinitely fast switching is impossible, a limit cycle would be created about the sliding line and a subsea robot would oscillate around its desired position. Slotine (1983) proposed a

solution to this problem with the introduction of a boundary layer in the immediate vicinity of the switching surface. The boundary layer would act as a buffer zone on either side of the sliding line. The thickness of the boundary layer depends upon the degree of system uncertainty and providing there were known limits for the system uncertainty the control would remain stable. As the boundary layer thickness increases, the tracking ability of the control strategy increases but the smoothness of the control action decreases.

A sketch of a constant thickness boundary layer for the present case is shown in Figure 3.5. Inspection of the sketch shows that a bandwidth, λ, can be defined in terms of boundary layer thickness, ϕ, and width, ε:

$$\lambda = \frac{\Phi}{\varepsilon} \tag{3.18}$$

where:

λ = bandwidth
ϕ = boundary layer thickness
ε = boundary layer width

Note that when S = 0, Equation 3.5 becomes $dE/dt = -\lambda E$, which represents a straight line through the origin (with slope $-\lambda$) in an $(E, \dot{E})$ plane. The boundary layer width, ε, is basically the control precision. In order to achieve the best compromise between tracking precision and robustness to unmodelled

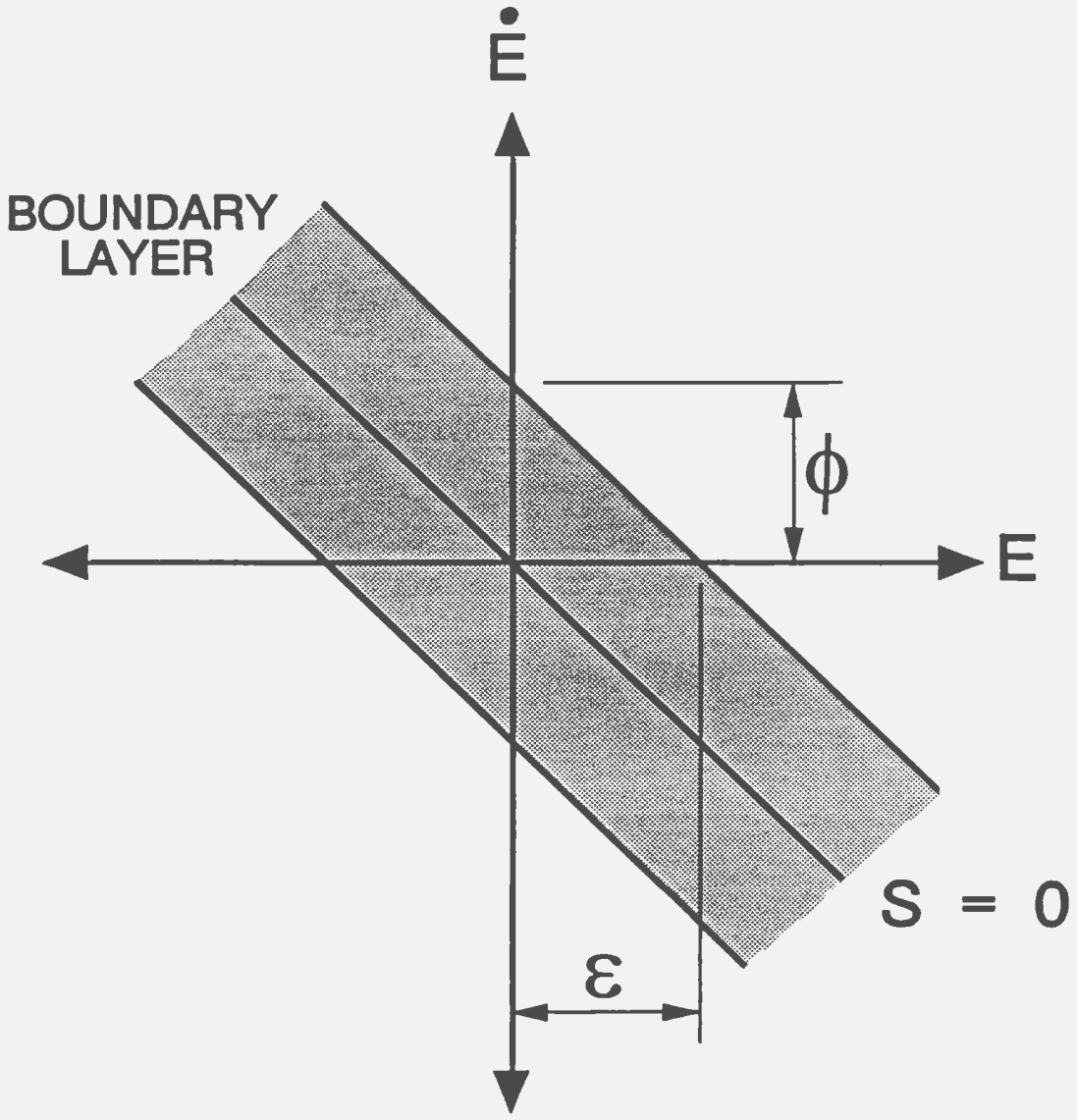

Figure 3.5 Boundary Layer Used in Sliding Mode for 1 DOF

dynamics, the boundary layer thickness, ϕ, is made to be time-varying and is monitored so as to always use the maximum control bandwidth available. Outside the boundary layer, a sliding mode control strategy tries to ensure movement towards the boundary layer. Since the boundary layer thickness, ϕ, is now allowed to vary with time, the sliding condition (Equation 3.7) must be modified:

$$\frac{dV}{dt} \leq \left(M\frac{d\phi}{dt} + \gamma\right)|S|, \qquad for\ |S| \geq \phi \tag{3.19}$$

The additional term M $d\phi/dt$ |S| represents how the boundary layer attraction condition is more forceful during boundary layer contraction ($d\phi/dt < 0$) and less forceful during boundary layer expansion ($d\phi/dt > 0$).

In order to satisfy the modified sliding condition (Equation 3.19), the quantity -M $d\phi/dt$ is added to the control discontinuity gain, K_R. The term K_R sign(S) from the switched control law is replaced by (K_R - M $d\phi/dt$) sat(S/ϕ). The propulsion force, F, for this case becomes

$$F = F^o + \left(K_R - M\frac{d\phi}{dt}\right) sat\left(\frac{S}{\phi}\right) \tag{3.20}$$

where:

F = force generated by the propulsion system
F^0 = propulsion force that would keep S fixed
K_R = relay gain
M = inherent and added water mass of the robot

S = measure of the algebraic distance to the sliding surface, S(t)
ϕ = boundary layer thickness

$sat(S/\phi) = sign(S/\phi)$ $\quad |S/\phi| > 1$
$sat(S/\phi) = S/\phi$ $\quad |S/\phi| \leq 1$

System trajectories within the boundary layer may be described in terms of S:

$$\frac{dS}{dt} + \left(\frac{K_R}{M} - \frac{d\phi}{dt}\right)\frac{S}{\phi} = Q \tag{3.21}$$

where Q represents forcing due to uncertainty.

Equation 3.21 resembles the original equation for the sliding line (Equation 3.5):

$$\frac{dE}{dt} + \lambda E = S \tag{3.22}$$

Letting each have the same bandwidth, λ, gives

$$\frac{\left(\frac{K_R}{M} - \frac{d\phi}{dt}\right)}{\phi} = \lambda \tag{3.23}$$

Manipulation of Equation 3.23 gives

$$\frac{d\phi}{dt} + \lambda\phi = \frac{K_R}{M} \tag{3.24}$$

Equation 3.24 gives an equation for the boundary layer in terms of the basic ideal relay gain, K_R.

For a constant thickness boundary layer (ϕ = constant), substitution of Equation 3.18 into Equation 3.24 gives

$$\lambda^2 \varepsilon = \frac{K_R}{M} \tag{3.25}$$

The precision of the control strategy is based on the relay gain and the bandwidth. A large gain value or a small bandwidth value will reduce precision. The bandwidth is like a filter break frequency and cannot be set arbitrarily. It is generally preferable to have a large bandwidth to ensure the tracking ability of the control action, however it is not desirable to have a bandwidth so large that it excites unmodelled dynamics and signal sampling and reconstruction phenomena. With λ and K_R known, Equation 3.25 gives an estimate of ε. It is only an estimate, because it ignores changes in uncertainty. To obtain robust control, estimates of the uncertainty in M, C and disturbance, D, must be reasonable: such an estimate may be difficult to obtain for D. If good estimates of uncertainty are unknown, the use of sliding mode seems hard to justify. A better method may be to simply tune the following combination of computed load and error-driven compensation by trial and error:

$$F = M^{o}\frac{d^{2}I}{dt^{2}} + C^{o}\frac{dI}{dt}\left|\frac{dI}{dt}\right| - D^{o} + K_{R}\,sign(E) + K_{P}\,E + K_{I}\,\Sigma E\Delta t + K_{D}\frac{\Delta E}{\Delta t} \quad (3.26)$$

where:

M^{o} = best estimate of inherent and added water mass of the robot
C^{o} = best estimate for term which accounts for wake drag
D^{o} = best estimate of disturbance force from the surroundings
K_R = relay gain
K_P = proportional gain
K_I = integral gain
K_D = derivative gain

The main benefit of sliding mode, as a control strategy, is its robustness. It is, however, computationally expensive like computed load control and can lack accuracy due to uncertainty in the system and its surroundings. Unfortunately, for the underwater environment, good estimates of uncertainty are difficult to obtain (partly due to the lack of hydrodynamic data). Thus, sliding mode control does not appear to be the best choice for subsea robot control.

3.2 Supervisory Control Strategies

Supervisory control strategies try to mimic a human operator by making decisions or adjustments that a human operator would make for proper control of a robot. A hierarchy of layers is often formed with supervisory strategies on the top and classical strategies on the bottom. Generally, the supervisory layers choose the appropriate classical layer for the immediate task. For example, one classical layer may try to make a subsea robot follow an underwater pipeline for inspection purposes. When an obstacle is encountered, however, the supervisory layers choose another classical layer designed for obstacle avoidance. Once the obstacle is avoided, control is returned to the pipeline following layer.

Supervisory control in combination with classical control often produces a more robust control. Since robustness is of such high importance for the operation of subsea robots for underwater tasks, supervisory control may be the way of the future for subsea robotics.

The three main control strategies used for supervisory control are:

- neural networks
- expert systems
- fuzzy logic

Each of these control strategies is described in the following sections. Further information on neural networks may be found in *Neural Networks: Theoretical Foundations and Analysis* and *Artificial Neural Networks: Paradigms, Applications, and Hardware Implementations* (IEEE, 1992(a) and 1992(b), respectively). Further reading on expert systems may be found in books by Waterman (1986) and Harmon and King (1985). Details of fuzzy logic may be found in papers by Lee (1990) and Cox (1992).

These strategies may be used in a supervisory role partnered with classical control strategies, but they may also be used for classical control. Here, they are described in a supervisory role. To illustrate each of the control strategies, an example of a subsea robot operating in storm conditions will be used. In severe storms, a subsea robot would need to sink to a safe operating depth, d. This operating depth would depend on, among other things, the wave steepness, R, and wave period, T. For given values of R and T, a supervisory controller is used to choose an appropriate value of d for classical strategies to achieve.

3.2.1 Neural Networks

Neural networks try to imitate the way the human brain processes information. In the human brain, there are many simple processing elements, known as

neurons, connected together in a complex manner. In a biological network, as shown in Figure 3.6, dendrites feed information into each neuron. At each dendrite/neuron interface, a synapse controls the strength of the signal which is fed into the neuron. Each neuron sums its inputs and, providing the sum is above a certain threshold, sends out a signal along its single axon. The axon branches into dendrites which feed into other neurons. The human brain contains over 10 000 million of these neuron units which respond in parallel to inputs presented to them to form an extremely powerful computing system.

Artificial neural networks are biologically-inspired information-processing models, which try to reproduce the way in which the human brain is believed to function. The three main elements of an artificial neural network are:

- set of processing elements or neurons
- connection pattern between neurons including interconnection weights
- learning law, which updates the weights between neuron connections

Each of these elements will be discussed further in terms of a typical mapping neural network and in an example in which a neural network is used to simplify the implementation of a depth selector for a subsea robot.

A typical mapping neural network is shown in Figure 3.7. It consists of an input layer, a hidden layer or middle layer and an output layer of neurons. The number of hidden layers can be chosen by the designer, but one hidden layer is often

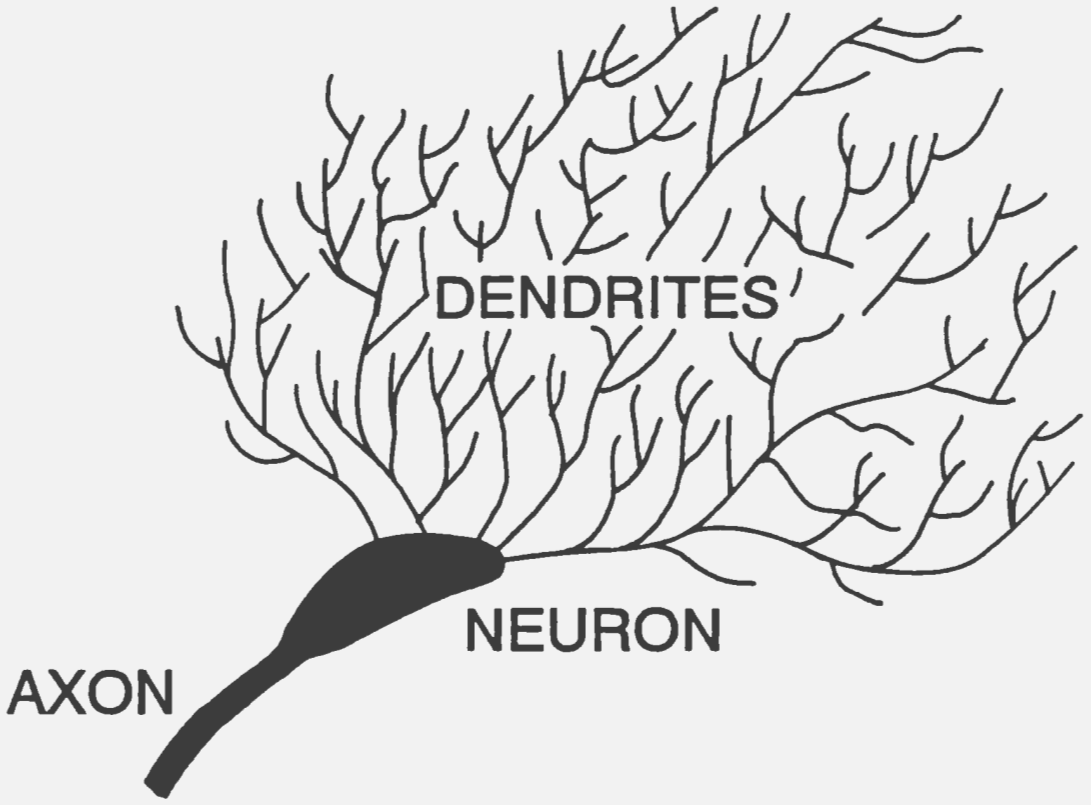

Figure 3.6 Biological Neuron

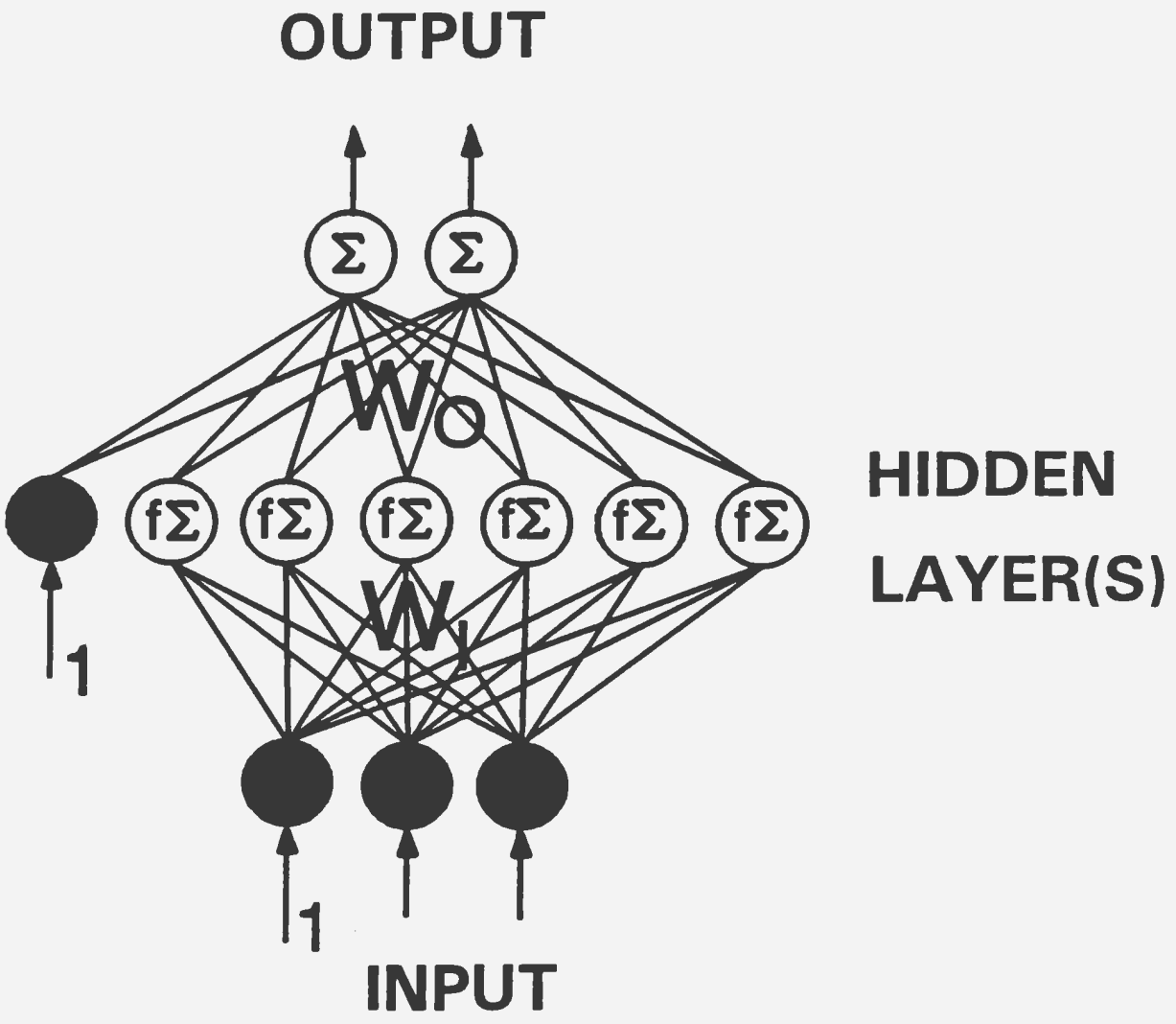

Figure 3.7 Typical Mapping Neural Network

sufficient to give a good fit. The input and hidden layers each contain one bias neuron with input unity. Every neuron in one layer is connected through a weight to every nonbias neuron in the next layer.

A set of known facts or input/output pairs is used to train the network. Once it has 'learned' known facts and can interpolate from them, it is called a 'trained network'.

The input layer receives input values from the training pair and each value is passed on to the hidden or middle layer once it has been multiplied by its interconnecting weight (W_I). The summed input into each hidden layer neuron is processed by a nonlinear squashing function as it passes through the neuron. Squashing turns out to be critical in the production of a good fit for the system, because it simulates the firing action of biological neurons. The sigmoidal or S shape function is used by most researchers as the squashing function:

$$f(i) = \frac{1}{1 + e^{-i}} \tag{3.27}$$

As the output from each middle layer neuron is fed on to each network output, it is multiplied by an interconnecting output weight (W_O). The network output(s) are compared to the expected output(s) based on the input/output pair. The network weights are continuously adjusted in an attempt to match the network

output to the output in the training pair. If, when tested, the network generates the correct output for all inputs with known outputs, the network weights have been sufficiently adjusted and the network is ready to be used for inputs not in the training set.

Information flows forward through the network from input to output. For a single input, single output case, the mapping equation for a single neuron is

$$O_N = W_{OB} + W_{OM}\ f\ (W_{IM}\ I_N + W_{IB}) \qquad (3.28)$$

where:

I_N = network input
O_N = network output
f = squashing function
W_{OB} = output weight for middle layer bias neuron
W_{OM} = output weight for middle layer neuron
W_{IM} = input weight for middle layer neuron
W_{IB} = input weight for input bias neuron

A neural network is basically an input/output map formed by patching together scaled and shifted nonlinear squashing functions. Equation 3.28 shows how in an input/output map the network weights can be used to scale and shift the squashing function both horizontally along the input axis and vertically along the output axis (refer to Figure 3.8). The result gives the network a local character similar to that of finite elements and makes very good fits possible.

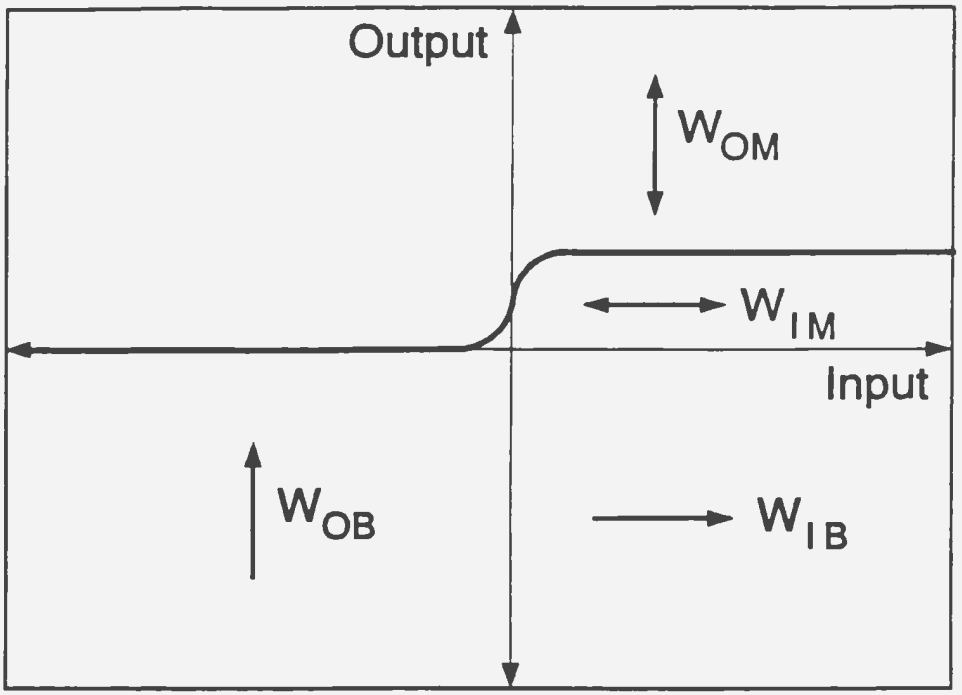

(a)

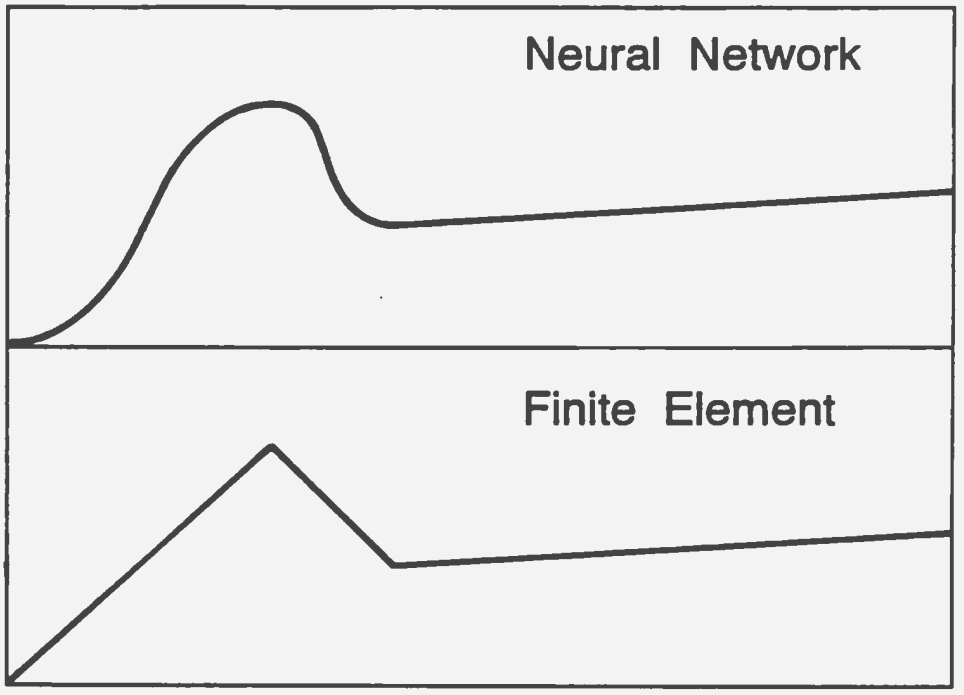

(b)

Figure 3.8 Single Input / Single Output Maps
(a) Role of each neural network weight
(b) Local character fit

For the depth selector case, the goal is to find the weights W_O and W_I which make the network depths, O_N, match the corresponding target depths, O_T. Most neural network codes use a steepest descent algorithm to adjust the weights in an iterative fashion starting from a random distribution. First, the error, E_N, between the network output and the target output is formed:

$$E_N = O_N - O_T \; ; \qquad O_N = \Sigma \; W_O \; M_N \tag{3.29}$$

where:

O_N = network output
O_T = target output
W_O = output weight
M_N = squashed output from middle layer neuron

The goal is to minimize the total squashed error, ΣE_N^2, for the training set. For each input/output training pair, the squared error is dependent on each of the outputs from the middle layer neurons (M_N) and their interconnecting output weights (W_O). For small changes in W_O and M_N, one can write

$$\Delta E_N^2 = \sum \frac{\partial E_N^2}{\partial W_O} \Delta W_O + \sum \frac{\partial E_N^2}{\partial M_N} \Delta M_N \tag{3.30}$$

Differentiation of M_N with I_N fixed gives an equation for ΔM_N in terms of W_I :

$$M_N = f\left[\Sigma\ W_I\ I_N \right]$$

$$\Delta M_N = \sum \frac{\partial M_N}{\partial W_I}\ \Delta W_I \tag{3.31}$$

Substituting ΔM_N from Equation 3.31 into Equation 3.30 gives

$$\Delta E_N^2 = \sum \frac{\partial E_N^2}{\partial W_O}\ \Delta W_O + \sum \frac{\partial E_N^2}{\partial M_N} \left(\sum \frac{\partial M_N}{\partial W_I}\ \Delta W_I \right) \tag{3.32}$$

According to the steepest descent algorithm:

$$W_O\ (NEW) = W_O\ (OLD) - \kappa\ \frac{\partial E_N^2}{\partial W_O}$$

$$W_I\ (NEW) = W_I\ (OLD) - \kappa\ \frac{\partial E_N^2}{\partial M_N}\ \frac{\partial M_N}{\partial W_I} \tag{3.33}$$

When the network is fed many times with various input/output pairs from its training set, this iteration, when stable, usually goes towards a global minimum. Graphically, it is said to back down the global E_N^2 versus weight bowl in hyperspace towards the global minimum. A small value for κ promotes iteration stability. To avoid convergence of the iteration to local minima, noise could be

periodically added to the weights. Once the network is trained, an output value may be computed by the network for any new input value which is supplied to the network. In the case of the depth selector, the network will be able to predict safe operating depths for inputs not in the training set.

Neural networks generally give robust control, however, problems in accuracy may occur if large changes to the system or surroundings occur. This method is computationally expensive in the learning mode, but not in the operating mode once the network has been trained.

In an underwater environment, where parameters are not known exactly, neural networks can provide good fits as long as the system does not vary substantially. Overall, as a control strategy for subsea robots, neural networks have high potential, especially when partnered with other control strategies.

3.2.2 Expert Systems

Expert systems incorporate judgement, experience and rules-of-thumb to solve problems which are not well defined algorithmically. Knowledge from human 'experts' are used to develop a set of rules or guidelines to follow for different scenarios of a problem. An expert system is developed for a particular situation and decisions are incorporated based on knowledge of 'experts' in that

particular field. An expert system would contain the supervisory experience of one or more human 'experts' in a set of IF/THEN rules.

A typical expert system structure is shown in Figure 3.9. Substructures include: knowledge base, context and inference engine. The knowledge base contains a set of IF/THEN rules, which often have a tree-like structure with outputs from one set feeding into a following set. The context starts with known information about the problem to be solved. The inference engine connects the knowledge base with the context and generates a solution to the problem; the solution is then stored in an expanded context. The simplest inference engine processes the known information through each tree path one path at a time to determine if there are any matches. When several matches occur, a priority or weighting scheme is used to choose the best path. The solution to the problem is returned to the user via the user interface and the explanation facility allows the user to query any decision the system generates.

Currently, expert systems do not appear to be the best choice for supervisory control of subsea robots. Expert systems require 'experts' to be able to determine all the possible scenarios and thus be able to predict the output(s) for every input(s). Unfortunately, the present knowledge in the field of underwater robotics is not substantial enough to provide sufficient information for an expert system. There may be situations in which expert systems can be used for tasks

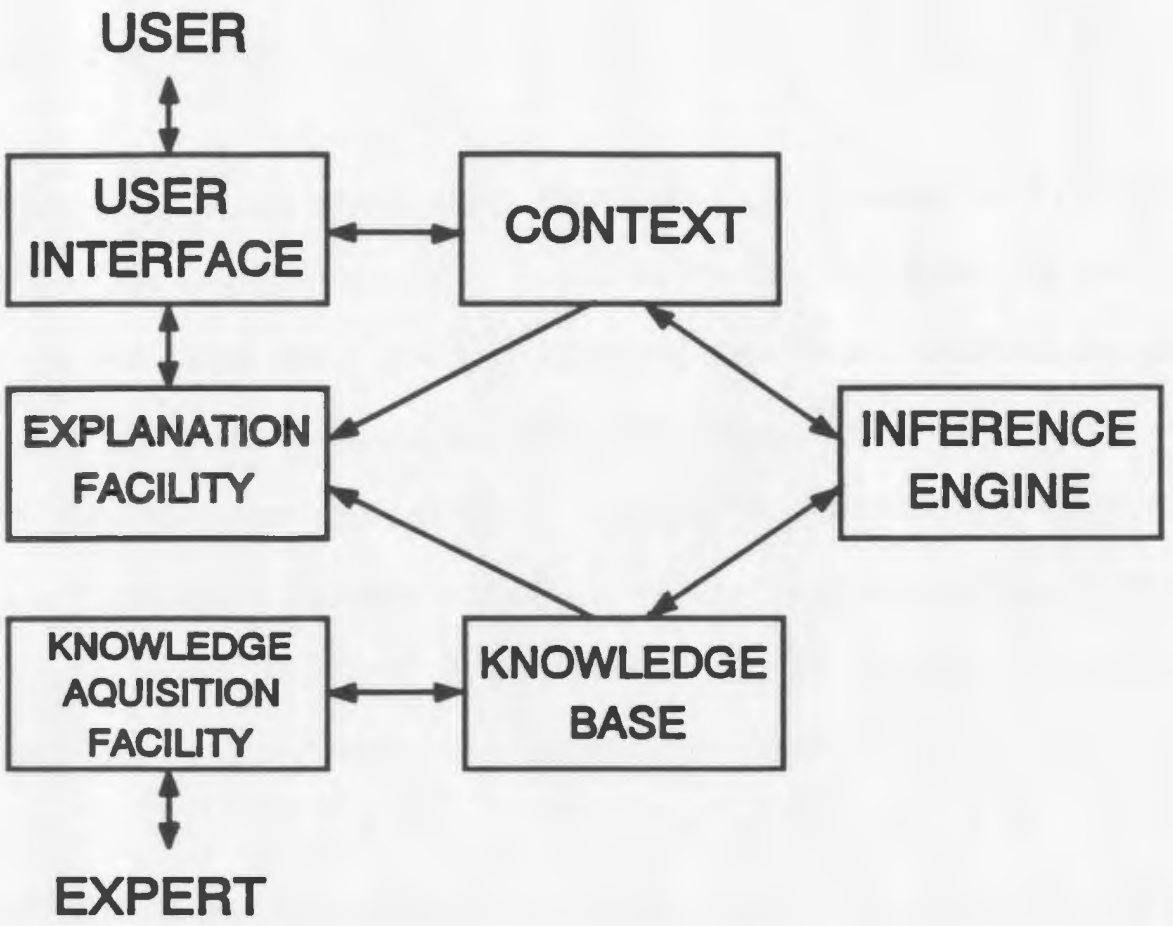

Figure 3.9 Expert System Structure

in which an operator has become skilled and has adequate experience to develop IF/THEN rules to form a knowledge base. As the oceans are explored and more information regarding the dynamics and uncertainties of the ocean is gathered, expert systems may find a place in subsea robot control.

3.2.3 Fuzzy Logic

Fuzzy logic grew out of the concept of a 'fuzzy set' developed by Lotfi A. Zadeh, of the University of California at Berkeley, in 1965. Zadeh realized that humans were able to control some systems better than machines because humans can base decisions on imprecise, nonnumerical information. He postulated that machine performance for imprecise inputs would increase if control could follow the way in which humans reason. The value of fuzzy logic is thus based on its ability to simulate human reasoning by incorporating imprecision which is inherent in all physical systems.

Zadeh introduced the concept of a linguistic variable: a variable whose values are words rather than numbers. For example, speed could be a linguistic variable with linguistic values of 'slow', 'medium' and 'fast'. 'Slow', 'medium' and 'fast' are each terms used to describe a fuzzy set. Membership functions are used to determine which fuzzy set something would belong to and the degree of membership in that set. For instance, a membership function would

determine if 50 km/hr belonged to the fuzzy set 'slow', 'medium' or 'fast' and to what degree it belonged to that particular set. The degree of membership is the confidence or certainty that a particular value belongs to a fuzzy set and is represented by a value from zero to one. A zero value would represent no membership to a particular fuzzy set and a value of one would mean it completely belongs in that fuzzy set.

Fuzzy logic uses the same IF/THEN structure as expert systems, but unlike expert systems it utilizes only a small number of rules. These rules are based on decisions a human operator would make and are often called heuristic rules or rules-of-thumb. A set of rules is developed for a control problem and when inputs are fed into each rule a fuzzy contribution to a graphical range of output is produced. A final output is determined by a process of 'defuzzification', which is a means of choosing a 'crisp' number from the graphical output. Different methods such as mean of maxima, centre of gravity or height method may be used to select an output value, but the centre of gravity method is most commonly used.

For depth selection, each fuzzy logic statement or rule would have a format like "If wave steepness, R, is large and wave period, T, is large then safe operating depth, d, should be very large". Membership functions would be used to quantify the degree to which a parameter belongs to a particular class or fuzzy

set like 'large'. The experience of one or more human 'experts' would be used to generate rules and membership functions, however, unlike expert systems, an 'expert' would not have to estimate a safe operating depth for each specific value of wave steepness and wave period.

Membership functions can have different shapes including triangles, trapezoids and smooth bell shapes. Figure 3.10 shows what typical membership functions might look like for the depth/wave case: the thick lines denote the first rule. There could be many more classes or fuzzy sets like 'large' than the few given here. Generally, neighbouring membership functions overlap, however, here to simplify the presentation, the depth functions are not allowed to overlap. Referring to Figure 3.10, the inputs are denoted by arrows (R is approximately 0.25 'large' and 0.75 'small', while T is 1.00 'large' and 0.00 'small').

For a specific pair of values for wave steepness, R, and wave period, T, manipulation of each fuzzy logic rule produces a contribution to an overall fuzzy range of depth. This manipulation for the first rule is given in Figure 3.11 and the overall range is shaded black: the contribution of each rule is identified by its number. Since each of the rules has an IF/AND/THEN structure, the minimum membership value for each rule dominates. The maximum membership function dominates for rules with an IF/OR/THEN structure. Whether the minimum or maximum membership function dominates follows the standard

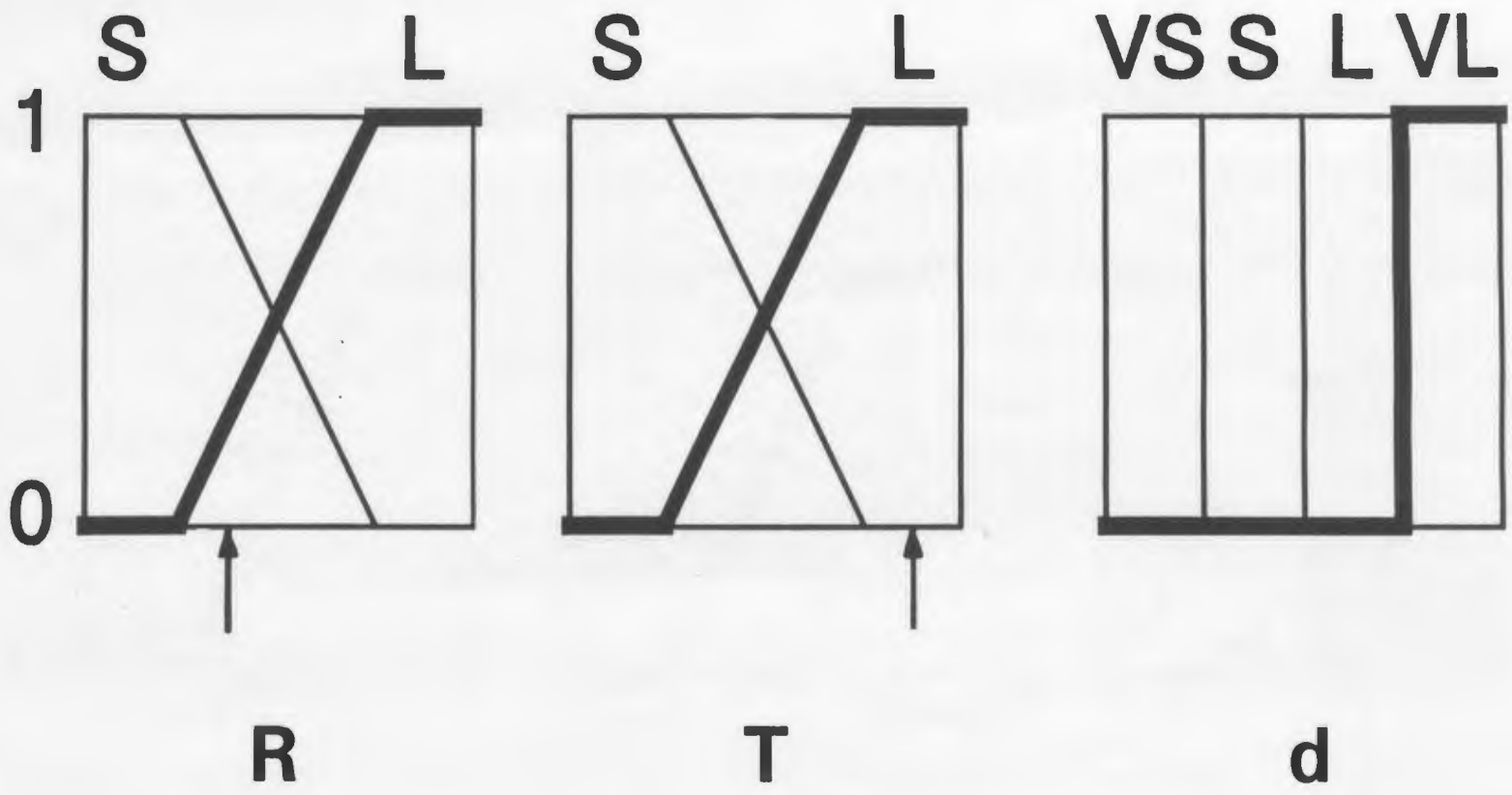

1) IF R IS LARGE AND T IS LARGE THEN d IS VERY LARGE
2) IF R IS SMALL AND T IS LARGE THEN d IS LARGE
3) IF R IS LARGE AND T IS SMALL THEN d IS SMALL
4) IF R IS SMALL AND T IS SMALL THEN d IS VERY SMALL

Figure 3.10 Fuzzy Logic Depth/Wave Membership Functions

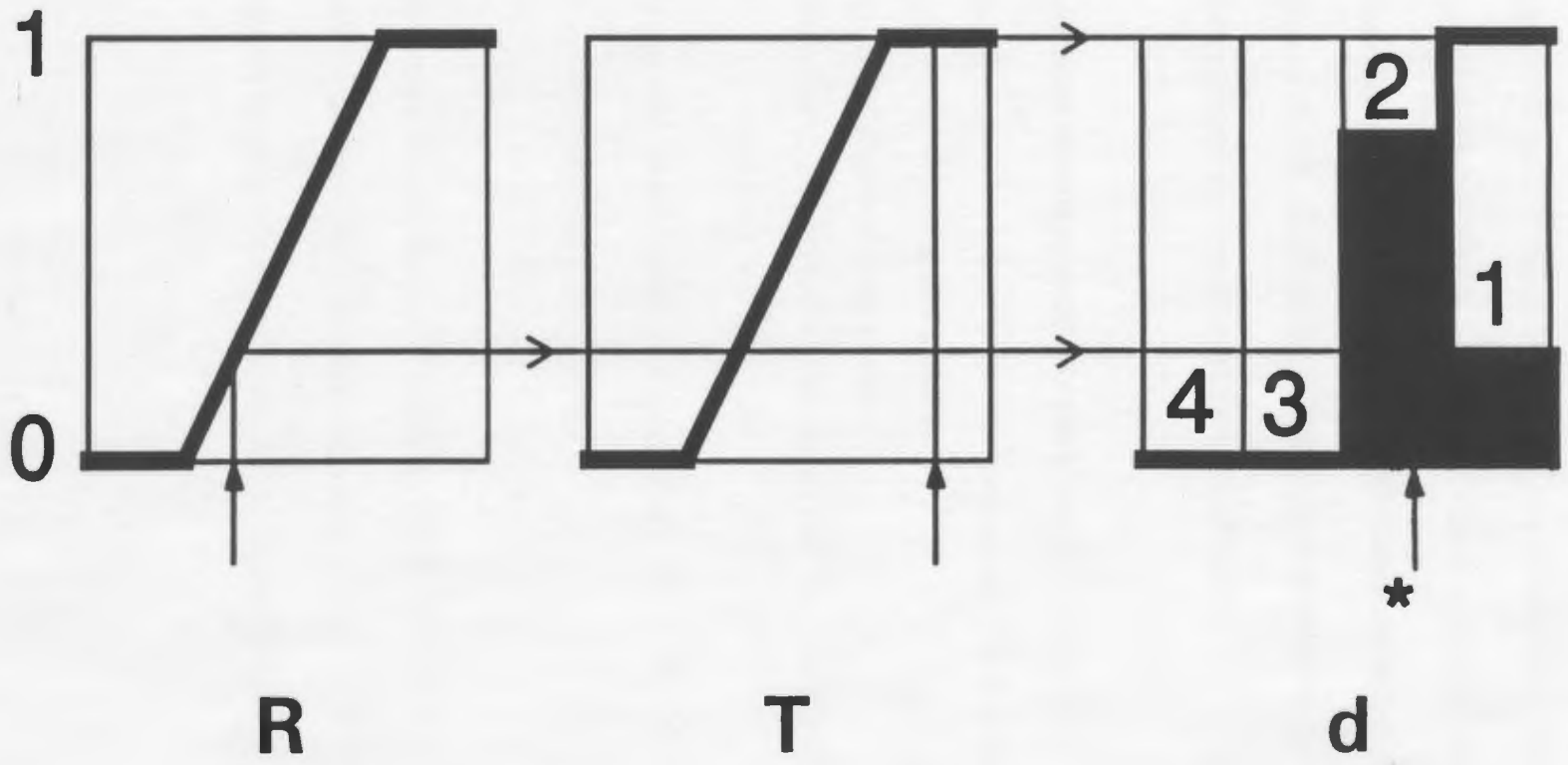

Figure 3.11 Generalization of Fuzzy Depth Range and Defuzzification

AND versus OR logic. A 'crisp' depth would be obtained from the overall depth range through a process of 'defuzzification'. In this case, the centroid of area method was used for 'defuzzification'. The output, which is the safe operating depth for the specific inputs of wave steepness and wave period, is denoted by an asterisk in Figure 3.11. Calibration of fuzzy logic is often necessary through adjustment of membership break points and shapes.

A fuzzy-logic control strategy may be very useful in the following situations:

- when control objectives are difficult to express numerically
- in both linear and nonlinear systems
- for time-varying dynamic systems
- when all solutions for possible patterns can not be described

The disadvantage of this control strategy is there is no rigorous way to determine beforehand if it will be stable.

As a control strategy for underwater robots, fuzzy logic provides the flexibility needed to control continuously variable systems. Since fuzzy logic is a robust control strategy, it is a great candidate for underwater robotic control.

3.2.4 Discussion

Of the three supervisory control strategies discussed in this thesis, neural networks and fuzzy logic are the most promising for accurate subsea control. Although expert systems are similar to fuzzy logic, far better control is expected with fuzzy logic. A fuzzy-logic system is also easier to implement than an expert system, since not as many rules are needed and human 'experts' are not required to determine an outcome(s) for each set of possible inputs. Fuzzy logic when combined with an error-driven control strategy provides reliable control which is both robust and stable. Neural networks would also make a great partner for fuzzy logic for the control of subsea robots, since neural network mapping could be used to obtain a good fit for the overall dynamics of the system. Neural networks may even be able to generate a fuzzy rule base to be used for fuzzy-logic control.

4 PROPULSION MECHANISMS

Performance of an underwater vehicle depends not only on its strategy for control but the accuracy of its propulsion mechanism, navigation system and sensors. Current propulsion mechanisms and problems relating to their use are described in this section. Problems relating to current navigation systems and sensors are also very important, however, they are beyond the scope of this thesis.

The type of vehicle propulsion system used is generally determined by the mode of operation of the vehicle. If the vehicle is towed by a surface vessel at mid-water depth, the vehicle normally has no onboard propulsion mechanism. Some vehicles use two means of propulsion depending on the mode of operation of the vehicle. For example, a vehicle would rely on the towing of the surface vessel for propulsion while in search mode and then use onboard thrusters while in inspection and sampling mode. For vehicles operating on the ocean floor, methods for propulsion include: caterpillar-like tracks; different wheel arrangements; and a system which allows the vehicle to winch itself forward on a pre-laid wire. Free-swimming vehicles generally use propellers for propulsion. A number of propellers are commonly used to give the vehicle a number of degrees of freedom. Stern mounted free propellers are also used in combination with elevators for vehicle movement in different directions.

Of the propulsion mechanisms previously described, propellers (which are often referred to as thrusters) are the most widely used. The most common type of propeller is a ducted propeller (a propeller surrounded by a shroud which gives the propeller a higher efficiency). Propellers have fixed or variable pitch and can run at a variable speed. A fixed-pitch propeller is designed to give the highest efficiency at the maximum operating speed. Variable-pitch propellers give constant efficiency over a range of speeds which is suitable for underwater vehicle operation. Variable-pitch propellers, however, add complexity to the system and are often not as reliable as the simpler fixed-pitch propeller. Variable-speed fixed-pitched propellers tend to be more reliable, but such systems may be slow to respond to changes in shaft speed which may cause a restriction on bandwidth (Farbrother and Stacey, 1993).

The number and arrangement of thrusters for underwater vehicles vary substantially, but full manoeuvrability in six degrees of freedom can be achieved with four thrusters arranged in a 'vertrans' configuration. Two thrusters are located at the rear of the vehicle providing forward motion and yaw control. The other two thrusters are located in the front of the vehicle and are vertically positioned in a 'V' formation on either side of the longitudinal centreline of the vehicle. These thrusters are orientated so they point towards the centre of mass of the vehicle and give the vehicle the other four degrees of freedom (up and down, side to side, roll and pitch) through vector thrust.

Thrusters are known to produce complex effects as reported by Farbrother and Stacey (1993). The complex effects associated with vehicle thrusters include: thruster / vehicle interaction; momentum drag; and mechanical nonlinearities. Thruster / vehicle interaction mainly refers to the blockage of flow in or out of the thruster by equipment on the vehicle body. Thrusters are generally placed inside the envelope of the hull to avoid snagging of the umbilical cord or other cables. Momentum drag is caused by a variation in the rate of change of momentum due to a significant velocity differential between the fluid velocity outside the thruster and the velocity the fluid is forced to adopt (the velocity vector of the vehicle) as it enters or leaves a ducted thruster. Mechanical nonlinearities include backlash, hysteresis and saturation.

Thruster placement significantly influences the force-coupling between degrees of freedom. To minimize these effects, it is preferable to have all forces acting through the centre of mass of the vehicle. Thus, thrusters would be positioned so their axes all pass through the centre of mass. In practice, this is almost impossible since the centre of mass changes with speed due to the shift in virtual mass distribution (Farbrother and Stacey, 1993). A hydrodynamic study by Baker and Sayer (1990) showed significant reduction in performance for poorly positioned thrusters. Tests included measuring the forces incurred on a test configuration in a towing tank for various types of thruster blockages. Results showed that it would be beneficial to position thrusters clear from

internal equipment and preferably clear from the main hull, provided they can be protected.

Yoerger, Cooke and Slotine (1990) have linked poor vehicle control to thruster dynamics. Through model tank tests, the thruster dynamics were found to dominate vehicle behaviour by restricting the maximum closed-loop bandwidth and creating a limit cycle. Closed-loop positioning performance of Jason, a 1200 kg ROV, during a dockside test in calm water without compensation for thrusters is shown in Figure 4.1. A stable oscillation with a fixed frequency and a magnitude of about 10 cm developed around the desired vehicle position. Similar behaviour was plotted for the RV Knorr, an 1800-ton oceanographic research vessel, under dynamic positioning control in calm water. Most marine vessels ranging from ships under dynamic positioning control to servo-controlled ROVs have also been known to exhibit limit cycle behaviour. Through testing of a thruster unit from the ROV Jason, the limit cycle behaviour was found to be a result of the nonlinear response of the torque-controlled thruster. The thruster represented a sluggish filter, however, its speed of response increased with higher input.

The nonlinear response of the ROV Jason thruster was used to explain problems with other ROVs (Yoerger, 1990). Jason's thrusters are small for its size, so normal hovering and manoeuvring use a substantial portion of the dynamic

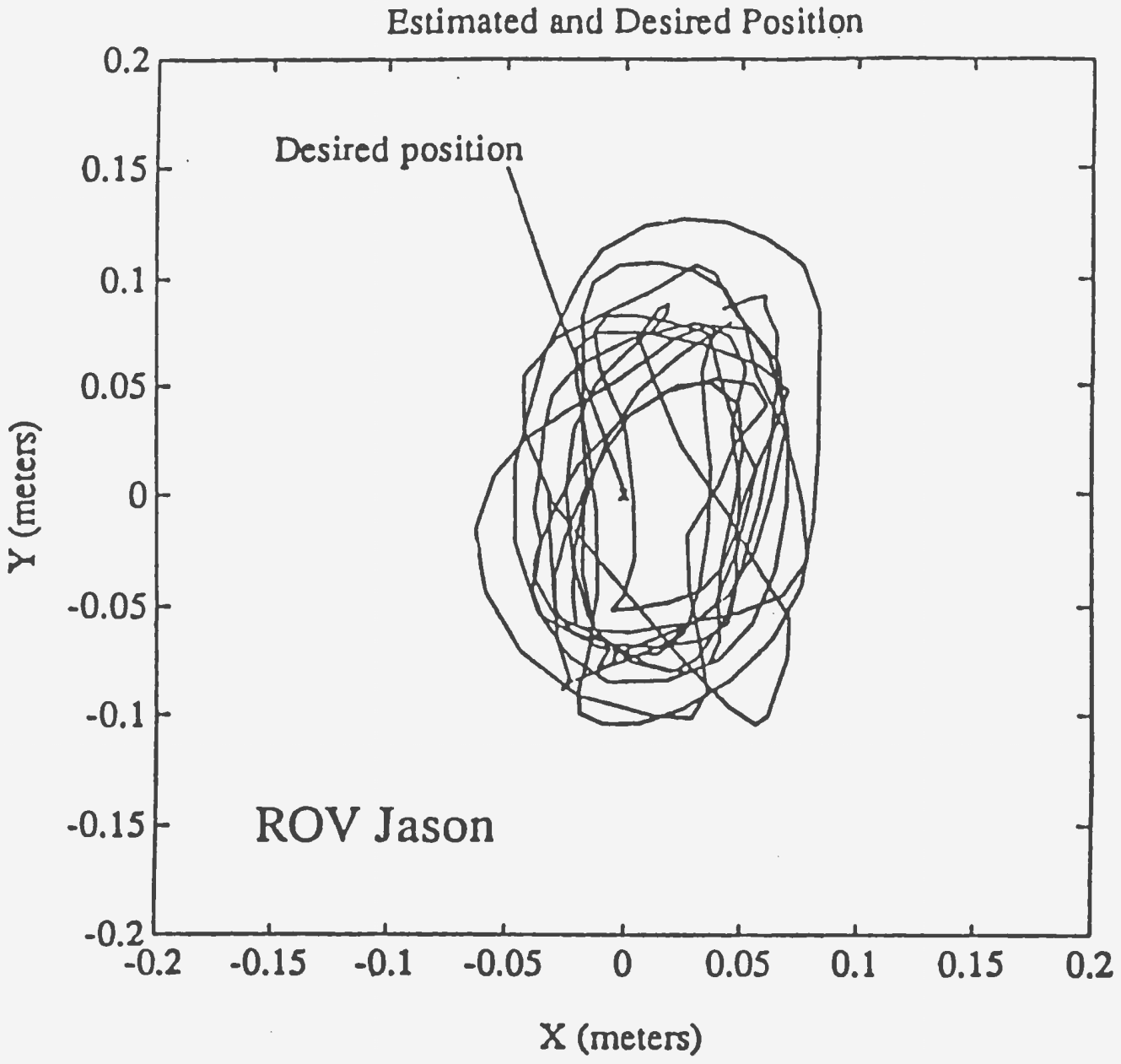

Figure 4.1 Limit Cycle of ROV Jason (Yoerger, Cooke and Slotine, 1990)

range of the thrusters. Other vehicles with very large powered thrusters use only a small portion of their thruster potential for fine manoeuvring, and thus the thruster response will be highly nonlinear resulting in further decline in vehicle positioning accuracy.

Many underwater tasks require accurate positioning of the vehicle. In slow speed control (for tasks such as automatic docking and combined vehicle manipulator tasks), the nonlinearities related to thruster behaviour were found to influence the overall system behaviour in a manner which was fundamentally different from most hydrodynamic and inertial nonlinearities. It has been found that thruster performance particularly diminishes at low speeds and during hover.

The poor performance of thrusters, especially at low speeds and during hover, prompted the design of an alternate propulsion device to provide accurate vehicle control. The propulsion device was designed to produce short duration fine-positioning control for tasks which would require the vehicle to remain stationary or manoeuvre at low speeds. Most low speed tasks require accurate control and it is at these speeds that thrusters are known to have low efficiency and high nonlinear behaviour. The design proposal for this new positioning device for small subsea robots is described in the following chapter.

5 HYDRAULIC ACTUATOR MECHANISM

A propulsion device using a hydraulic actuator mechanism was proposed to provide short duration accurate positioning of subsea robots. The proposed device would include its own energy source and provide high efficiency performance by mimicking the jet mechanism used by squids (Muggeridge and Hinchey, 1992 and Hinchey, Muggeridge and Rivera, 1992). The proposed device would be used in conjunction with current propulsion mechanisms. For instance, general positioning of a subsea robot would be performed by ducted propellers and fine positioning would be performed by the proposed device.

The proposed propulsion device would use compressed gas as an energy source to pressurize hydraulic fluid in an accumulator to operate an actuator. The hydraulic actuator mechanism, through a plunger-type motion of the actuator, produces a water jet. The water jet motion would provide small movements of the vehicle which react quickly to the control strategy used to operate the actuator. The resultant motion would be similar to the smooth ride of an airplane created by the fast acting but small movements of its wing ailerons and tail elevators. The implication of such a self-contained compact device is that fine-positioning control could be achieved for an autonomous submersible.

The scope of the experimental work and descriptions and observations of tests

conducted on the positioning device are described in the following sections.

5.1 Purpose and Scope of Experimental Work

The experimental work for the new positioning device is developmental in nature as research in the area of subsea robot control has not previously been conducted at Memorial University of Newfoundland.

The purpose of the research work was to develop and test the concept of using compressed gas as an energy source to operate an actuator for the proposed positioning device.

The scope of the research work was to determine the feasibility of the new device through preliminary testing. Tests included trying to operate a hydraulic actuator via computer control and determining how long an actuator would operate with a certain size accumulator. However, in-water tests were not conducted. Instead, the goal of the tests was to determine if the potential existed for development of the fine-positioning device.

5.2 Development of Test Configuration

The test configuration, shown schematically in Figure 5.1, illustrates the concept

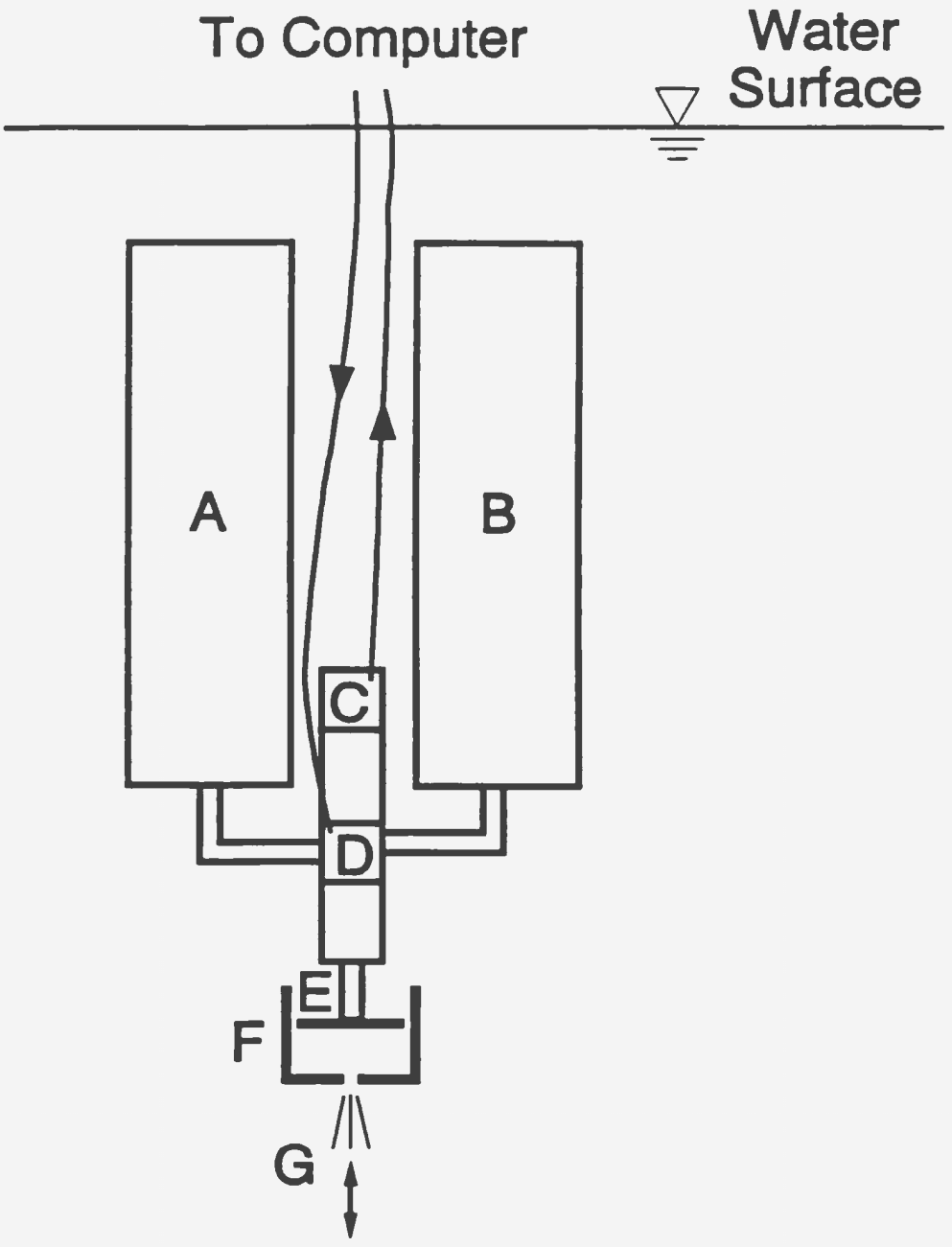

A - Low pressure chamber
B - Accumulator
C - Linear variable differential transformer (LVDT)
D - Servovalve
E - Piston
F - Cylindrical chamber
G - Water jet

Figure 5.1 Test Configuration Schematic

of the new device. An accumulator is used to store compressed gas and high pressure hydraulic fluid. Compressed gas provides the energy source to operate the hydraulic actuator. As the high pressure hydraulic fluid from the accumulator passes through the servovalve during its operation, it is returned to a low pressure chamber. The servovalve controlled actuator is used to generate a flow of water into or out of a cylindrical chamber. Rapid back-and-forth motion on the plunger assembly produces a water jet that may be used for vehicle position keeping. Another way the water jet may be utilized would be to produce a series of fast 'kicks' with a slow return mechanism which would provide vehicle motion in one direction based on the difference in momentum (Muggeridge and Hinchey, 1992). A complicated valve system would increase the efficiency of the motion but is beyond the scope of this work. The controller in the prototype would be located onboard the vehicle, however, for the test configuration it would be located externally to simplify the setup. A computer would generate control signals for the servovalve and sensors would provide information on the system and its surroundings for closed-loop feedback control.

The preliminary test setup is shown in Figure 5.2 and 5.3. The apparatus, shown in Figure 5.2, listed left to right, consisted of: a pressure gauge; a MTS 111.11B-04 accumulator; a MTS 242.01 actuator; a MTS 252.21 servovalve; and an ENERPAC hand pump. Product information for the accumulator, actuator

Figure 5.2 Preliminary Setup: Apparatus

Figure 5.3 Preliminary Setup: Control Console

and servovalve is provided in Appendix A. The structures lab control unit manufactured by MTS Systems Corporation, shown in Figure 5.3, was used to control the actuator. The control console included: a MTS 440.13 servocontroller; a MTS 440.22 linear variable differential transformer (LVDT) controller; and a MTS 440.14 valve driver.

The servovalve was used to control the operation of the actuator. The servovalve converts electrical signals from the servocontroller for position control to flow of hydraulic fluid to the actuator. The flow of fluid through the servovalve is directly proportional to the electrical input current supplied to the valve. The electrical input generated by the servocontroller is based on the relationship between the desired and actual position of the actuator piston.

The MTS 252.21 servovalve is a two stage servovalve which is designed for low flow rate, high response servohydraulic systems. The servovalve consists of a torque motor and two stages of hydraulic power regulation. Servovalve components are shown in Figure 5.4. The torque motor is used to control the first stage hydraulic power regulation. The control signal energizes the motor coil and the armature/flapper is rotated clockwise or counter clockwise depending on the polarity of the signal. The position of the flapper influences the amount of flow through two nozzles which are located on either side of the flapper. As the flow increases through one nozzle, it decreases through the

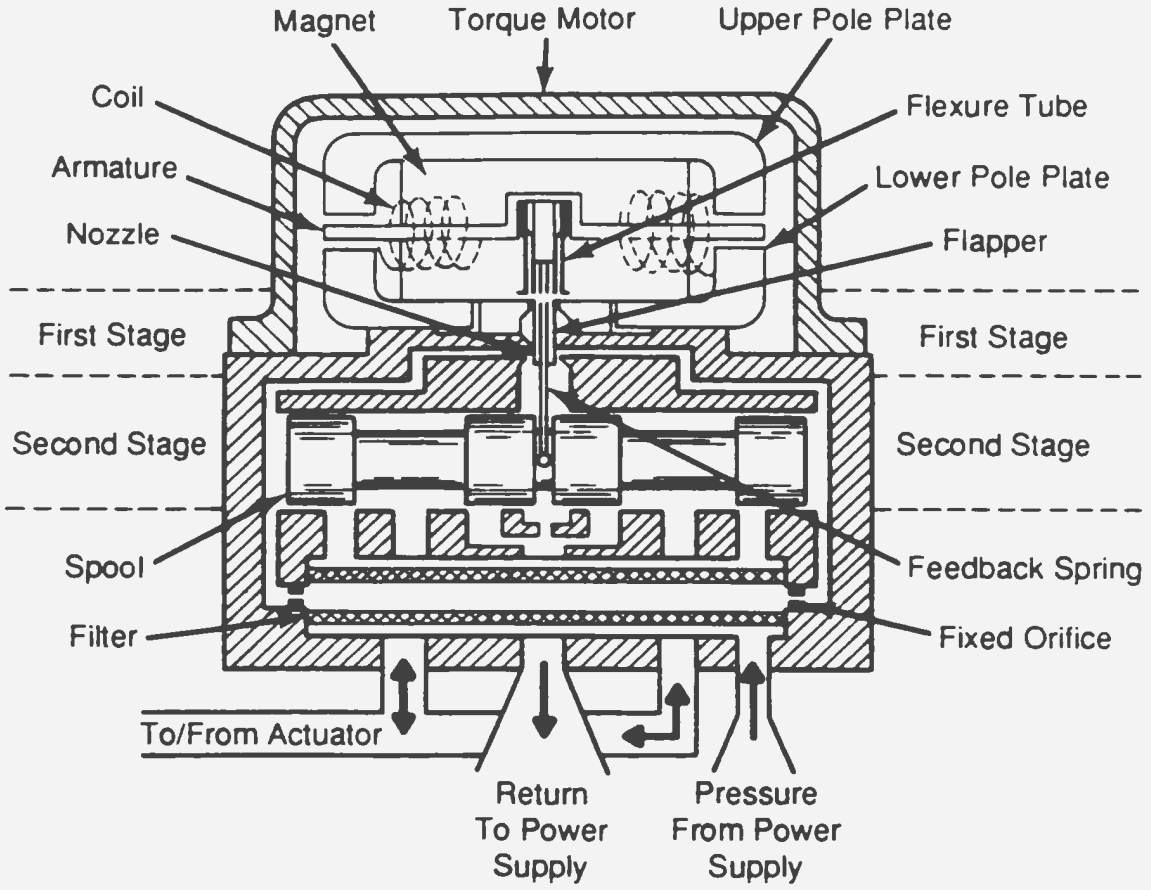

Figure 5.4 Cutaway Drawing of Model #252 Servovalve (MTS brochure)

other nozzle creating a differential pressure on the spool in the second stage. The spool moves in response to the difference in pressure. A feedback spring (which is attached to the flapper and is in contact with the spool) exerts an opposite torque to the one produced by the armature/flapper. The spool continues to move until the torque experienced by the feedback spring is equal to the torque of the control signal. As the spool comes to its correct position, the flapper is recentred and the flow from both nozzles equalize. A balance of pressure on each end of the spool causes the spool to remain stationary while hydraulic fluid continues to flow to the actuator.

When a new control signal is sent to the servovalve, the spool position changes. For every control signal, there is a position of the spool which is dependent on the magnitude and polarity of the control signal.

The MTS 242.01 hydraulic actuator used is a small linear actuator which is operated by servovalve control. The actuator contains an internally mounted linear variable differential transformer which provides an accurate indication of piston rod displacement. High pressure hydraulic fluid is supplied to the pressure port and internal passages direct the fluid to the servovalve. The servovalve sends the fluid to one side of the piston or the other in order to extend or retract the piston rod. As the hydraulic pressure is applied to one side of the piston, the fluid on the other side is passed out of the actuator through the

return port.

A MTS 111.11B-04 piston-type accumulator was used in the preliminary setup. One side of the internal piston of the accumulator is charged with nitrogen gas while the other side of the piston is filled with hydraulic fluid. Using the hand pump, the hydraulic fluid is pressurized to 21 MPa which forces the piston upward and compresses the nitrogen gas to 21 MPa. The compressed nitrogen gas acts as an energy source for the flow of hydraulic fluid.

The MTS 440.13 servocontroller in the lab's MTS control console was used to control the actuator. Signals are sent from the servocontroller to the valve driver (MTS 440.14) where they are amplified and passed on to the servovalve. An LVDT signal conditioner (MTS 440.22) is used to condition the output from the actuator's LVDT. It provides the feedback signal, the actual position of the actuator piston, for the controller.

The preliminary test setup was used to determine the null flow for the servovalve and whether the actuator could be operated using the accumulator to supply high pressure hydraulic fluid. The null flow for the servovalve is defined as the leakage through the servovalve with a zero input error signal from the controller. The valve is said to be nulled when the internal spool is in its centre position and hydraulic fluid is not being passed to the actuator.

Once the initial tests were conducted and it was determined that the actuator could operate from the accumulator, a test frame was designed to allow further testing. The test frame was designed as a housing for the original actuator and servovalve (MTS 242.01 and MTS 252.21, respectively), a new accumulator (MTS 111.12C-06), a reservoir and high pressure hoses and fittings. A new larger accumulator was purchased to increase the hydraulic fluid capacity to allow longer duration tests. A steel reservoir designed to withstand high pressure was built to hold the return hydraulic fluid from the actuator.

The test frame was constructed from 50 mm square aluminum box tubing. This material was chosen for its strength, low weight and corrosion resistant properties. A dimensional drawing of the test frame is shown in Figure 5.5. A horizontal aluminum channel was used to support the reservoir, actuator and accumulator. The overall dimensions for the test frame are 0.61 m wide by 0.46 m deep by 1.52 m high.

Once the aluminum test frame was constructed, the main components were mounted in the test frame (a photograph of the test frame and its components is shown in Figure 5.6). All the necessary high pressure valves, fittings and hoses were procured. An adapter plate was made for the accumulator because it normally was flush-mounted to a base and in this case a threaded connection was needed for pipe fittings. The test apparatus was designed to be contained

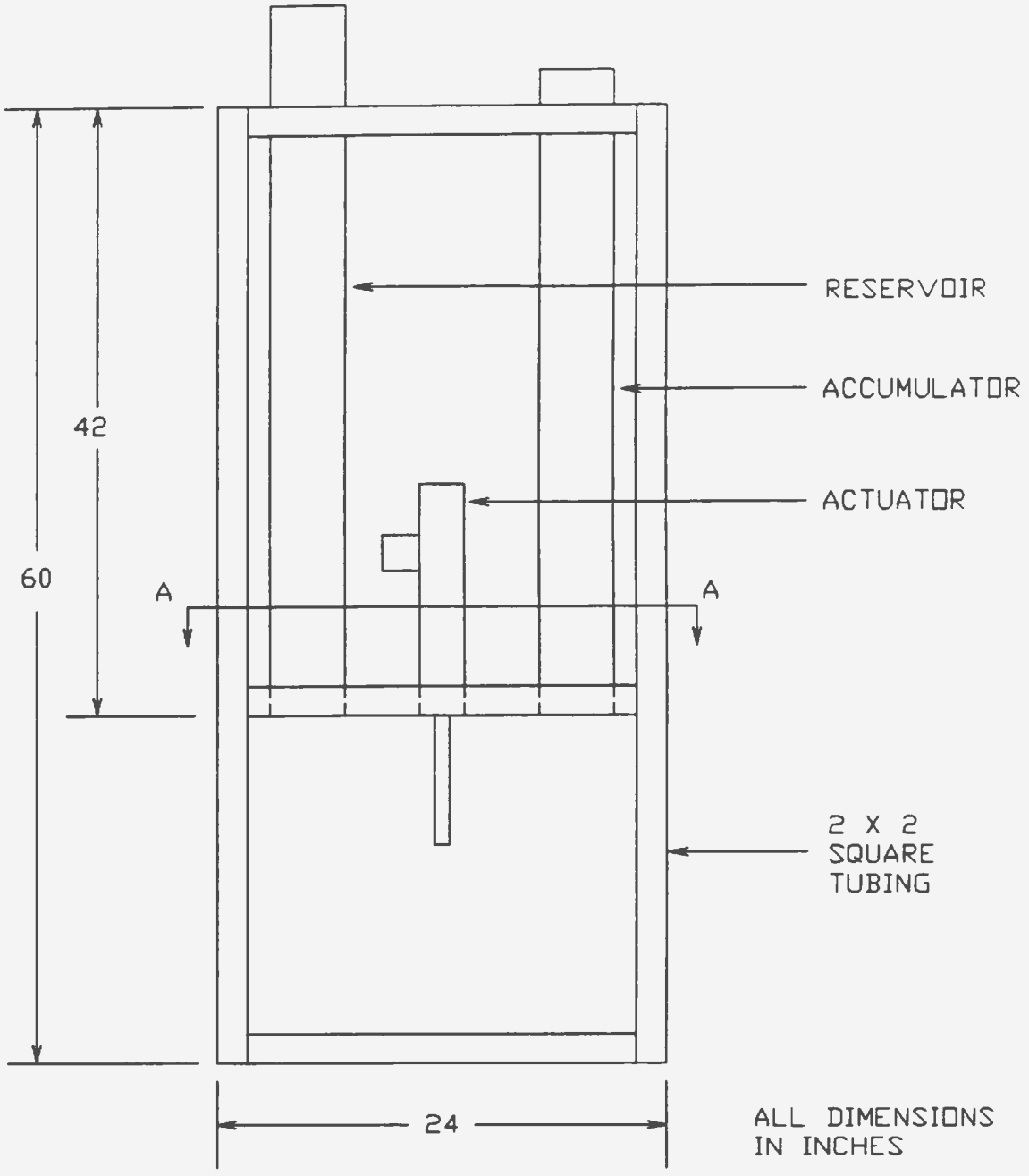

(a)

Figure 5.5 Dimensional Drawing of Test Frame
(a) Front view
(b) Plan view and section A-A

PLAN VIEW

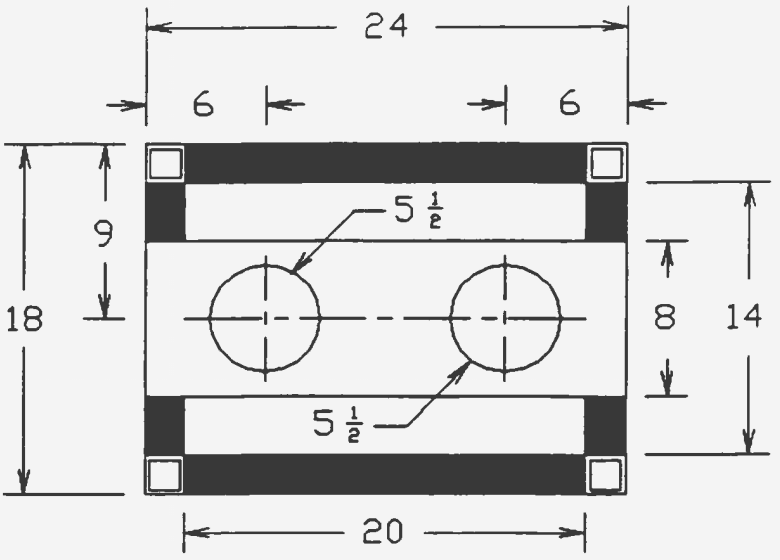

SECTION A-A

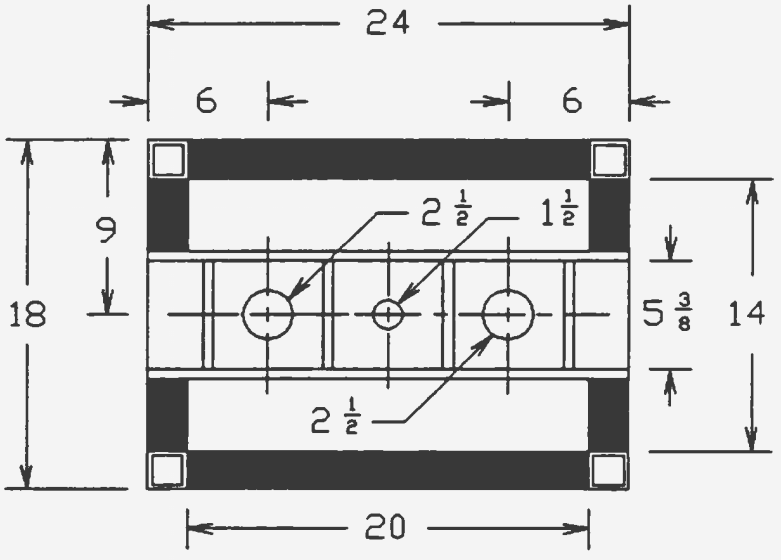

ALL DIMENSIONS IN INCHES

(b)

Figure 5.6 Test Frame and Components

within the aluminum frame. The actuator was housed in the centre of the test frame with the accumulator on one side and the reservoir on the other side. The actuator was rotated 90 degrees so less hose was required to connect the accumulator and the reservoir to the actuator, which resulted in a more compact design.

The test frame and components, shown in Figure 5.6, were set up with an independent system for control of the actuator. The lab's MTS control console was replaced by: a computer; a separate servovalve driver (LC500 load commander); a power supply; a separate LVDT conditioner (Transducer Exciter-Demodulator Daytronic Model 201C); and a data acquisition system (Keithley KDAC500 data requisition and control software). The computer generates the control error signal which drives the actuator. The Keithley system converts the signal from digital to analog before the signal is sent to the servovalve via the servovalve amplifier. The signal from the LVDT, which indicates the position of the actuator piston rod, is conditioned before it is converted from analog to digital by the Keithley system. This feedback signal is used by the computer program to generate a new control signal and the process is repeated.

A simple computer program, which interfaced with the Keithley system control software, was written in Quick BASIC and used to generate the control signal. The difference between the desired and the actual piston rod position was used

to drive the system. The desired motion of the piston was set as a sinusoidal motion. Its set point, amplitude and frequency were inputs to the computer program which could be selected at the time of the test. A copy of the program can be found in Appendix B.

5.3 Observations

Null flow measurements for the servovalve (MTS 252.21) have been tabulated in Table 5.1. All flow rates measured were found to fall below the maximum specified null flow rate of 1.1 litres per minute for the servovalve. The average null flow rate observed was 65 mL per minute.

Table 5.1 Null Flow Measurements

Trial Number	Initial Pressure (MPa)	Volume of Oil (mL)	Time Elapsed (min)	Flow Rate (mL/min)
1	21.37	230	4	58
2	21.37	190	3	63
3	20.68	330	3	110
4	20.68	275	10	28

The results from tests in which the actuator (MTS 242.01) was operated from the recharged accumulator (MTS 111.12C-06) are given in Table 5.2. For all of

the tests, the piston was commanded to produce a sinusoidal motion with a set frequency and stroke length. The elapsed time refers to the duration that the actuator operated from the accumulator. From the initial pressure and the elapsed time, the rate of loss of pressure was calculated. Based on the rate of loss of pressure for each trial, the time expected for the actuator to operate with an initial pressure equal to its normal operating pressure of 21 MPa was estimated.

Table 5.2 Actuator Operation from Accumulator

Trial No.	Initial Press. (MPa)	Freq. (Hz)	Stroke Length (mm)	Elapsed Time (min/sec)	Rate of Press. Loss (MPa/min)	Calc. Time from 21MPa (min/sec)
1	18.27	0.1	70	8'	1.85	9' 18"
2	18.27	0.5	20	6' 30"	2.28	7' 34"
3	18.27	0.5	20	5' 30"	2.70	6' 24"
4	18.27	0.5	20	5' 10"	2.87	6'
5	18.27	0.5	20	6'	2.47	6' 59"
6	18.27	0.5	20	5'	2.96	5' 49"
7	18.27	0.5	20	5'	2.96	5' 49"
8	17.93	0.5	20	5' 50"	2.13	7' 7"
9	17.93	0.5	20	4' 50"	2.57	5' 54"
10	18.00	0.5	20	4' 50"	2.58	5' 52"
11	18.00	0.5	20	4' 44"	2.64	5' 45"
12	18.00	0.5	20	4' 25"	2.83	5' 22"

In order to check that the piston was moving at its set frequency and stroke length, the piston motion during trials two, three, five and six were plotted. All plots depicted perfect sinusoidal wave forms at the commanded frequency until the piston came to a stop.

Twelve trials with slightly different scenarios were conducted to determine whether certain operating conditions affected the system performance. These alterations were made to simulate actual underwater operating conditions. In trials one through five, the reservoir was not used. For trials six and seven, the reservoir was used in the system with its vent open. In trial eight, the reservoir was used in the system with its vent closed. For trials nine and ten, the vent on the reservoir was closed and silicone was used to block the LVDT port holes. The reservoir was not used in the system for trial eleven. In trial twelve, the reservoir was used in the system with its vent closed.

The average rate of pressure loss for all trials was 2.57 MPa per minute. There were no significant differences in the average rate of pressure loss for trials that did not include the reservoir in the system and trials with the reservoir in the system with its vent closed. The expected test duration from a normal operating pressure of 21 MPa was estimated to be just over 6 minutes.

A number of problems were encountered during the experiential work due to its

developmental nature. For instance, during tests to determine null flow and volume of fluid used in the test, an emulsion of oil was seen leaving the return line when the return line was left open to atmosphere. Upon inspection, o-rings in the servovalve were found to be unseated. It was determined that in order to prevent air from entering the servovalve the return line must remain full with hydraulic fluid. The problem was corrected by bending the return hose into a 'U' shape when the return line was not connected to the reservoir or to the lab hydraulics system.

Several problems relating to equipment were encountered. Difficulties arose when electronic equipment, not designed to be used in conjunction with other test equipment, was interfaced to the test equipment. As some of the equipment was old and worn, alterations and repairs to several pieces were required before they could be used.

One equipment problem observed was that the actuator piston rod would undergo full scale movements when medium values of gain and amplitude were used and serious vibrations occurred when small gain and amplitude values were used as inputs. In order to isolate the problem, print statements were inserted in the computer program and a voltmeter and oscilloscope were connected to the test equipment. The oscilloscope was used to track the output from the Keithley system since oscillation and humming suggested AC voltages.

It was discovered that the servovalve driver was operating in the noisy range. At small voltages, noise was very disruptive and produced vibration. At high voltages, the amplification was so high that piston was already in its extreme position.

Calculations for the test system were performed to determine the water jet speed; the water jet force; the speed of the test system (ignoring drag); and the terminal speed of the test system (considering drag). Data used in the calculations included: the full-flow rating of 4 L/min for the MTS 252.21 servovalve; the force rating of 4.5 kN for the MTS 242.01 actuator; a plunger diameter of 0.15 m; a chamber height of 0.10 m; and a water jet diameter of 0.025 m. Details of the calculations are given in Appendix C.

The maximum jet speed was calculated to be 9 m/s based on the full-flow rating of the MTS 252.21 servovalve and the piston area and maximum stroke for the MTS 242.01 actuator. This method was used since the full-flow rating of the servovalve (not the force rating of the actuator) was found to be the limiting factor in determining the maximum jet speed.

The jet force was calculated to be 40 N based on the calculated jet mass flow rate of 4.42 kg/s and the jet speed of 9 m/s.

The force on the test system, according to Newton's third law of motion and d'Alembert's principle, is the force of inertia and is equal in magnitude, but opposite in direction, to the force produced by the water jet. Conservation of momentum was used to determine the momentum added to the test system by the water jet (neglecting drag). Using a mass of 225 kg for the test system, which included an additional 50 percent for added inertia, the speed of the test system was calculated to be 0.07 m/s.

In an attempt to ascertain the effect of drag on the system, a terminal speed of the test system was determined by letting the drag force equal the force provided by the jet. The equation for the drag force used an assumed drag coefficient of one and the surface area of the rectangular cross section of the test frame. The equation for the drag force was rearranged in terms of the test system speed and the force provided by the water jet was substituted for the drag force. It was determined that at a speed of 0.53 m/s the drag force would equal the force produced by the water jet. This speed is beyond the expected speed required for fine positioning of the test system.

If necessary, there are a number of methods which could be used to increase the jet force and thus the speed of the test system. The simplest method would be to decrease the jet diameter without changing any other system parameter. Based on the pressure balance between the pressure the actuator can deliver

(from the force rating of the actuator) and the pressure beneath the plunger, Bernoulli's equation was used to determine the minimum jet diameter. The calculated minimum jet diameter of 0.016 m corresponds to a jet force, test system speed and terminal test system speed of 97 N, 0.17 m/s and 0.83 m/s, respectively.

Other options available for increasing the jet force, if a larger jet force is required, include:

- use a servovalve with a higher full-flow rating
- use an actuator with a higher force rating
- decrease the piston diameter to increase the pressure in the chamber
- decrease the drag force on the test system by altering its shape
- decrease the weight of the test system by using a slighter frame and a plastic reservoir

Some of these options would have compromises. For instance, if the present system with a jet diameter of 0.025 m was used and the current servovalve was replaced with a MTS 252.22 servovalve (full-flow rating of 9.5 L/min) a jet force of 217 N would be produced. However, a higher flow rate servovalve would drain the hydraulic fluid stored in the accumulator more quickly and reduce the operational time of the device.

In conclusion, the experimental work conducted demonstrated the potential for the proposed positioning device. The feasibility of using compressed gas as the

energy source to operate an actuator for a sufficient period of time was established. A test frame was constructed and an independent test setup was developed for future work in the area.

6 CONCLUSIONS

The ocean environment has become of ever-increasing interest in the world, since reserves of nonrenewable resources on the earth's land areas are diminishing. The need for the exploration and development of these resources from the seabed has emphasized the role of robot technology for performing various underwater tasks.

The trend in underwater vehicles has focused on increased autonomy, developing from manned vehicles to remotely operated vehicles (ROVs) to autonomous underwater vehicles (AUVs). In order to achieve this goal, control methods must be robust in face of dynamic uncertainties encountered in the unstructured seawater environment.

The main control strategies were examined and evaluated in terms of their potential for underwater robot control. The control strategies were subdivided into two main groups: classical and supervisory. The classical strategies have been used for robotic applications for many years and are generally error-driven or based on the governing equations for the system. Supervisory control strategies try to mimic a human operator by making decisions or adjustments a human operator would make for proper control of a robot.

The classical strategies evaluated were: combination of proportional, integral and derivative; switching; computed load; and sliding mode. The control strategies evaluated for supervisory control were: neural networks; expert systems; and fuzzy logic. Supervisory control in combination with classical control shows great potential for robust control. In particular, fuzzy logic and neural networks in combination with error-driven control are proposed to be the most promising mix for accurate subsea robot control.

Control of subsea robots was found not only to be dependent on the control strategy but also greatly influenced by the vehicle's propulsion mechanism. Propulsion devices for underwater vehicles were reviewed and the most common type, ducted propellers, were found to have low efficiency and poor performance due to dynamic nonlinear characteristics. Thus, control strategies no matter how sophisticated will give poor vehicle performance with current propulsion mechanisms, especially at low speeds and during hover.

A new propulsion device was proposed to give short-duration fine-positioning control. The device used a hydraulic actuator mechanism to convert the up and down motion of an actuator's piston to a water jet in an attempt to mimic the jet propulsion used by squids. The water jet produced would give smooth control of the vehicle through small but rapid motions similar to the movement of aircraft control surfaces used to produce a smooth ride. Compressed gas

stored in an accumulator was used as an energy source for a hydraulic actuator.

The experimental work conducted demonstrated the potential for the proposed positioning device. The feasibility of using compressed gas as the energy source to operate an actuator for a sufficient period of time was established. A test frame was constructed and an independent test setup was developed for future work in the area.

In a more general sense, the project represented not only a new positioning device for subsea robots, but a significant beginning in the new area of underwater robotics at Memorial University of Newfoundland. A number of individuals have since joined the group conducting research in the area of underwater robotics.

7 RECOMMENDATIONS

Areas for future work include testing the proposed positioning device in the wave tank at Memorial University of Newfoundland. Feedback from pressure and wave sensors used to monitor the system surroundings could be incorporated into the feedback loop. Various control strategies could be tested and their performance on the in-water system monitored. In particular, those strategies mentioned in this thesis, which have been recommended for accurate subsea control, should be tested.

8 REFERENCES

Asada, H., and Slotine, J.J.E. (1986). *Robot Analysis and Control*, John Wiley and Sons, Inc., New York, New York, pp. 133-179.

Baker, J.H.A., and Sayer, P. (1990). "Selection of Experimental Facility and Measurements of Hydrodynamic Coefficients for ROVs," *Proceedings of the First European Offshore Mechanics Symposium*, Trondheim, Norway.

Blidberg, D., and Yoerger, D. (1990). Guest Editorial, *IEEE Journal of Oceanic Engineering*, Vol. 15, No. 3, pp. 141-143.

Brooks, R.A. (1991). "Intelligence without Representation," *Artificial Intelligence*, Vol. 47, No. 2, pp. 139-159.

Busby, F., and Vadus, J.R. (1990). "Autonomous Underwater Vehicle R&D Trends," *Sea Technology*, Vol. 31, No. 5, pp. 65-73.

Caudill, M. (1987). "Neural Networks Primer - Part I," *AI EXPERT*, Dec. issue, p. 48.

Cox, E. (1992). "Fuzzy Fundamentals," *IEEE Spectrum*, Vol. 29, No. 3, pp. 58-61.

Cristi, R., Papoulias, F.A., and Healey, A.J. (1990). "Adaptive Sliding Mode Control of Autonomous Underwater Vehicles in the Dive Plane," *IEEE Journal of Oceanic Engineering*, Vol. 15, No. 3, pp. 152-160.

Farbrother, H.N., and Stacey, B.A. (1993). "Aspects of Remotely Operated Vehicle Control - A Review," *Underwater Technology*, Vol. 19, No. 1, pp. 24-36.

Fujii, T., and Ura, T. (1990). "Development of Motion Control System for AUV using Neural Nets," *Proceedings of the Symposium of Autonomous Underwater Vehicle Technology*, pp. 81-86.

Hall, W., and Adams, M. (1992). "Autonomous Vehicle Software Taxonomy," *Proceedings of the 1992 Symposium on Autonomous Underwater Vehicle Technology*, sponsored by the Oceanic Engineering Society of IEEE, Washington, DC, pp. 49-64.

Harmon, P., and King, D. (1985). *Expert Systems*, John Wiley and Sons, Inc., New York, New York.

Hinchey, M.J. (1994). "Potential for Subsea Robot Control," *Ocean Engineering Journal*, Pergamon Press, at press.

Hinchey, M.J., Muggeridge, K.J., and Rivera C. (1992). "Subsea Robotics Research at OERC/MUN," *Proceedings of the Third Newfoundland Electrical and Computer Engineering Conference*, sponsored by the Newfoundland and Labrador Section of IEEE, St.John's, Newfoundland.

IEEE. (1992a). *Neural Networks: Theoretical Foundations and Analysis*, ed. C. Lau, IEEE Press, Piscataway, New Jersey.

IEEE. (1992b). *Artificial Neural Networks: Paradigms, Applications, and Hardware Implementations*, ed. E. Sánchez-Sinencio and C. Lau, IEEE Press, Piscataway, New Jersey.

Irish, J.D., and Brown, W.S. (1990). "Chapter III The Environment", *Submersible Vehicle Systems Design*, ed. E.E. Allmendinger, The Society of Naval Architects and Marine Engineers, New Jersey, pp. 71-73.

Jain, R. (1980). "Fuzzyism and Real World Problems," *Fuzzy Sets: Theory and Applications to Policy Analysis and Information Systems*, ed. P.P. Wang and S. K. Chang, Plenum Press, Plenum Publishing Corp., New York, New York, pp. 129-132.

Josin, G. (1988). "Integrating Neural Networks," *AI Expert*, Aug. issue, pp. 50-58.

Kawato, M., Uno, Y., Isobe, M., and Suzuki, R. (1988). "Hierarchical Neural Network Model for Voluntary Movement with Application to Robotics," *IEEE Control Systems Magazine*, Vol. 8, No. 2, pp. 8-15.

Lee, C.C. (1990). "Fuzzy Logic in Control Systems: Fuzzy Logic Controller - Part I and II," *IEEE Transactions on Systems, Man, Cybernetics*, Vol. 20, No. 2, pp. 404-435.

Mamdani, E.H., and Sembi, B.S. (1980). "Process Control Using Fuzzy Logic," *Fuzzy Sets: Theory and Applications to Policy Analysis and Information Systems*, ed. P.P. Wang and S. K. Chang, Plenum Press, Plenum Publishing Corp., New York, New York, pp. 249-265.

Miyamoto, H., Kawato, M., Setoyama, T., and Suzuki, R. (1988). "Feedback-Error-Learning Neural Network for Trajectory Control of a Robotic Manipulator," *Neural Networks*, Vol. 1, pp. 251-265.

Muggeridge, K.J., and Hinchey, M.J. (1992). "A New Jet Propulsion Device for Small Subsea Robots," *Proceedings of the 1992 Symposium on Autonomous Underwater Vehicle Technology*, sponsored by the Oceanic Engineering Society of IEEE, Washington, DC.

Muggeridge, K.J., and Hinchey, M.J. (1991). "Underwater Robot Control," *Proceedings of the Third Newfoundland Electrical and Computer Engineering Conference*, sponsored by the Newfoundland and Labrador Section of IEEE, St.John's, Newfoundland.

Nomoto, M., and Hattori, M. (1986). "A Deep ROV Dolphin 3K: Design and Performance Analysis," *IEEE Journal of Oceanic Engineering*, Vol. OE-11, pp. 373-391.

Ogata, K. (1990). *Modern Control Engineering*, Second Edition, Prentice-Hall, Inc., Englewood Cliffs, New Jersey.

Rumelhart, D.E., Hinton, G.E., and Williams, R.J. (1986). "Learning Internal Representations by Error Propagation," *Parallel Distributed Processing: Explorations in the Microstructure of Cognition*, ed. vol.1 D.E. Rumelhart and J.L. McClelland, MIT Press, Cambridge, Massachusetts, pp. 318-362.

Self, K. (1990). "Designing With Fuzzy Logic," *IEEE Spectrum*, Vol. 27, No. 11, pp. 42-44, 105.

Slotine, J.J.E. (1984). "Sliding Controller Design for Nonlinear Systems," *International Journal of Control*, Vol. 40, No. 2, pp. 421-434.

Slotine, J.J.E. (1983). "Tracking Control of Nonlinear Systems Using Sliding Surfaces," *PhD thesis*, Massachusetts Institute of Technology, Cambridge, Massachusetts.

Slotine, J.J.E., and Coetsee, J.A. (1986). "Adaptive Sliding Controller Synthesis for Nonlinear Systems," *International Journal of Control*, Vol. 43, No. 6, pp. 1631-1651.

Slotine, J.J.E., and Sastry, S.S. (1983). "Tracking Control of Nonlinear Systems Using Sliding Surfaces, with Application to Robot Manipulators," *International Journal of Control*, Vol. 38, No. 2, pp. 465-492.

Togai, M. (1991). "Fuzzy Logic: Applications and Perspectives," *The 41 st Video Conference Seminar via Satellite*, produced by IEEE, Inc., Piscataway, New Jersey, pp. 1-50.

Ura, T. (1990). "Development of AUV PTEROA," *First Workshop on Mobile Robots for Subsea Environments*, Monterey, California, pp. 195-200.

Waterman, D. (1986). *A Guide to Expert Systems*, Addison-Wesley, New York, New York.

Yoerger, D.R. (1990). "Precise Control of Underwater Robots: Why and How," *First Workshop on Mobile Robots for Subsea Environments*, Monterey, California, pp. 113-117.

Yoerger, D.R., Cooke, J.G. and Slotine, J.J.E. (1990). "The Influence of Thruster Dynamics on Underwater Vehicle Behaviour and Their Incorporation Into Control System Design," *IEEE Journal of Oceanic Engineering*, Vol. 15, No. 3, pp.167-178.

Yoerger, D.R., and Slotine, J.J.E. (1985). "Robust Tracking Control of Underwater Vehicles," *IEEE Journal of Oceanic Engineering*, Vol. OE-10, pp. 462-470.

Yuh, J. (1990). "A Neural Net Controller for Underwater Robotic Vehicles," *IEEE Journal of Oceanic Engineering*, Vol. 15, No. 3, pp.161-166.

Yuh, J., Lakshmi, R., Lee, S.H., and Oh, J. (1990). "An Adaptive Neural-net Controller for Robotic Manipulators," *Robotics and Manufacturing*, ed. M. Jamshidi and M. Saif, ASME, New York, New York.

Zadeh, L.A. (1965). "Fuzzy Sets," *Information and Control*, Vol. 8, pp. 338-353.

Zheng, X., Jackson, E., and Kao, M. (1990). "Object-oriented Software Architecture for Mission-configurable Robots," *First Workshop on Mobile Robots for Subsea Environments*, Monterey, California, pp. 63-73.

APPENDIX A Product Information

(excerpts from MTS Systems Corporation product brochures)

Series 242 Hydraulic Actuators

Features

- Available with force ratings of 1.0 kip or 2.2 kip (4.5 kN or 10.0 kN).
- Nonmetallic bearings provide high sideload capabilities and eliminate bearing-to-rod galling failures.
- Accepts a wide range of MTS Series 252 Servovalves, with flow ratings from 1 gpm to 15 gpm (4 ℓ/m to 57 ℓ/m).
- Standard Series 242 Actuators use low-pressure piston rod seals. This provides low friction operation, while minimizing fluid leakage and keeping contaminants out of the actuator.
- Single-piece, chrome-plated, hollow piston rod constructed to provide strength and extended seal and bearing life.
- Built-in hydraulic cushions protect the end caps during full-stroke, high-velocity operation.
- The displacement transducer is coaxially mounted in the hollow piston rod for increased accuracy and transducer protection.

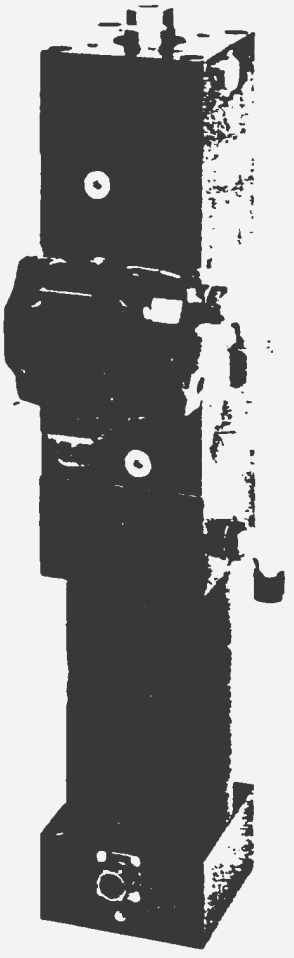

Series 242 Hydraulic Actuator shown with attached servovalve

Description

The Series 242 Hydraulic Actuators are small, low force, linear actuators which operate under precision servovalve control in MTS closed-loop servohydraulic systems. Typical applications include component fatigue tests, structural resonance searching and modal analysis.

Series 242 Actuators are available in two models. Model 242.01 has a force rating of 1.0 kip (4.5 kN) and has a standard stroke length of 4 in. (101.6 mm). Model 242.02 has a force rating of 2.2 kip (10.0 kN) and has standard stroke lengths of 1 in. or 4 in. (25.4 mm or 101.6 mm). Other stroke lengths are available as options for both models (refer to Table 1).

Each 242 Actuator contains a closed-housing LVDT (linear variable differential transformer) to provide an accurate indication of piston rod displacement, and has a pedestal base which allows the actuator to be rigidly mounted to a reaction mass. The actuator may also be installed in an MTS load frame. A swivel mounting accessory is available and is typically used in structural testing applications where pivotal freedom of the actuator is necessary.

The Series 242 Actuators are designed for the severe requirements of servo-controlled, closed-loop testing applications without compromising long-term reliability. Lab tested and field proven, this design features the latest technology in seal and bearing materials.

Design Characteristics

All MTS actuators are carefully manufactured to close tolerances. This attention to precision ensures reliability, performance, long life, and complete part interchangeability (within a given actuator model). The following characteristics are common to all Series 242 Actuators (refer to Figure 1).

1. Piston Rod End (fixture attachment end): The piston rod end has a center position internal thread for mounting fixtures, swivels, load cells, etc.

2. Porting: High-pressure hydraulic fluid is supplied through the pressure port, marked on the actuator with a **P**. Internal passages direct the fluid to a servovalve. The servovalve sends the fluid to one side of the piston or the other in order to extend or retract the piston rod. As hydraulic pressure is applied to one side of the piston, the fluid on the other side is ported through the servovalve to the return port, marked on the actuator with an **R**.

3. Piston Rod: The Series 242 Actuators are equipped with a double-ended piston rod. The double-ended piston has equal areas on both sides for balanced performance. The piston rod is machined from a single piece of heat-treated alloy steel, hard chrome plated, and precision ground to a fine finish to increase seal and bearing life. The hollow rod permits convenient installation and accurate alignment of the LVDT.

4. Piston Rod Bearings: The Series 242 Actuators are supplied with high-capacity nonmetallic bearings bonded directly to the end caps. The nonmetallic bearings are standard due to their high sideload tolerance and resistance to failure from galling and seizure.

   The close tolerance fit between the piston rod and bearing surface creates a low leakage viscous seal. A small amount of hydraulic fluid is allowed to flow across the bearing for lubrication, and is then ported back to the system hydraulic power supply reservoir.

5. Piston Rod Seals: The standard Series 242 Actuators use one low-pressure seal in each end cap. The seal wipes excess hydraulic fluid from the piston rod and guides the fluid into the drainback port.

6. Viscous Piston Seal: The close tolerance fit between the piston and cylinder provides an effective viscous seal. Grooves on the piston ensure adequate lubrication of the piston surface during short-stroke, sideloaded tests.

7. Cushions: Hydraulic cushions protect the end caps during full-stroke, high-velocity operation.

8. LVDT Assembly: The internally mounted LVD provides a displacement indication of the actuator piston rod. The LVDT core is securec to the inside of the hollow piston rod by a locking setscrew and can be adjusted to establish a zero reference point for the actuator.

9. Pedestal Base: The pedestal base allows the actuator to be rigidly mounted to a reaction mass, or permits attachment of a swivel mounting accessory.

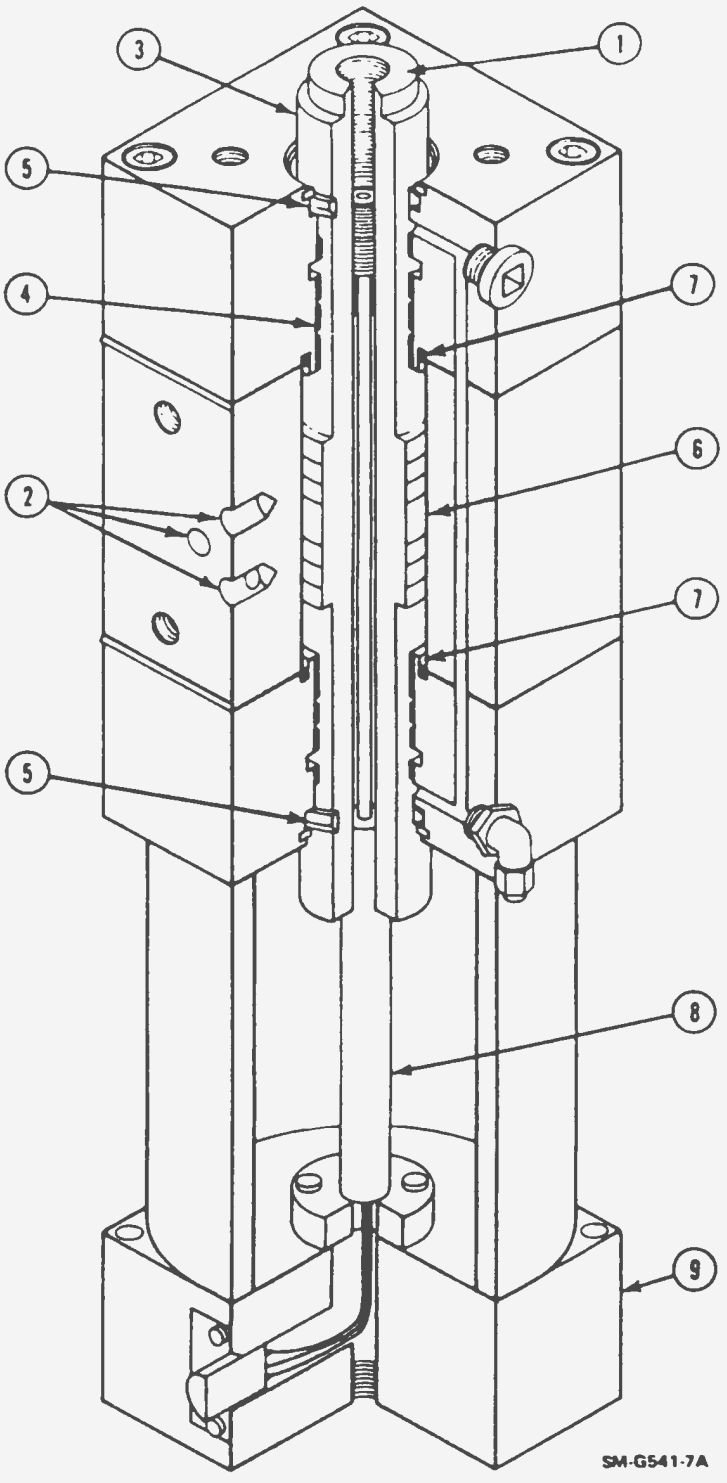

Figure 1. Cutaway View of a Typical Series 242 Actuator

Options

- Stroke: Model 242.01 has a standard dynamic stroke of 4 in. (101.6 mm). Model 242.02 has a standard dynamic stroke of 1 in. or 4 in. (25.4 mm or 101.6 mm). Other stroke lengths are available as options for both models (refer to Table 1).

- Special Porting: Series 242 Actuators may be ordered with porting designed to accommodate flow requirements greater than the maximum 15 gpm (57 ℓ/min) recommended for the standard Series 242 Actuators. Contact MTS Systems Corporation for information on special flow requirements.

- High-Pressure Seals: An optional high-pressure seal kit is available and may be used to increase the efficiency of the actuator during static test applications. One high-pressure seal is installed in each end cap, reducing the amount of fluid that flows across the piston rod bearings. Another high-pressure seal is installed on the piston, to reduce the amount of fluid transfer across the viscous piston seal. High-pressure seals are not recommended for high-velocity dynamic applications. High-pressure seal kits may be ordered with a new actuator or may be ordered separately and added to an existing actuator.

Swivel Mounting Accessory

The swivel mounting accessory consists of a swivel eye and a mounting bracket assembly. The swivel eye may be threaded into either end of the Model 242.01 or 242.02 Actuators. Two swivel mounting accessories are necessary to provide pivotal freedom of both ends of the actuator, reducing sideloads on the piston rod. The mounting bracket may be bolted to a fixture, or to a reaction mass, structural base, or bedplate. Figure 3 provides the specifications and dimensions for the swivel mounting accessory.

Specifications

Specifications for the Series 242 Actuators are listed under the actuator model number in Table 1. Actuator and accessory dimensions are illustrated in Figures 2 and 3. Lettered dimensions called out in Figure 2 are listed in Table 2.

Ordering Information

When ordering a Series 242 Hydraulic Actuator, first specify the desired actuator by the model number corresponding to the force rating, and the required dynamic stroke (refer to Table 1). Next, specify any additional options and accessories as follows:

- Special Porting
- High-Pressure Seals
- Swivel Mounting Accessory

Table 1. Actuator Specifications

	Model 242.01		Model 242.02	
	U.S. Customary	SI Metric	U.S. Customary	SI Metric
Force Rating[1]	1.0 kip	4.5 kN	2.2 kip	10.0 kN
Piston Area	0.42 in.^{2}	270.9 mm^2	0.92 in.^{2}	593.5 mm^2
Rod Diameter	1.12 in.	28.4 mm	1.12 in.	28.4 mm
Available Dynamic Stroke Lengths[2]	1.00 in.	25.4 mm	1.00 in.[3]	25.4 mm[3]
	2.00 in.	50.8 mm	2.00 in.	50.8 mm
	4.00 in.[3]	101.6 mm[3]	4.00 in.[3]	101.6 mm[3]
	6.00 in.	152.4 mm	6.00 in.	152.4 mm

[1] Nominal force with 2500 psi (17.2 MPa) pressure drop across the piston. Actual force may be up to 20% higher depending on servovalve size and test conditions.

[2] The value shown is total stroke minus the total cushion length, 0.50 in. (12.7 mm).

[3] Standard stroke lengths.

Specifications are subject to change without notice. Contact MTS for verification of specifications critical to your needs.

Table 2. Actuator Dimensions

Stroke (Both Models)		Dimension[1]					
		A		B		C	
in.	mm	in.	mm	in.	mm	in.	mm
1	25.4	1.60	40.64	8.50	215.9	12.68	322.07
2	50.8	2.60	66.04	8.50	215.9	13.68	347.47
4	101.6	4.60	116.84	11.00	279.4	18.18	461.77
6	152.4	6.60	167.64	13.00	330.2	22.18	563.37

[1] The dimensions listed are shown in Figure 2.

Dimensions are subject to change without notice. Contact MTS for verification of dimensions critical to your needs.

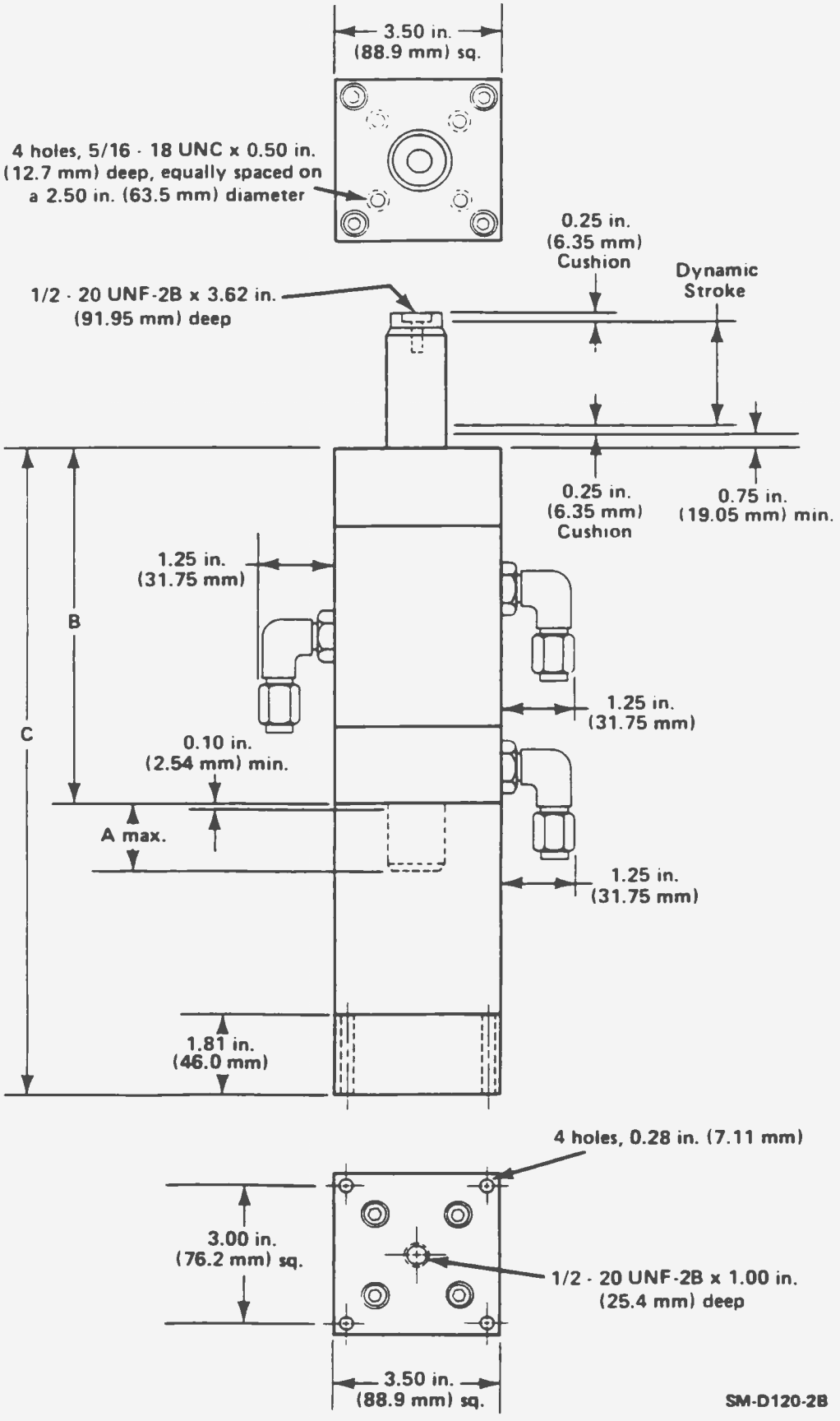

Figure 2. Basic Series 242 Hydraulic Actuator with Closed Housing LVDT and Pedestal Base

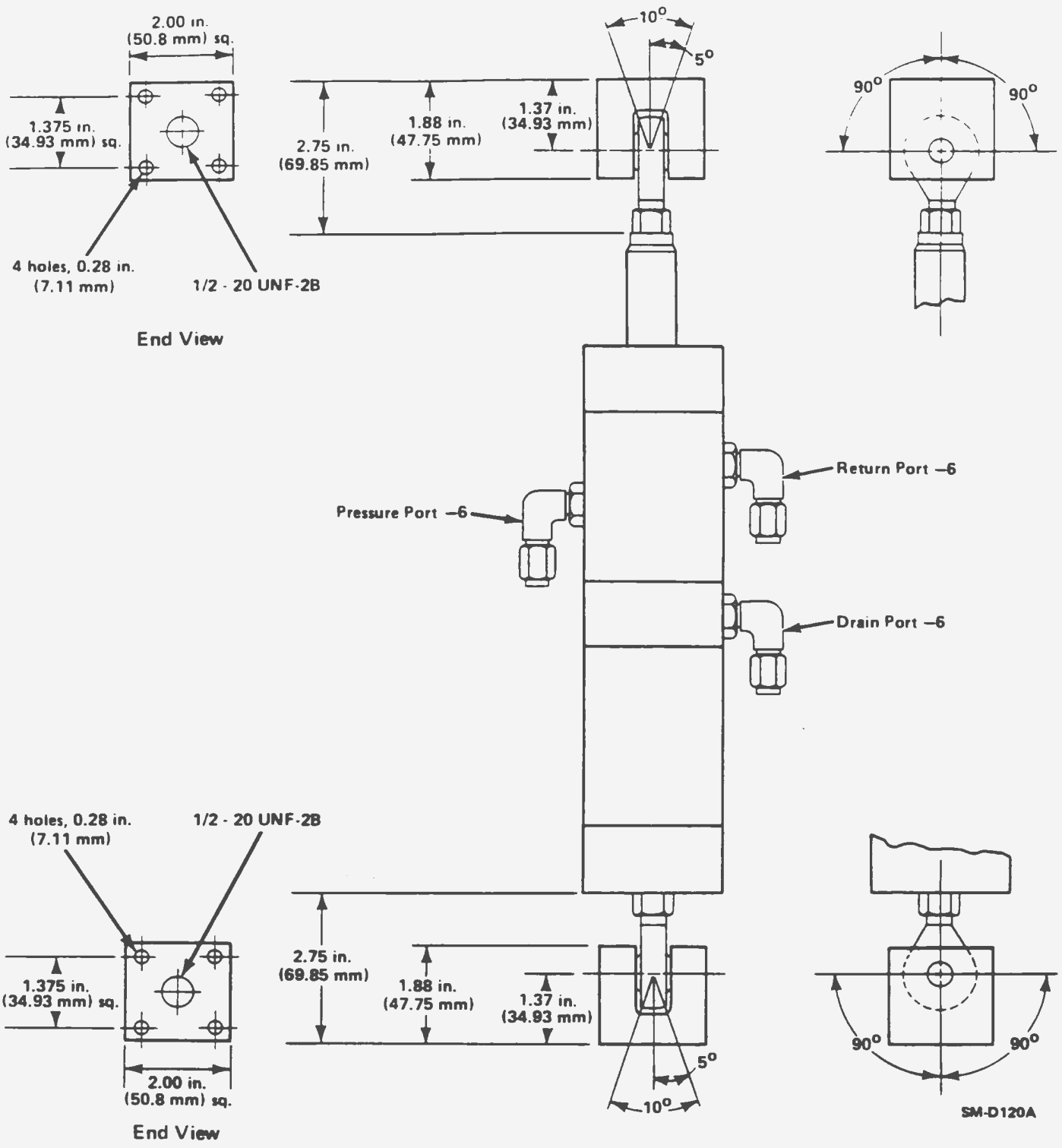

Figure 3. Series 242 Hydraulic Actuator with Swivel Accessories

Series 252 Servovalves

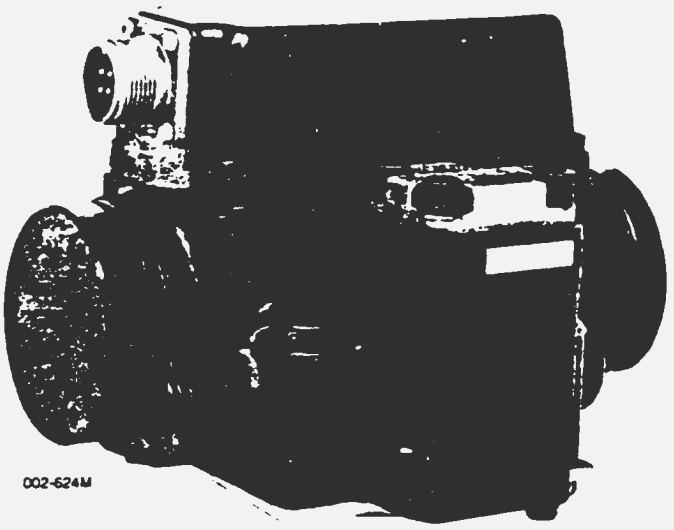

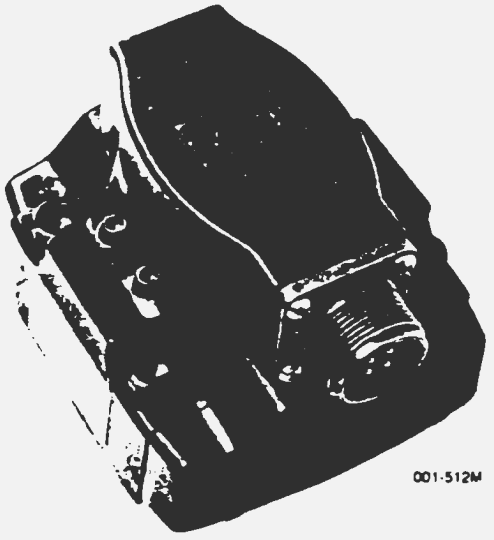

Features

- Nozzle-flapper design with mechanical feedback from the spool to provide positive internal closed-loop flow control
- Internal filtration to protect nozzle orifices from contamination
- Unpeaked response over servo-system frequency range
- Fifth port on some servovalves for separating pilot pressure from system pressure
- 3000 psi (21 MPa) operating pressure for optimum system performance and reliability; operating pressures up to 5000 psi (34.5 MPa) available on special request
- Mounting configuration within 252.2X and 252.4X series and within 252.3X series allows interchangeability between servovalves of different flow ratings
- High spool-driving forces (over 100-pounds-force) provide low contamination sensitivity

Description

MTS Series 252 Servovalves are two-stage, four-way servovalves that are designed for low-to-medium flow rates (1 to 60 gpm or 3.8 to 227 ℓ/min) in high-response, servo-hydraulic systems. Typical applications include hydraulic power control and regulation in fatigue test systems, simulators, and servo-hydraulic process and industrial controls.

Each servovalve consists of a torque motor and two stages of hydraulic power regulation (refer to Figure 2). The torque motor controls the first stage by positioning a flapper. The flapper controls the flow of hydraulic fluid from two nozzles in the first stage in an inversely proportional manner. As the flow from one nozzle increases, the flow from the other decreases. The resultant change in the flow of hydraulic fluid creates a differential pressure which is used to position the second stage spool. The second stage spool directly controls the direction and rate of hydraulic fluid flow to the actuator.

All the advantages of closed-loop control are incorporated in a complete loop within the servovalve. As the second stage spool reacts to the differential pressure created by the position of the torque motor flapper, a feedback spring is positioned by the spool which counters the action of the torque motor and flapper. When the spool reaches the commanded position, the torque motor and flapper will be completely counteracted. The flow from both nozzles will be equal; therefore, the differential pressure will balance and the spool will stop. This design provides precise control of the spool position, a high hydraulic driving force on the spool and a high error-force gradient (spool driving force per percent of spool position error).

Applications which require a higher flow rate than are available in the standard Series 252 Servovalves may use two servovalves connected in parallel to double the flow rating (refer to Figure 3). A special dual-valve manifold is required to operate the servovalves in parallel. Dual 252 Servovalves provide the advantages over a larger valve through reduced cost, increased availability and (in some applications) increased response rate.

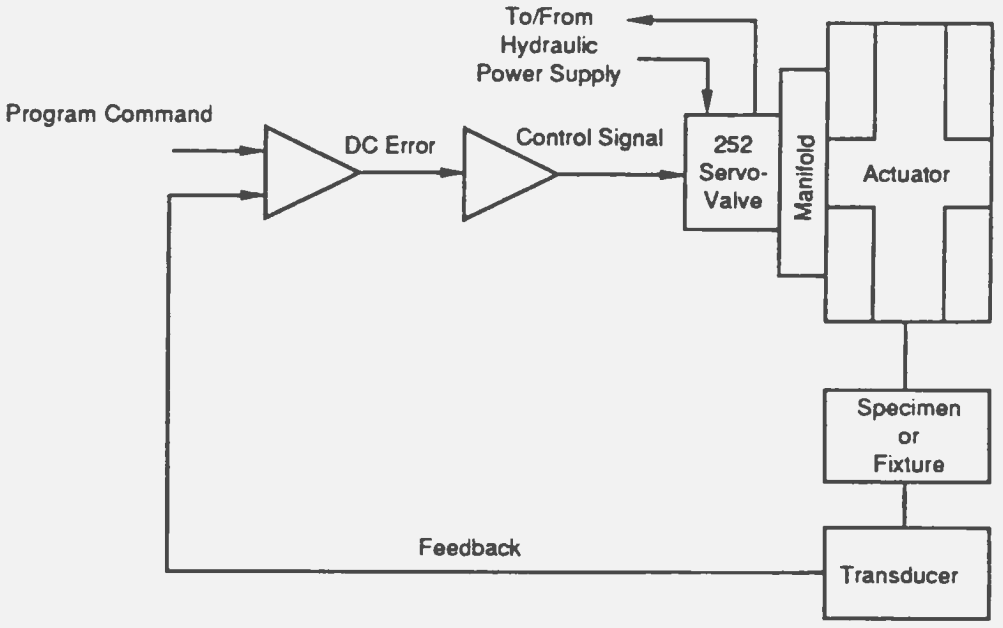

Figure 1. Servovalve in Closed Loop

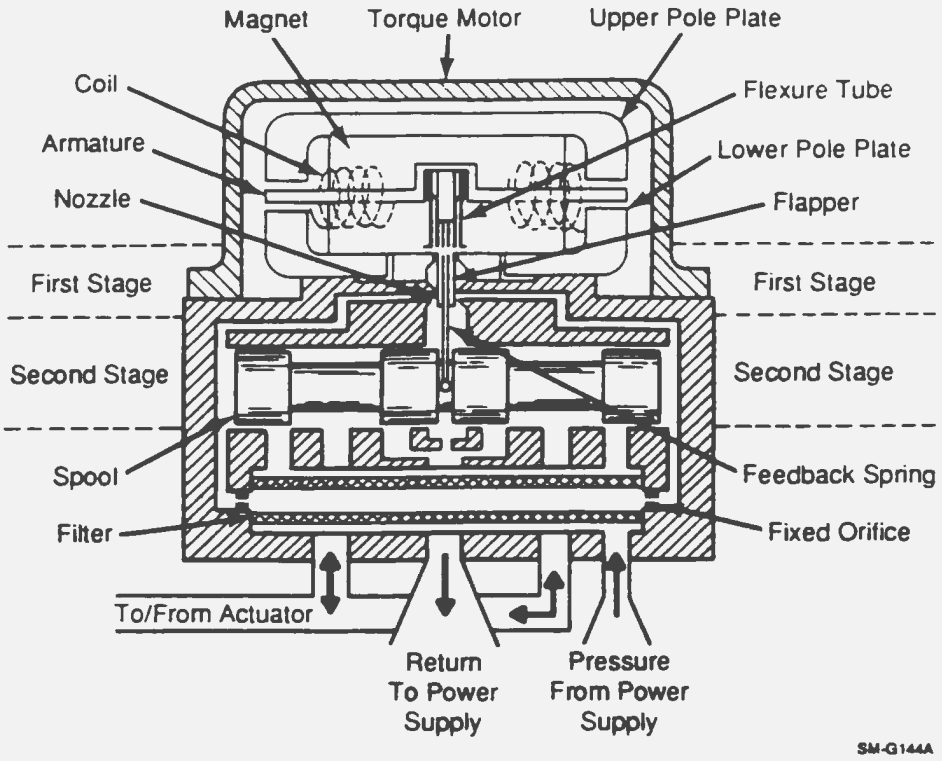

Figure 2. Parts Identification

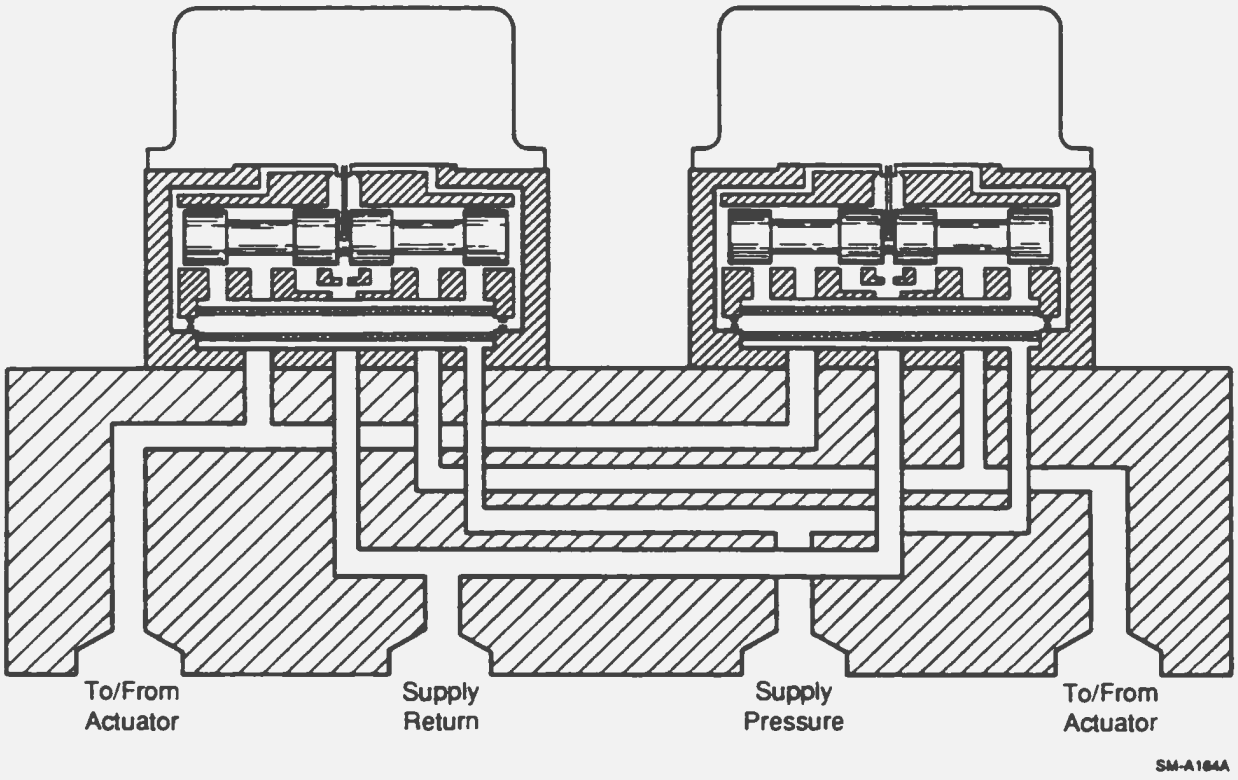

Figure 3. Dual Servovalves

Performance Curves

The flow-frequency performance curves (refer to Figure 4) indicate the relative performance capability of the servovalves. The curves are for full-flow conditions where a full valve opening command signal of 50 mA is applied at the indicated frequency. Servovalve performance at higher frequencies, particularly where the curves are shown dashed, is a function of many variables introduced by system components, actuator response and characteristics of the load or specimen.

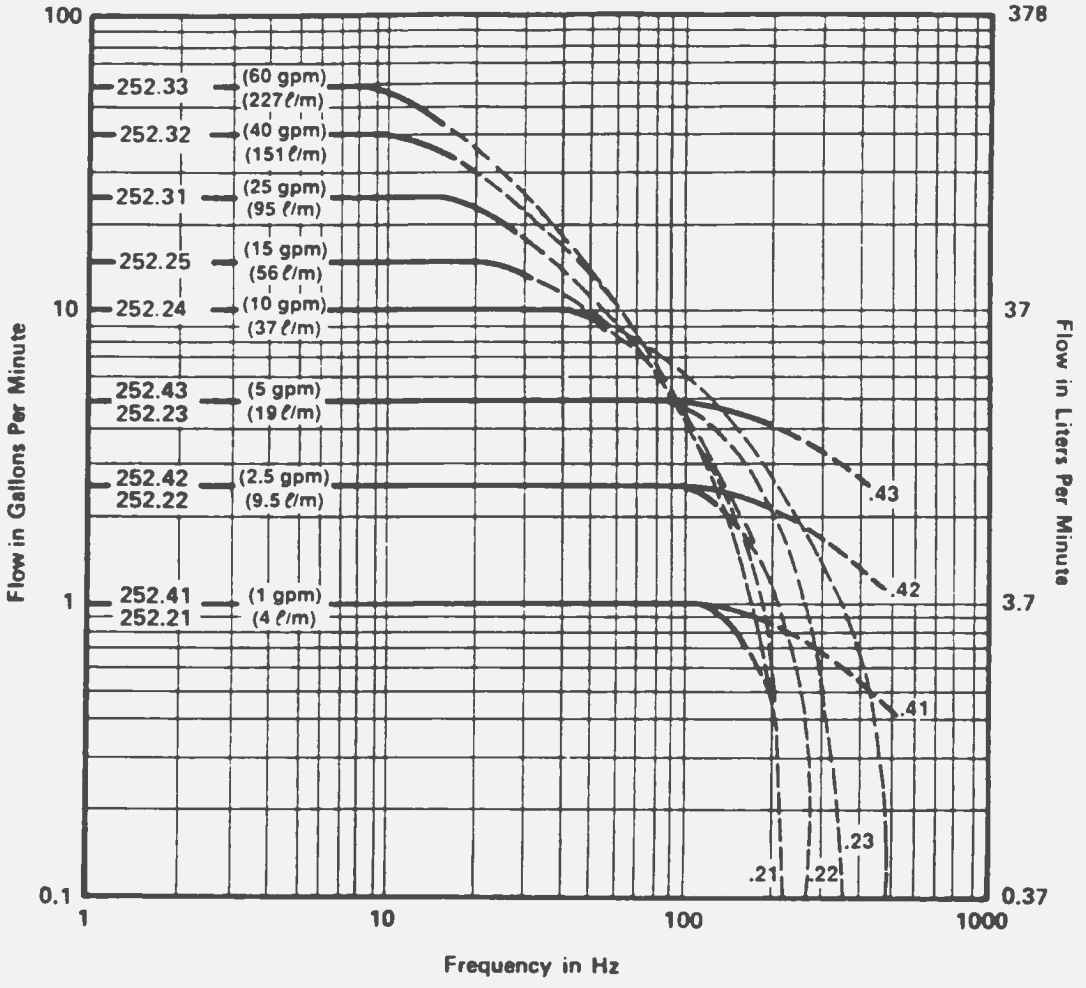

Note: Performance is with 3000 psi (21 MPa) pressure supplied and a 1000 psi (7 MPa) pressure drop across the Servovalve.

SM-K001E

Figure 4. Flow - Frequency Performance Curves

Dimensions

The 252.4X and 252.2X Series Servovalves have the same port pattern, bolt pattern, electrical connector and seal options. Full command is 50 mA for both. The 252.4X, however, has higher flows at higher frequencies than the 252.2X (Figure 4). The 252.4X also has a higher 90° point than its counterpart (refer to Table 1). At lower frequencies the 252.4X and 252.2X are comparable.

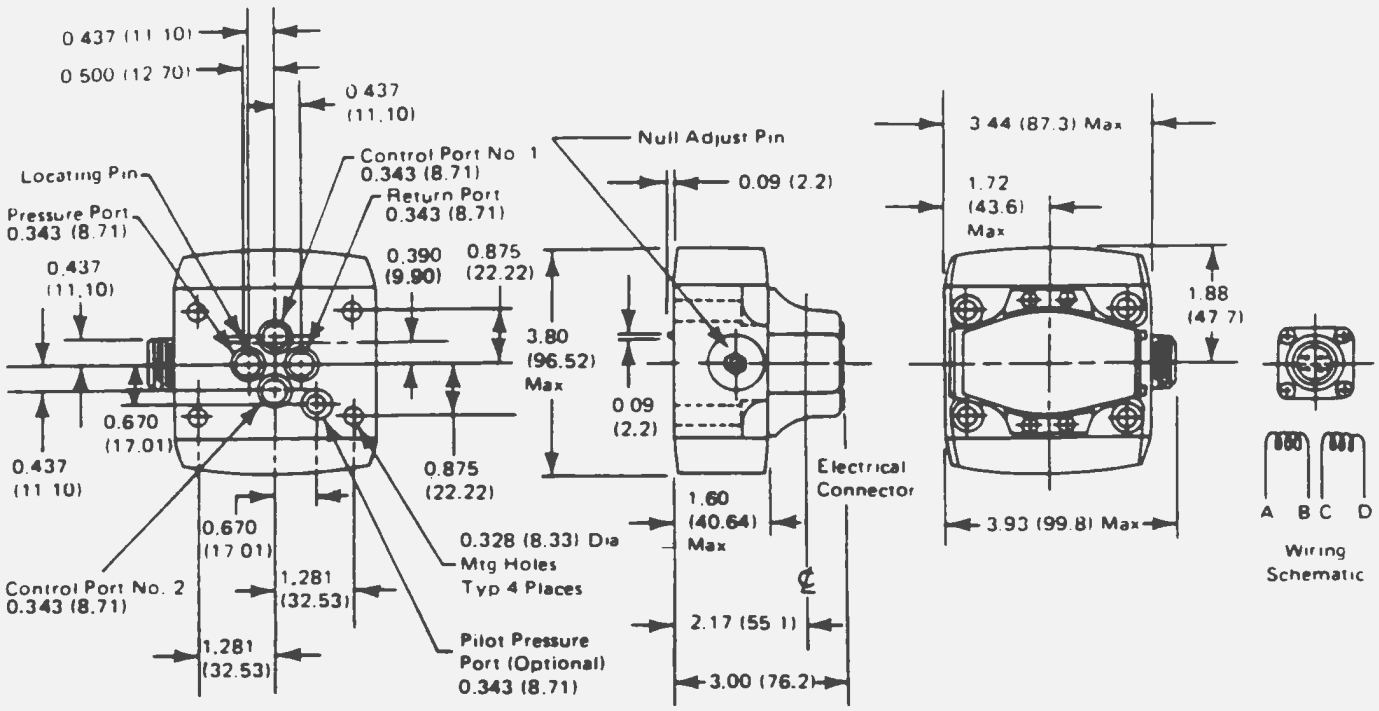

Note: Dimensions are in inches with millimeters in parentheses. The pressure port, control ports 1 and 2, and return port use O-ring size -013, and the optional pilot pressure port uses O-ring size -012. For the mounting screws use 5/16 - 18 x 1 3/4.

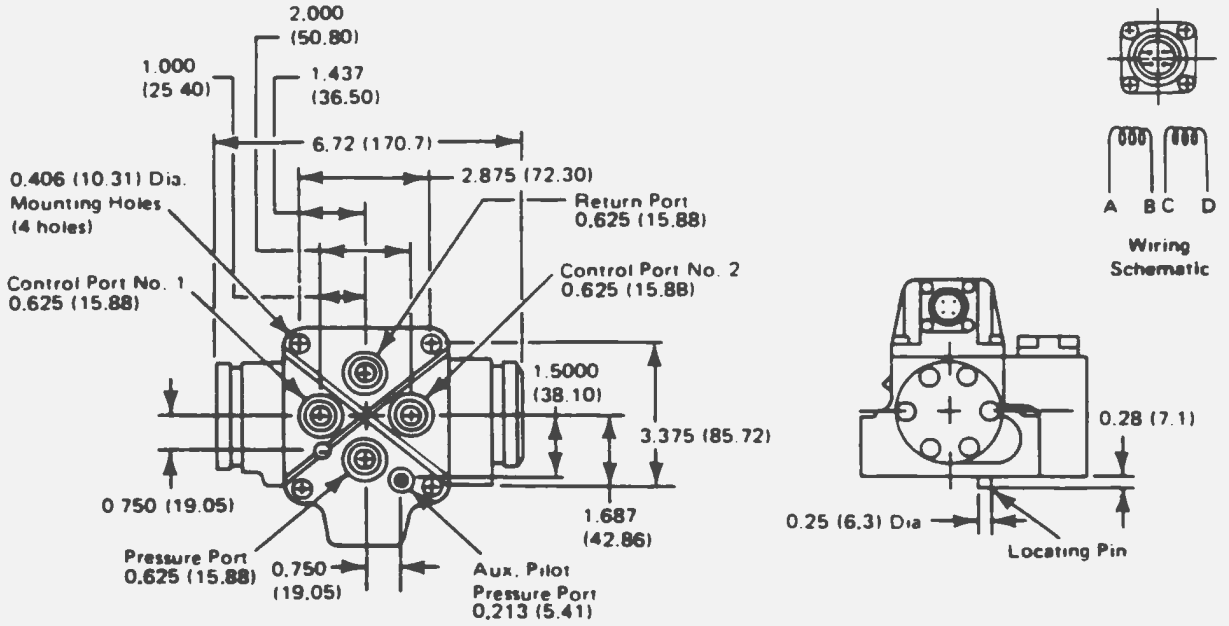

Note: Dimensions are in inches with millimeters in parentheses. The pressure port, control ports 1 and 2, and return port use O-ring size -019. The auxiliary pilot pressure port uses O-ring size -012. For the mounting screws use 3/8 - 16 x 2.

SM-G165D

Figure 5. Dimensions

Specifications

Series 252 Servovalve specifications are listed in Tables 1 and 2. Servovalve dimensions and O-rings are provided in Figure 5 for all Series 252 Servovalves.

Table 1. Performance Characteristics

Model No.	Full Flow Rating*		90° Point at 10% Command	Null Flow†	
	gpm	ℓ/min		gpm	ℓ/min
252.21C	1.0	4.0	240 Hz	0.29	1.10
252.41A‡	1.0	4.0	300 Hz	0.29	1.10
252.22C	2.5	9.5	240 Hz	0.38	1.44
252.42A‡	2.5	9.5	280 Hz	0.38	1.44
252.23C	5.0	19	240 Hz	0.60	2.27
252.43A‡	5.0	19	280 Hz	0.60	2.27
252.24C	10	37	200 Hz	0.60	2.27
252.25C	15	56	170 Hz	0.60	2.27
252.31A**	25	93	80 Hz	0.95	3.60
252.32A**	40	151	60 Hz	1.47	5.56
2152.33A**	60	227	50 Hz	2.20	8.33

* The flow ratings are specified with a 1000 psi (7 MPa) pressure drops across the servovalve. Higher flows are available with greater pressure drops.

† The maximum internal null flow is specified at 3000 psi (21 MPa). The null flow at the first stage is 0.20 gpm (0.76 ℓ/min) for all Series 252 Servovalves.

‡ This servovalve has a higher 90° point than the Series 252.2X Servovalves. Contact MTS for further performance characteristics.

** This servovalve can be operated with pilot pressure by removing a plug from the auxiliary pilot pressure port. 90° point is at 40% command.

Specifications are subject to change without notice. Contact MTS for verification of specifications critical to your needs.

Table 2. Static Specifications

Parameter	Specification
Maximum operating pressure	3000 psi (21 MPa)*
Minimum operating pressure	200 psi (12.4 MPa)
Operating temperature range	-40°F to +275°F (-40°C to +135°C)
Seals	Buna-N standard†
Rated full-flow input signal current‡	25 mA (series) 50 mA (differential) 50 mA (parallel)
Coil resistance‡	80 Ω per coil
Weight 252.2X/.4X 252.3X	 2.3 lb (1.03 kg) 7.75 lb (3.5 kg)
Recommended hydraulic fluid**	Mobil DTE 25 or Shell Tellus 46

* Higher operating supply pressures up to 5000 psi (34.5 MPa) are available on special request (contact MTS for more information).

† Special seals are available as options. Refer to *Ordering Information*.

‡ Refer to Figure 6.

** For more information regarding hydraulic fluid, refer to the MTS *Hydraulic Fluid and Hydraulic System Care* manual (MTS pn 115681-00).

Specifications are subject to change without notice. Contact MTS for verification of specifications critical to your needs.

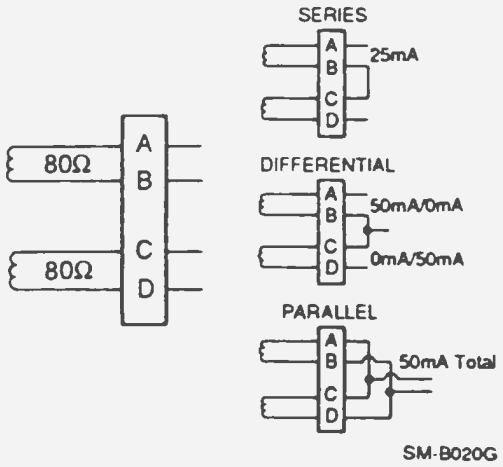

Figure 6. Coil, Connector and Wiring Illustration

Series III Accumulators

Features

- Rated Fatigue Pressure (RFP) conforms to NFPA Recommended Standard, NFPA/T3.47-1980, category 3/99
- Threaded gas and hydraulic end caps allow disassembly for maintenance
- Seamless thick wall construction increases service life
- Piston seals provide long operating life with minimum leakage

Description

The MTS Series 111 Accumulators are piston-type, nitogen-gas-charged accumulators, used in hydraulic systems. They can be used to reduce fluctuations due to sudden changes in flow rate, to act as an energy source for short term tests and to absorb hydraulic system shock fluctuations. They may be connected to the main pressure line or to the return line.

The Model 111.11B Accumulator (refer to Figure 1), together with a nipple coupling, forms a boss port mounted accumulator. The Model 111.12C Accumulator (refer to Figure 2), is a flange mounted accumulator which typically has a nitrogen gas capacity larger than the Model 111.11B.

Specifications

Table 1. General Specifications

Parameter	Specifications
Minimum burst pressure: Model 111.11B Model 111.12C	 12,000 psi (82.7 MPa) 20,000 psi (137.9 MPa)
Rated fatigue pressure: Model 111.11B Model 111.12C	 3000 psi (21 MPa) 3200 psi (22 MPa)
Operating temperature:	-40°F to 200°F (-40°C to 93.3°C)
Hydraulic fluid:	Petroleum based hydraulic fluid. Contact MTS for use with other fluids
Charge gas:	Dry nitrogen gas

Specifications are subject to change without notice. Contact MTS for verification of specifications critical to your needs.

Table 2. Capacity, Dimension[1] and Weight Specifications U.S. Customary and SI Metric

Model[2]	Nitrogen Gas Capacity		Length		A		B		Hydraulic Fluid Port Connection	Maximum Gross Weight	
			in	cm	in.	cm	in.	cm		lbs	kg
111.11B-01	5 in.^{3}	82 cm^3	6.12	15.54	3.12	7.92	2.50	6.35	12 SAE (1-1/16 - 12 UNF-2B)	9.4	4.26
111.11B-02	10 in.^{3}	164 cm^3	7.12	18.08	3.12	7.92	2.50	6.35	12 SAE (1-1/16 - 12 UNF-2B)	10.2	4.63
111.11B-03	1 pt	475 cm^3	11.00	27.94	3.12	7.92	2.50	6.35	16 SAE (1-5/16 - 12 UNF - 2B)	13.1	5.94
111.11B-04	1 qt	950 cm^3	16.88	42.88	3.12	7.92	2.50	6.35	20 SAE (1-5/8 - 12 UNF - 2B)	17.6	7.98
111.12C-02	1 qt	950 cm^3	11.62	29.51	5.00	12.70	4.00	10.16	1-1/2 SAE 4-bolt flange[3]	40.6	18.45
111.12C-03	1/2 gal	1.9 ℓ	15.38	39.07	5.00	12.70	4.00	10.16	1-1/2 SAE 4-bolt flange[3]	48.0	21.77
111.12C-04	1 gal.	3.8 ℓ	24.38	61.93	5.00	12.70	4.00	10.16	1-1/2 SAE 4-bolt flange[3]	65.8	29.87

[1] Refer to Figure 1 for Model 111.11B diagram and Figure 2 for Model 111.12C diagram.

[2] The models listed in this table are considered standard models. Other models may be manufactured with different capacities, lengths or hydraulic fluid port connections than listed here. Contact MTS for information on non-standard models.

[3] Standard pressure series (Code 61)

Specifications are subject to change without notice. Contact MTS for specifications critical to your needs.

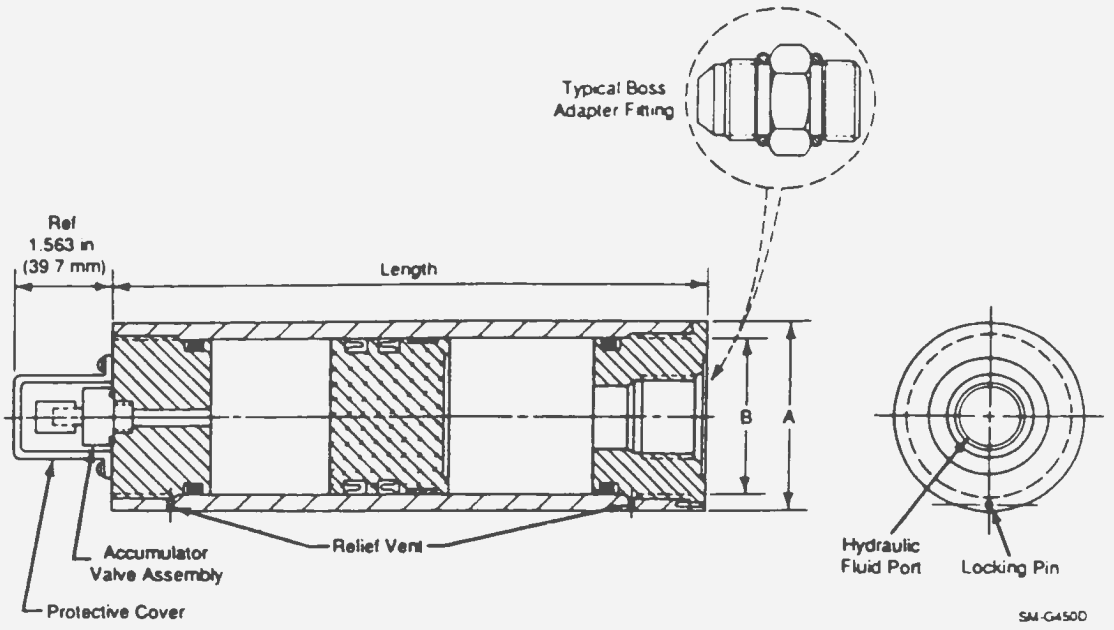

Figure 1. Cross-Sectional View of Model 111.11B Accumulator

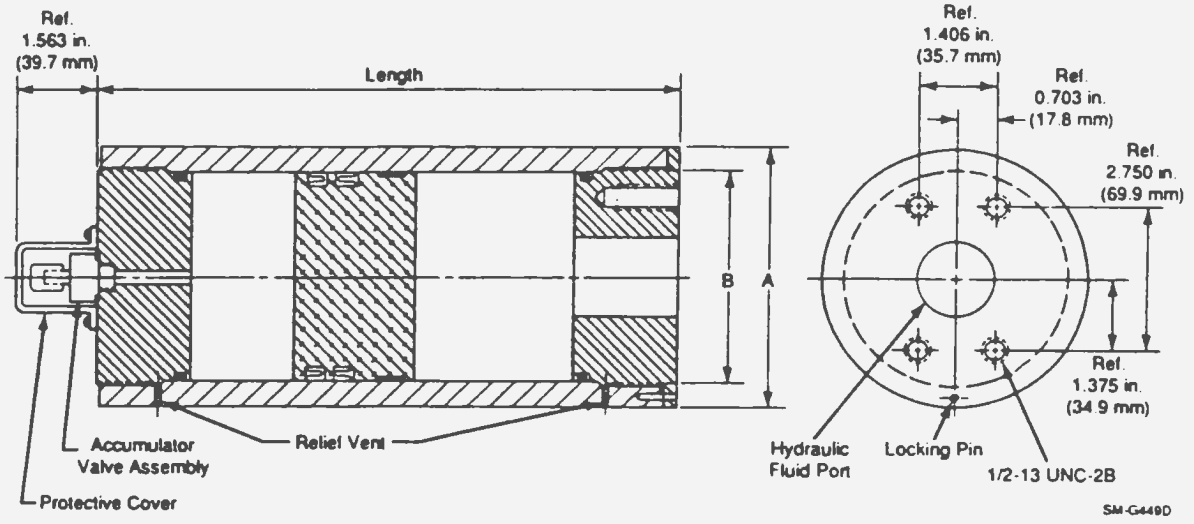

Figure 2. Cross-Sectional View of Model 111.12C Accumulator

APPENDIX B Computer Program

Computer Program for Actuator Operation

This is a simple program that was used to operate the actuator in a sinusoidal motion. The value of the LVDT signal, which gives the actual position of the actuator piston rod, was used as feedback. The difference between the command signal and the feedback value was used to generate an error value. The error value was multiplied by a gain value and the result used to drive the servovalve.

```
' $ INCLUDE: 'kdac500.bi'
CALL kdinit (BASIC.)
INPUT "MTS ACTUATOR CONTROL"
INPUT "GAIN"; gain
INPUT "ACTUATOR REST POINT"; rest
INPUT "ACTUATOR AMPLITUDE"; amp
INPUT "TIME SCALE"; scale
count = 0
DO
CALL fgread ("vin1", NONE, VARSEG (lvdt), VARPTR (lvdt), C.VOLTS, NT)
set = rest + amp * SIN (count / scale)
error = set - lvdt
mts = gain * error
CALL fgwrite ("vout1", VARSEG (mts), VARPTR (mts), C.VOLTS, NT)
count = count + 1
LOOP UNTIL INKEY$ < > " "
END
```

APPENDIX C Calculations

Calculations for Water Jet Force

Given:

MTS 242.01 actuator: - force rating is 4.5 kN
- piston area is 270.9 mm^2
- maximum stroke is 101.6 mm

MTS 252.21 servovalve: full-flow rating is 4 L/min

Chamber: - diameter of plunger is 0.15 m
- height of chamber (stroke of piston) is 0.10 m

Jet: diameter is 0.025 m

Sketch:

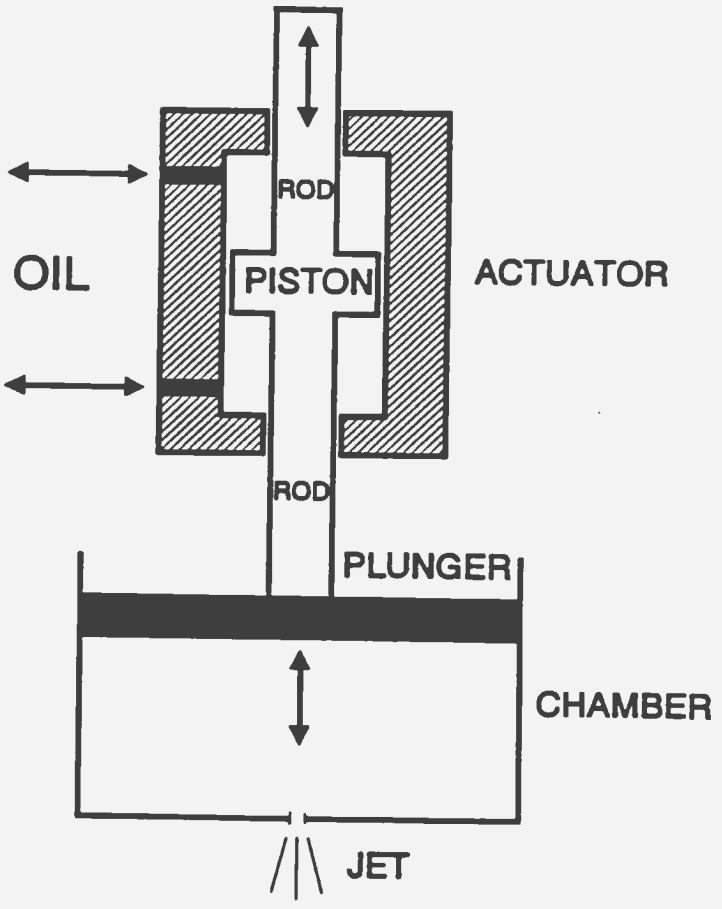

Maximum Jet Speed Calculations:

The maximum jet speed was determined based on the full-flow rating of the MTS 252.21 servovalve, the piston area and maximum stroke for the MTS 242.01 actuator. This method was used since the full-flow rating of the servovalve (not the force rating of the actuator) was found to be the limiting factor in determining the maximum jet speed. The maximum piston (and hence plunger) speed that can arise was calculated and the maximum jet speed was determined from continuity.

Maximum piston/plunger speed:

Volume of hydraulic fluid, V, used by the actuator for maximum piston stroke:

$$V = (270.9 mm^2)(101.6 mm)$$

$$= 27523.44\ mm^3$$

$$= 2.7523 \times 10^{-5}\ m^3$$

Flow rate of hydraulic fluid into actuator based on full-flow rating:

$$
\begin{aligned}
Q &= 4 \ litres \ per \ minute \\
&= \frac{4L}{\min}\left(\frac{(1\times10^{-1}m)^3}{1L}\right)\left(\frac{1\min}{60s}\right) \\
&= \frac{4\times10^{-3}\ m^3}{60\ s}
\end{aligned}
$$

Time, t, required to fill volume in actuator:

$$
\frac{4\times10^{-3}m^3}{60s} = \frac{2.7523\times10^{-5}m^3}{t}
$$

$$
t = 0.41s
$$

Maximum piston (and hence plunger) speed, denoted $V_{plunger}$:

$$
\begin{aligned}
V_{plunger} &= \frac{stroke}{time} \\
&= \frac{101.6mm}{0.41s} \\
&= 0.25m/s
\end{aligned}
$$

Maximum jet speed:

$$Q = VA$$

$$V_{plunger} A_{plunger} = V_{jet} A_{jet}$$

Rearranging and solving for the jet speed:

$$V_{jet} = \left(\frac{A_{plunger}}{A_{jet}} \right) (V_{plunger})$$

$$= \left(\frac{D^2_{plunger}}{D^2_{jet}} \right) (V_{plunger})$$

$$= \left(\frac{(0.15m)^2}{(0.025m)^2} \right) (0.25m/s)$$

$$= 9 \ m/s$$

The jet speed of 9 m/s was calculated using a jet diameter of 0.025 m, a piston diameter of 0.15 m and a piston stroke of 101.6 mm.

Jet Force Calculations:

The jet force for the system is calculated by first determining the mass flow rate for the jet. The mass flow rate is then multiplied by the jet speed to give the jet force.

Mass flow rate calculated for a 0.025 m diameter jet:

$$\dot{M}_{jet} = \frac{\pi D_{jet}^{\ 2}}{4} V_{jet}\ \rho$$

$$= \frac{\pi (0.025\,m)^2}{4}(9\,m/s)(1000\,kg/m^3)$$

$$= 4.42\ kg/s$$

Jet force, F_{jet}, for a 0.025 m diameter jet:

$$F_{jet} = \dot{M}_{jet} V_{jet}$$

$$= (4.42\,kg/s)(9\,m/s)$$

$$= 39.78\ N$$

Based on the current system, the jet force and jet speed were calculated to be approximately 40 N and 9 m/s, respectively.

Calculations for the Speed of Test Frame and its Components:

The force on the test frame and its components, according to Newton's third law of motion and d'Alembert's principle, is the force of inertia and is equal in magnitude but opposite in direction to the force produced by the water jet.

Added momentum is provided by the jet to the test frame and its components (which will be referred to as 'the rig' hereafter). Considering the control volume of the rig and the surrounding water (ignoring the drag force), conservation of momentum gives

$$M_{jet}\ V_{jet} = M_{rig}\ V_{rig}$$

Mass of jet is

$$\begin{aligned} M_{jet} &= mass\ of\ water\ inside\ the\ chamber \\ &= \left(\frac{\pi\ (0.15m)^2}{4}\ (0.10m)\right)(1000kg/m^3) \\ &= 1.77\ kg \end{aligned}$$

Speed of jet from previous calculations:

$$V_{jet} = 9\ m/s$$

Mass of rig including all components and test frame and 50 percent added inertia:

$$M_{rig} \approx 225\ kg$$

Rearranging the equation for the conservation of momentum and solving for the rig speed:

$$V_{rig} = \frac{M_{jet}\, V_{jet}}{M_{rig}}$$

$$= \frac{(1.77\,kg)(9\,m/s)}{225\,kg}$$

$$= 0.07\ m/s$$

Based on the added momentum provided by the water jet, the rig speed was calculated to be 0.07 m/s.

Considering the Drag Force of the Rig in its Rectangular Configuration:

Drag force on the rig is equal to

$$F_D = C_D\, A\, \rho\, \frac{V_{rig}^2}{2}$$

Drag coefficient for the rig would be poor based on its large rectangular configuration. The drag coefficient is assumed to be:

$$C_D = 1$$

The surface area of the rectangular cross section of the test frame is used to determine the drag force.

$$A = (0.61m)\ (0.46m)$$
$$= 0.28m^2$$

Terminal rig speed:

A terminal rig speed is determined based on the speed at which the drag force would equal the force provided by the jet. The equation for the drag force is rearranged and the force previously calculated for the jet force is substituted for the drag force. The terminal speed for the rig becomes

$$(V_{rig})_{max} = \sqrt{\frac{2\ F_{jet}}{C_D\ A\ \rho}}$$
$$= \sqrt{\frac{2\ (39.78N)}{(1)\ (0.28m^2)\ (1000kg/m^3)}}$$
$$= 0.53\ m/s$$

The speed of the rig cannot exceed 0.53 m/s or the negative force of drag will counteract the positive force produced by the water jet. This speed is beyond the expected speed required for fine positioning of the test system.

Methods to Increase Jet Force:

The simplest method to increase the jet force and thus the rig speed is to decrease the jet diameter without changing any other system parameter. Based on the pressure balance between the pressure the actuator can deliver and the pressure beneath the plunger, Bernoulli's equation can be used to determine the minimum jet diameter.

Pressure beneath the plunger, $P_{plunger}$, based on the force rating of the actuator:

$$P_{plunger} = \frac{F_{provided\ by\ actuator}}{area\ of\ plunger}$$

$$= \frac{F_{provided\ by\ actuator}}{\left(\frac{\pi D^2_{plunger}}{4}\right)}$$

$$= \frac{4.5\,kN}{\left(\frac{\pi (0.15\,m)^2}{4}\right)}$$

$$= 255\ kPa$$

Bernoulli's equation in standard form:

$$\frac{P_1}{\gamma} + \frac{V_1^2}{2g} + z_1 = \frac{P_2}{\gamma} + \frac{V_2^2}{2g} + z_2$$

Bernoulli's equation, letting point one refer to beneath the plunger and point two refer to beneath water jet:

$$\frac{P_{plunger}}{\gamma} + \frac{V^2_{plunger}}{2g} + z_{plunger} = \frac{P_{jet}}{\gamma} + \frac{V^2_{jet}}{2g} + z_{jet}$$

Ignoring unsteady dynamics and cancelling $z_{plunger}$ and z_{jet} since they are close in elevation, Bernoulli's equation becomes

$$\frac{P_{plunger}}{\gamma} + \frac{V^2_{plunger}}{2g} = \frac{P_{jet}}{\gamma} + \frac{V^2_{jet}}{2g}$$

Writing the jet speed in terms of the plunger speed:

$$V_{jet} = V_{plunger}\left(\frac{A_{plunger}}{A_{jet}}\right)$$

$$= V_{plunger}\left(\frac{D_{plunger}}{D_{jet}}\right)^2$$

Substituting into Bernoulli's equation:

$$\frac{P_{plunger}}{\gamma} + \frac{V^2_{plunger}}{2g} = \frac{P_{jet}}{\gamma} + \frac{V^2_{plunger}\left(\frac{D_{plunger}}{D_{jet}}\right)^4}{2g}$$

Rearranging the equation in terms of D_{jet}:

$$D_{jet} = \sqrt[4]{\frac{V^2_{plunger} D^4_{plunger}}{\frac{2gP_{plunger}}{\gamma} + V^2_{plunger} - \frac{2gP_{jet}}{\gamma}}}$$

Value of P_{jet} is taken to be 30 kPa based on the test frame operating in water depth of 3 m, which would be the case for in-water tank tests.

Substituting values for $V_{plunger}$, $D_{plunger}$, $P_{plunger}$, P_{jet}, g and γ and solving for D_{jet}:

$$D_{jet} = \sqrt[4]{\frac{(0.25\,m/s)^2\ (0.15\,m)^4}{\frac{2(9.81\,m/s^2)(255\,kPa)}{9.79\,kN/m^3} + (0.25\,m/s)^2 - \frac{2(9.81\,m/s^2)(30\,kPa)}{9.79\,kN/m^3}}}$$

$$= 0.016m$$

The jet diameter must be larger than 0.016 m.

Table A1 contains values for the jet force, rig speed and terminal rig speed for a number of jet diameters below 0.025 m and above the minimum diameter of 0.016 m. All other system parameters were the same as in previous calculations.

Table A1: Jet Force, Rig and Terminal Rig Speeds for Various Jet Diameters

Jet Diameter (m)	Jet Speed (m/s)	Jet Mass Flow Rate (kg/s)	Jet Force (N)	Rig Speed (m/s)	Terminal Rig Speed (m/s)
0.025	9.00	4.42	40	0.07	0.53
0.020	14.06	4.42	62	0.11	0.67
0.019	15.58	4.42	69	0.12	0.70
0.018	17.36	4.42	77	0.14	0.74
0.017	19.46	4.42	86	0.15	0.78
0.016	21.97	4.42	97	0.17	0.83

Summary:

The jet force, rig speed and terminal rig speed were calculated to be 40 N, 0.07 m/s and 0.53 m/s, respectively for the present system. However, by simply reducing the jet diameter (without changing any other parameters or components) the jet force, rig speed and terminal rig speed can be increased to 97 N, 0.17 m/s and 0.83 m/s, respectively.

The following options are available if a larger jet force is required:

- use a servovalve with a higher full-flow rating
- use an actuator with a higher force rating
- decrease the piston diameter to increase the pressure in the chamber
- decrease the drag force on the rig by altering its shape
- decrease the weight of the rig by using a slighter frame and a plastic reservoir

Some of these options would have compromises. For instance, using the present system with a jet diameter of 0.025 m but replacing the current servovalve with a MTS 252.22 servovalve (full-flow rating of 9.5 L/min) the jet force becomes 217 N. However, a higher flow rate servovalve would mean the stored hydraulic fluid in the accumulator would be drained faster during the operation of the device.